UNIVERSIDADE FEDERAL DO RIO GRANDE DO SUL
PROGRAMA DE PÓS-GRADUAÇÃO EM FÍSICA

Tese de Doutorado

Study of Quantum Phase Transitions in One-dimensional Spin Models

Estudo de Transições de Fases Quânticas em Modelos de Spin Unidimensionais

Marcos César Amor Pérez Leiva

Tese realizada sob a orientação do Prof. Dr. Gerardo Guido Martínez Pino e apresentada ao Programa de Pós-Graduação do Instituto de Física da Universidade Federal do Rio Grande do Sul para a obtenção do Título de Doutor em Ciências, na Área de Física Teórica.

Porto Alegre, RS, Brasil

Março de 2018

* Trabalho financiado pelo Conselho Nacional de Desenvolvimento Científico e Tecnológico (CNPq)

Index

Acknowledgments

This work was supported by the CNPq agency (Brazil). I would like to acknowledge Professor Germán Sierra (IFT-Madrid) and Professor Cristiane Morais Smith (ITP-Utrecht), who supported my visit to their research places and enriched the physical discussion of the preliminary results of this thesis. I am also grateful to IIP-Natal for the successful organization of events at a high scientific level, which allowed me to enrich my knowledge about topological states of matter and integrable models. I would also like to thank the IF-UFRGS for hosting me these four years, and especially to my advisor, Professor Gerardo Martínez, for his great patience.

I am grateful to many people who contributed to the completion of this thesis. Special thanks are endowed to my friends, colleagues, to my Brazilian family, to the people of the past and the future, and especially to my parents who, like many other parents in the world, support a huge percentage of the scientific production of our countries.

Abstract

In this thesis we address the subject of quantum phase transitions within the context of spin liquids using two different models and two theoretical approaches. The field of quantum phase transitions is quite vast and for that reason we selected two specific examples, which are exactly solvable. The first one is described by elementary excitations called majorana zero modes which are related to topological phases, and the second one is described by free spinons that obey fractional statistics. In both cases, these are elementary excitations from interacting many-body systems, which are essentially very different from fermions or bosons. Therefore, the usual second quantization rules are not available for these systems, opening the gate for developing new theories and techniques. In this thesis we have the opportunity, broadly speaking, to gather basic aspects of topological properties of low dimensional systems in one hand, and to bring into operation some details of the structure of the Yangian algebra to deal with the physics of free spinons, on the other hand.

We first start by studying the effect of spatial inhomogeneities in the Kitaev chain. This one-dimensional model describes a p-wave superconductor which is characterized by topological/non-topological phase transitions. Using an enlarged unit-cell method, we studied a suitable topological invariant to describe the effects of spatial modulations in the parameters of the model. We found the emergence of compact non-topological regions, we called them bubbles, that are described by topological protected states in the homogeneous case. To characterize these phases, we developed a polynomial description of the topological invariant, which led us to account for the emergence of bubbles in the topological region, as well as to identify an internal structure of the topological invariant, which has a notorious similar behavior with the spin correlation function of the XY spin-1/2 model. Both models exhibit the same oscillation region in their phase diagrams. This is an effect of duality, as both models are linked through a Jordan-Wigner transformation. As an application

of our method, we used it to characterize an effective model corresponding to a one-dimensional tight-binding model of spinless fermions with a nearest-neighbor charge interaction, which is periodically driven. Using the Floquet formalism, we found an effective Hamiltonian which is mapped into an inhomogeneous Kitaev chain described by a dimerized nearest-neighbor pairing and a next-nearest-neighbor pairing term. Applying our formalism, we accomplish a description of the effects of the time-dependence of this effective model.

In the second part of this thesis, we studied the one-dimensional Haldane-Shastry model plus a chiral interaction given by the z-component of the rapidity operator. The Haldane-Shastry model is a periodically bounded spin-1/2 homogeneous chain with a long-range exchange interaction that falls off with the inverse of the distance squared among the spins. This model is integrable, exactly solvable through the Yangian algebra and its symmetries describe elementary excitations given by free spinons which satisfy a fractional statistics. Since the chiral interaction is taken as the rapidity operator from the Yangian, the symmetry of the new model does not change, allowing us to use the Modified Young Tableaux formalism to describe their eigenstates. We found that the spectrum of the original model split when the chiral interaction is turned on. The split is governed by the Yangian algebra, resulting in non-trivial quantization rules which were studied by the representation theory of the algebra. After our numerical description for finite systems, we extended our results towards a thermodynamic limit, finding a general description of the ground-state transitions at low energy that is also valid for the infinite chain. Finally, as an application, we used the Haldane-Shastry model with a chiral interaction to introduce a family of spin models with different medium-range interactions whose coupling constants are extracted from this model. We describe how the solution of these models can be found by our approach and formulate the question about the link among them.

Resumo

Nesta tese abordamos o tema das transições de fases quânticas no contexto de líquidos de spins usando dois modelos e duas abordagens teóricas diferentes. A área das transições de fases quânticas é bastante vasta e, por esse motivo, escolhemos dois exemplos específicos, que tem solução exata. O primeiro exemplo é descrito por excitações elementares denominadas modos de majorana de energia zero que estão relacionadas às propriedades topológicas, enquanto que o segundo exemplo é descrito por spinons livres que obedecem a estatísticas fracionárias. Nos dois casos, estas excitações elementares vêm da sistemas interagentes de muitos corpos, as quais são fundamentalmente diferentes dos férmions e bósons. Portanto, as regras de segunda quantização usuais não estão disponíveis para esses sistemas, abrindo espaço para desenvolver novas teorias e técnicas. Nesta tese temos a oportunidade, em termos gerais, de reunir aspectos básicos das propriedades topológicas de sistemas de baixa dimensionalidade, por um lado, e colocar em operação alguns detalhes da estrutura da âlgebra Yangiana para lidar com a física de spinons livres, por outro lado.

Primeiramente começamos por estudar o efeito da inomogeneidade espacial na cadeia de Kitaev. Este modelo unidimensional descreve um supercondutor de onda p caracterizado por fases topológicas/não-topológicas. Usando o método de célula unitária ampliada, estudamos um invariante topológico apropriado para descrever os efeitos das modulações espaciais nos parâmetros do modelo. Encontramos o surgimento de regiões não-topológicas compactas, as que chamamos de bolhas, as quais são descritas por estados topológicos protegidos no caso homogêneo. Para caracterizar estas fases, desenvolvemos uma descrição polinomial do invariante topológico, o que nos levou a uma explicação do surgimento destas bolhas na região topológica, assim como a identificar uma estrutura interna do invariante topológico, tendo este um comportamento notoriamente semelhante à função de correlação de spins do modelo XY de spin-1/2. Ambos modelos exibem a mesma região de oscilações nos seus

diagramas de fase. Isto é um efeito da dualidade, já que ambos modelos estão ligados por uma transformação de Jordan-Wigner. Como uma aplicação do nosso método, utilizamos ele para caracterizar um modelo efetivo correspondente a um modelo de ligaduras-fortes de férmions sem spin, com uma interação de carga a primeiros vizinhos que é modulada periodicamente. Usando o formalismo de Floquet, achamos um Hamiltoniano efetivo o qual é levado à cadeia de Kitaev inomogênea descrita por um emparelhamento a primeiros vizinhos dimerizado e um emparelhamento a segundos vizinhos. Aplicando o nosso formalismo, conseguimos descrever os efeitos da dependência temporal deste modelo efetivo.

Na segunda parte da tese, estudamos o modelo unidimensional de Haldane-Shastry, mais uma interação quiral dada pelo componente-z do operador de rapidez. O modelo de Haldane-Shastry consiste numa cadeia homogênea com condições de borda periódicas de spins 1/2, com uma interação de troca entre os spins que decai com o inverso da distância ao quadrado. Este modelo é integrável, exatamente solúvel através da âlgebra Yangiana, e as suas simetrias descrevem as excitações elementares, dadas por spinons livres que satisfazem estatísticas fracionárias. Uma vez que a interação quiral é tomada como o operador de rapidez, da Yangiana, a simetria do novo modelo não muda, o que nos permite utilizar o formalismo das Tabelas de Young Modificadas para descrever seus autoestados. Descobrimos que o espectro do modelo original é separado quando a interação quiral é ligada. A âlgebra Yangiana é responsável por esta separação, resultando em regras de quantização não-triviais que foram estudadas pela teoria de representação da âlgebra. Após nossa descrição numérica para sistemas finitos, ampliamos nossos resultados para o limite termodinâmico, achando uma descrição geral das transições do estado fundamental para baixas energias, que é válida até para a cadeia infinita. Para finalizar, e como uma aplicação, utilizamos o modelo de Haldane-Shastry com interação quiral para introduzir uma família de modelos de spins com interações a mais vizinhos, cujas constantes de acoplamento são extraídas deste modelo. Descrevemos como a solução desses modelos pode ser achada por meio da nossa abordagem, o que nos permite formular a questão sobre o vínculo que têm entre eles.

Chapter 1

Motivation words

Quantum phase transitions have attracted the interest of both theoretical and experimental researchers in condensed matter physics from the beginning of the quantum mechanics to explain, for instance, the fate of magnetism. These quantum phase transitions occur at zero temperature as a result of competing ground states. Different approaches have been developed to study this competition, being the Landau's theory of second order phase transitions the most celebrated in the past. In our days, this theory is still used but cannot give answers to all questions behind the description of the quantum states of matter, requiring to develop new approaches that bring new concepts and answers, as well as new questions, about the features of quantum matter and their topological quantum phase transitions.

One example corresponds to the transitions from topological to non-topological phases, having in the Kitaev chain [1], a spinless fermion p-wave superconductor wire, a paradigmatic model that has been studied intensively in the last seventeen years. In this case, the transition is governed by global symmetries that keep the gap open. Such gap protection by symmetry is the main subject of study in this new area – the so-called topological invariant systems – for which the Landau description of local parameters and symmetry breaking no longer applies.

To cite another example, we mention the quantum phase transition from criticality of the isotropic Heisenberg model to an XXZ spin chain by quenching the system through the inclusion of a Dzyaloshinskii-Moriya interaction [2]. Critical behavior, like in the Heisenberg model, is a well studied subject and it is described as having correlation functions decaying algebraically instead as exponentially. This subject

is inserted in a broad area related to integrable systems, whose aim is to develop validated theoretical schemes in exactly solvable models. Exact solutions are scarce and the techniques to deal with them are sophisticated and cumbersome.

These models are generically denominated as quantum spin liquids, which may be considered as quantum disordered ground states of spin systems, in which zero-point fluctuations are so strong at low dimensionality that prevent conventional magnetic long-range order at very low or even at zero temperature. Although this definition has being sustained for a while in the specific literature, it is somehow loose in the sense that defines quantum spin liquids for what they do not do, as they do not order magnetically in the conventional sense. There is another, more specific, definition of quantum spin liquids in terms of maximally entangled systems [3], but we will not follow that line of reasoning. Although quite relevant, we will not touch the subject of quantum entanglement in this thesis either.

Having said what we will not deal with in this thesis, it is time to declare what the subjects of this work are. Within the general context described above, we divided the thesis work in two parts:

We first took the example of the Kitaev chain [1], a tight-binding model of spinless fermions with a p-wave superconducting pairing in a one-dimensional discrete lattice that presents topological properties, as described in more detail in the next (second) chapter, and we found that there was an incomplete description of the disordered situation. We therefore started to study how to implement theoretical rules to analyze the dependence of the topological phase diagram when disorder, in the form of distributions of the parameters of the Kitaev Hamiltonian, is introduced. We found out that there is already a formalism in the literature, the Enlarged Unit-Cell Method [4], and we adapted it to our case to obtain the modifications of the phase diagram of the Kitaev chain. We include this Kitaev model as a spin liquid because of its dual model, the anisotropic XY spin model [5], to which the Kitaev chain is converted through an exact Jordan-Wigner transformation [6]. Furthermore, another exact unitary transformation converts the Kitaev chain into a model described by Majorana fermions with zero energy bound states

(majoranas zero-modes). Different from Dirac fermions, Majorana fermions are their own antiparticles, and therefore we cannot define a usual Fock space for them as the occupancy of majoranas is not well defined. This is the context of the first part of the thesis and it is described in the second chapter, where a polynomial description for the topological invariant in the enlarged unit-cell method for disordered Kitaev models is developed. An application of our method is further worked out, in collaboration with Professor Cristiane Morais Smith (ITP-Utrecht), for a system with a driving time-dependent term using the Floquet formalism.

The second part, which is detailed in the third chapter, is devoted to another spin liquid model, namely the Haldane-Shastry spin chain. This model was proposed and solved simultaneously by F.D.M. Haldane [7] and B. S. Shastry [8] in 1988, and it is a sort of long-range spin interacting system with a $1/r^2$ exchange coupling. This long-range interacting system is exactly solvable and the elementary excitations are free spinons, which have a fractional statistics. The model is described by a Yangian algebra, beyond the SU(2) algebra. We took a suggestion proposed by Professor Germán Sierra (IFT-Madrid) to include a perturbation taken from the Yangian algebra of the model. We coupled the Haldane-Shastry Hamiltonian to the z-component of the rapidity vector operator and found very interesting results by numerical (exact diagonalization) and theoretical (Yangian representation theory [9]) approaches. Our outcomes exhibit a spin liquid behavior in the thermodynamic limit. The singlet character of the ground-state is preserved in the large size limit as the quantum phase transitions of the ground state always keep $S^z = 0$. Therefore, no magnetic long-range order is observed in an almost exact solution of the extended Haldane-Shastry to which a rapidity chiral interaction was applied as a perturbation. As an application of our results, we discuss a family of medium-range Heisenberg Hamiltonians with further neighbor chiral interactions to see whether our method can also be applied to such general situation.

Chapter 2

Quantum phases in topological inhomogeneous systems

2.1 Introduction

The topological properties in condensed matter physics appeared in 1980 with the discovery of the Quantum Hall Effect (QHE) by von Klitzing *et al.* [10]. When a perpendicular magnetic field is applied in a 2D metallic material at low temperature, the QHE relates to the null longitudinal conductance of this system while its edge is metallic with a quantized conductance, as we can see in the Fig. 2.1. Soon after, in 1981, Laughlin [11] explained the quantum conductance of a 2D semiconductor using his argument of "charge pumping", whereas in 1982, Thouless, Kohmoto, Nightingale and den Nijs (TKNN) [12] were the firsts to give topological arguments to explain the QHE. In 1983, Laughlin [13] proposed his notorious wavefunction whose topological features describe the Fractional Quantum Hall Effect (FQHE), where the quantum of conductance is now fractionalized. At this time, Berry [14] published a work in 1984 about the observable effects of a geometric phase in a quantum system after a cyclic adiabatic evolution. This phase is known as the *Berry Phase* and is characterized by an integer multiple of π. Furthermore, Zak [15] in 1989 showed that the eigenstates of a periodic system with a band structure can accumulate a geometrical phase in the momentum space, in the same way as the adiabatic evolution exposed by Berry. In the 1990s, the topological properties of

semiconductor models were studied and characterized by their global symmetries. In 1997, Altland and Zirnbauer [16] reported a *Periodic Table* of the topological invariant for non-interacting systems, paving the discussion about which type of topological invariant can be used to characterize the topological features of a system using their symmetries and dimensions.

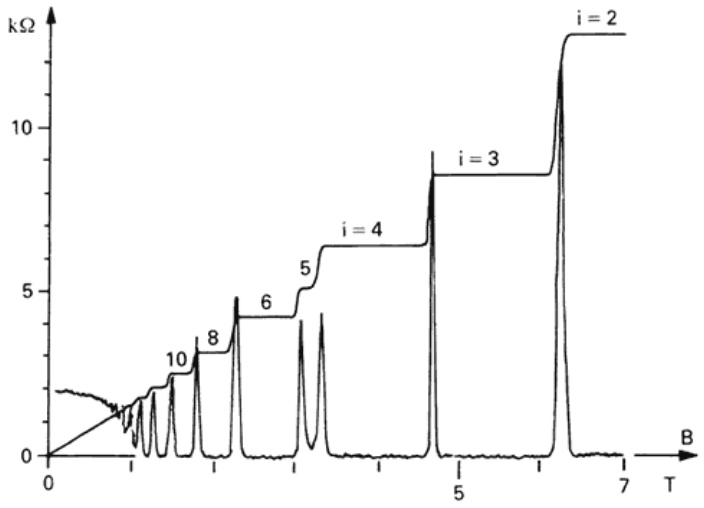

Fig. 2.1: *Longitudinal and transversal resistance as a function of an external magnetic field. This figure is the signature of the quantum Hall effect. Source: K. von Klitzing, G. Dorda, M. Pepper: Phys. Rev. Lett.,* **45***, 494–497, Aug. 1980* [10].

The list of models and successful theoretical predictions that the topology give us is composed of milestones in the theoretical physics. An example is related to the Quantum Spin Hall Effect (QSHE), from which a theoretical prediction can be build following the ideas of Kane and Mele [17]. They adapted the Haldane model [18] to study graphene that was subsequently improved by Bernevig and Zhang [19]. Here, the spin-orbit coupling is crucial to experimental purposes, which allowed Molenkap's team to detect the QSHE in HgTe quantum wells [20].

The successful topological description of this quantum effect in semiconductor materials discussed above, invites us to focus on another kind of materials, the superconductors. After the BCS theory, the superconductivity has motivated many

new approaches, which allow to build amazing phase diagrams that describe a lot of features about this state of matter but without a clear unification [21]. One approach to face this problem is topology, where the Kitaev chain is one of celebrated results, not just for exploring theoretically the topological protection of the superconductor gap, but also for its potential technological application in quantum computing.

In 2001, Kitaev [1] published his seminal work about the topological properties of a p-wave superconductor wire, where the edge effects hide an elusive emergent quasiparticle, the majoranas [22]. In fact, it is not really a "particle" in the sense of an elementary particle, indeed it is more like a bound state at the edges that works as a quasiparticle, as it will become clear in the following.

The first solid hint of the majoranas observation was found by the group of Leo Kouwenhoven in Indium Antimonide wires [23] and shortly after the group of Charlie Marcus detected the same signature in Indium Arsenide nanowires [24]. They are currently working together in the fabrication of quantum devices useful for storage quantum information on quantum computers. To detect the zero-energy mode the researchers studied the conductivity of a superconductor wire, which is characterized by a perfect Andreev reflection, characterized by a resonance at zero bias in the conductance curve. Those measurements did not convince the whole community, motivating the creation of new methods and techniques to detect and control this state in the lab. On the other hand, theoretical approaches evolve into more realistic features about this model, including interactions, long-range couplings, disorder and so forth. As claims for more robust arguments about the effects of spatial modulation on the Kitaev chain on the topological characterization grow stronger, we developed an approach to study the internal structure of the topological invariant and describe the effects of any spatial modulation. Using an enlarged unit-cell formalism we found a polynomial description, where oscillatory functions give information about the topology.

In this chapter, we present our approach, starting by a summary of the homogeneous Kitaev chain, discussing its solution as well as its topological properties. Subsequently, we extend these results including spatial modulated parameters of the

Hamiltonian. Here, we introduce the enlarged unit-cell method and build a suitable topological invariant. Using a polynomial description, we analyze the analytical structure of this topological invariant, which we apply to the study of the homogeneous and inhomogeneous cases, where the chemical potential and the hopping are modulated. Finally, we discuss our results in the concluding section.

2.2 The Kitaev chain: The homogeneous case

The Kitaev chain is a one-dimensional tight-binding model of spinless fermions with a p-wave pairing term, whose band structure is characterized by a superconducting gap protected topologically. This model was studied by Kitaev [1] and extended to many different systems for the last 15 years, including long-range hopping and pairing, further interactions, as well as extra dimensions [4, 25–41] .

Different approaches and mathematical tools have been used to characterize the topological properties of this model. Kitaev used the Pfaffian of the ground-state [1], while other researchers count the zero modes at the edges using a transfer matrix approach or other numerical methods, such as exact diagonalization, DMRG and so on. Although different approaches are being used, the solution of this model and its topological features are a framework for theoretical research, which will be the main topic of the next sections.

2.2.1 Analytical solution

In this section, we show how the energy gap of this paradigmatic model is protected by symmetry using topological arguments. Let us start introducing the Hamiltonian of this model, which is given by

$$H = -\sum_{n=1}^{N} \mu \left(c_n^\dagger c_n - \frac{1}{2} \right) + \sum_{n=1}^{N-1} \left\{ -t \left(c_n^\dagger c_{n+1} + c_{n+1}^\dagger c_n \right) + \Delta \left(c_n c_{n+1} + c_{n+1}^\dagger c_n^\dagger \right) \right\}, \tag{2.1}$$

where N is the length of the chain, μ is the chemical potential, t is the hopping

(that will be positive in this section[1]) and Δ is the pairing term that makes this chain a p-wave superconductor when it is a real value[2]. The operators c_n and $c_n^\dagger$ are spinless fermion operators that satisfy the usual anticommutation relations

$$\{c_n, c_m\} = 0 \quad \text{and} \quad \left\{c_n, c_m^\dagger\right\} = \delta_{nm}. \tag{2.2}$$

To solve this model, we introduce the Fourier transformation of the fermion operators: $c_k = N^{-1/2}\sum_n c_n \exp(-ikna)$, with a being the lattice parameter, and where the sum is over discrete values of k from $-\pi/a$ to π/a, with steps of $2\pi/Na$. This transformation allows us to write the Hamiltonian as follows

$$H = \sum_k -\frac{\mu}{2}\left(c_k^\dagger c_k - c_k c_k^\dagger\right) - 2t\cos(ka)c_k c_k^\dagger + \Delta\exp(ika)\left(c_k c_{-k} + c_k^\dagger c_{-k}^\dagger\right). \tag{2.3}$$

Restricting the range of momenta k to positive values, the Hamiltonian then reads

$$H = -\sum_{0<k<\pi/a}\left(\mu + 2t\cos(ka)\right)\left(c_k^\dagger c_k - c_{-k}c_{-k}^\dagger\right) + 2i\Delta\sin(ka)\left(c_{-k}c_k - c_k^\dagger c_{-k}^\dagger\right). \tag{2.4}$$

At this point, it is useful to introduce the Bogoliubov-de Gennes (BdG) transformation, that maps this system into a two-band Hamiltonian with particle-hole symmetry, using a spinless like representation, which diagonalizes the Hamiltonian. In fact, the BdG transformation allows us to write the Hamiltonian in term of spinors $\hat{\psi}_k^\dagger = (c_k^\dagger\, c_{-k})$ as follows

$$H = \sum_k \hat{\psi}_k^\dagger\, h_k\, \hat{\psi}_k = \sum_{0<k<\pi/a}\begin{pmatrix} c_k^\dagger & c_{-k}\end{pmatrix} h_k \begin{pmatrix} c_k \\ c_{-k}^\dagger\end{pmatrix} \tag{2.5}$$

where

[1] If $t < 0$ we can change its sign by a unitary gauge transformation $c_n \to (-1)^n c_n$ and come back to our framework.

[2] If Δ is complex another unitary transformation returns it to real, ignoring phase effects, see ref. [1]

$$h_k = \begin{pmatrix} -(\mu + 2t\cos(ka)) & 2i\Delta\sin(ka) \\ -2i\Delta\sin(ka) & (\mu + 2t\cos(ka)) \end{pmatrix} = -(\mu + 2t\cos(ka))\sigma_z - 2\Delta\sin(ka)\sigma_y, \tag{2.6}$$

where σ_i $(i = x, y, z)$ are the Pauli matrices, which span the particle-hole space. This matrix h_k can be written in an off-diagonal form using a unitary transformation as follows

$$\tilde{h}_k = U\, h_k\, U^\dagger = \begin{pmatrix} 0 & \rho(k) \\ \rho^*(k) & 0 \end{pmatrix} \tag{2.7}$$

where $\rho(k) = -(\mu + 2t\cos(ka)) + 2i\Delta\sin(ka)$, and

$$U = \exp(-i\pi\sigma_y/4) = \frac{1}{\sqrt{2}} \begin{pmatrix} I & -I \\ I & I \end{pmatrix}. \tag{2.8}$$

The matrix $\tilde{h}_k$ can be written as $\tilde{h}_k = \mathbf{g}(k)\cdot\sigma$, where $\sigma = (\sigma_x, \sigma_y)$ and $\mathbf{g}(k) = (\mathbb{R}e\rho, -\mathbb{I}m\rho)$. As $\rho(k)$ is a complex number, we can introduce a phase $\phi(k)$ such that $\rho(k) = |\rho(k)|e^{-i\phi(k)}$ and the Anderson vector $\mathbf{g}(k)$ acquires the following expression

$$\mathbf{g}(k) = |\rho(k)| \begin{pmatrix} \cos\phi(k) \\ \sin\phi(k) \end{pmatrix}. \tag{2.9}$$

The phase $\phi(k)$ is given by the equation

$$\tan\phi(k) = \frac{2\Delta\sin(ka)}{\mu + 2t\cos(ka)}, \tag{2.10}$$

With this information, we are able to find the eigenvalues and eigenvectors of the Hamiltonian (2.5), they are given respectively by

$$\epsilon_{k,\pm} = \pm\sqrt{(\mu + 2t\cos(ka))^2 + (2\Delta\sin(ka))^2} = \pm|\rho(k)|, \tag{2.11}$$

$$|u_{k,\pm}\rangle = \frac{1}{2} \begin{pmatrix} \pm e^{-i\phi(k)} \\ 1 \end{pmatrix}. \tag{2.12}$$

The band structure, given by the equation (2.11), is characterized by a gap that is protected by the presence of the pairing term. In figure (2.2), we can visualize the energy bands as a function of the chemical potential. In (a), we can see how the band structure of the tight-binding model ($\Delta = 0$) turns it gapless for $\mu \leq 2$, while in (b), the Kitaev chain (for $\Delta = 1$) is gapped except at $\mu = 2$, where the topological phase transition takes place.

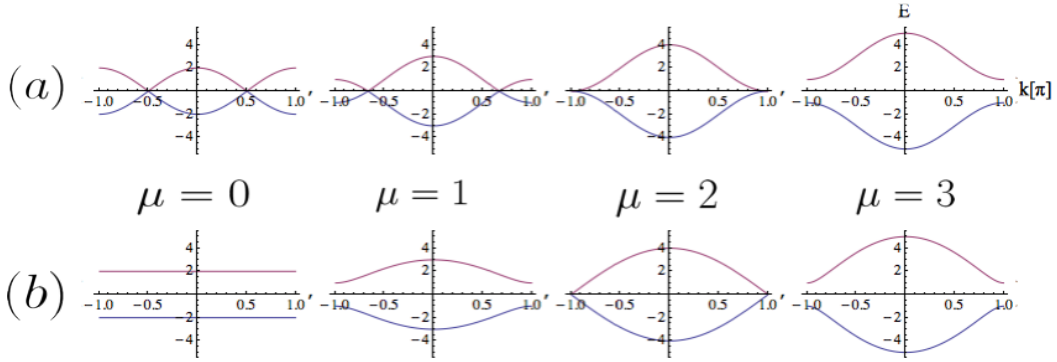

Fig. 2.2: *Band-structure E vs k (a) the tight-binding model: $\Delta = 0$ and (b) the Kitaev chain: for $\Delta = 1$, when $\mu = 0, 1, 2$ and 3 (in unit of t, the hopping), respectively. We see the gap closes at $\mu = 2t$ in (b).*

The gap protection is due to topological arguments, encoded in the geometrical features of the eigenstates in k-space. In figure (2.3), we show how the eigenstates of the Kitaev chain ($\Delta/t = 1$) evolve along the Brillouin Zone (BZ) in the non-topological (a) and topological phase (b). In both cases the system is gapped and the energy bands are similar. However, in the first case (a), for which $\mu = 3t$, the eigenstates in the extremes of the BZ are the same, while in the topological phase ($\mu = 1t$), the eigenstates rotate, accumulating a phase of π. This phase is a topological signature, whose physical features were introduced by Zak [15] taking the name of Zak phase, which will be explored mathematically in the next sections.

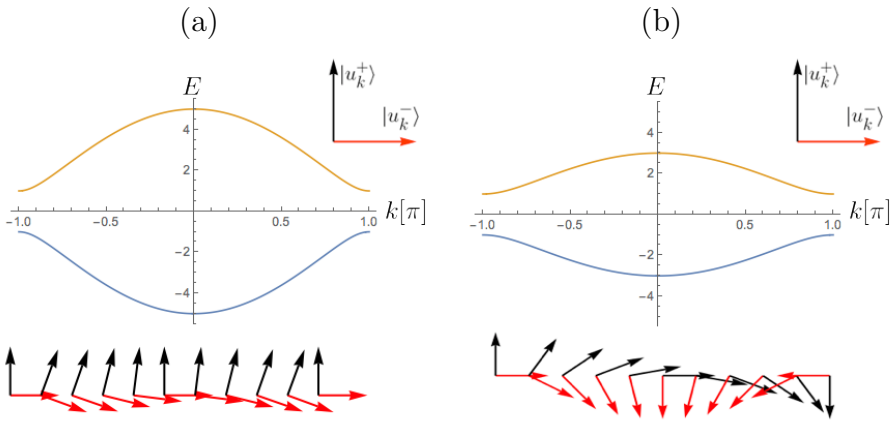

Fig. 2.3: *Band structure and eigenstates evolution of the Kitaev chain in (a) the non-topological phases for $\mu = 3t$ and (b) the topological phase for $\mu = 1t$. The two eigenstates are represented as orthogonal arrows that rotate in the Hilbert space when the system is topological, accumulating a phase.*

2.2.2 Topological description

In this section, we present a brief mathematical description about the topological properties in condensed matter physics. The exact solution of the Kitaev chain provided previously will be used as a framework, where the topological invariant is the Zak phase [15], which is the Berry phase of a periodic system, corresponding to the angle covered by the rotation of the eigenstates in the Hilbert space such as it was shown in the last section. Let $|u_k\rangle$ be an eigenstate of our model, the Zak phase is then given by

$$\mathcal{Z} = \frac{i}{\pi} \oint dk \langle u_k | \partial_k u_k \rangle, \tag{2.13}$$

where k is along the BZ. This phase can be an integer multiple of π that depends on the parameters of the model. The set of values that the topological invariant takes can be classified in three types. One of them is the $\mathbb{Z}$-type, where the Zak phase can take integer multiples of π; the other is $\mathbb{Z}_2$-type, where the phase can take just two values, zero or π; and the zero-type (0), which is related to a system without topological invariant. The type of topological invariant depends on the

symmetry and dimension of the system. This classification was studied by Altland and Zirnbauer [16], who encountered a topological classification for non-interacting systems with spatial periodicity described by time-reversal, particle-hole and chiral symmetries.

Table 2.1: *Periodic Table of Topological Invariants for non interacting systems.*

	Symmetry			d							
AZ	Θ	Ξ	Π	1	2	3	4	5	6	7	8
A	0	0	0	0	$\mathbb{Z}$	0	$\mathbb{Z}$	0	$\mathbb{Z}$	0	$\mathbb{Z}$
AIII	0	0	1	$\mathbb{Z}$	0	$\mathbb{Z}$	0	$\mathbb{Z}$	0	$\mathbb{Z}$	0
AI	1	0	0	0	0	0	$\mathbb{Z}$	0	$\mathbb{Z}_2$	$\mathbb{Z}_2$	$\mathbb{Z}$
BDI	1	1	1	$\mathbb{Z}$	0	0	0	$\mathbb{Z}$	0	$\mathbb{Z}_2$	$\mathbb{Z}_2$
D	0	1	0	$\mathbb{Z}_2$	$\mathbb{Z}$	0	0	0	$\mathbb{Z}$	0	$\mathbb{Z}_2$
DIII	-1	1	1	$\mathbb{Z}_2$	$\mathbb{Z}_2$	$\mathbb{Z}$	0	0	0	$\mathbb{Z}$	0
AII	-1	0	0	0	$\mathbb{Z}_2$	$\mathbb{Z}_2$	$\mathbb{Z}$	0	0	0	$\mathbb{Z}$
CII	-1	-1	1	$\mathbb{Z}$	0	$\mathbb{Z}_2$	$\mathbb{Z}_2$	$\mathbb{Z}$	0	0	0
C	0	-1	0	0	$\mathbb{Z}$	0	$\mathbb{Z}_2$	$\mathbb{Z}_2$	$\mathbb{Z}$	0	0
CI	1	-1	1	0	0	$\mathbb{Z}$	0	$\mathbb{Z}_2$	$\mathbb{Z}_2$	$\mathbb{Z}$	0

Altland and Zirnbauer found eight classes, which are summarized in Table 2.1. There, Θ is the time-reversal, Ξ the particle-hole and Π the chiral operators representing the global symmetries. The first column labels the topological classes. The following three columns correspond to the square value of the operator symmetries, which can be ± 1, and the other columns show the kind of topological invariant as a function of the dimension of the system, from $d = 1$ to 8.

In our model, we have that the time-reversal symmetry –linked with the spatial periodicity– is $\Theta = \mathcal{K}$ (where $\mathcal{K}$ takes the complex conjugate) that satisfies $\Theta H_k \Theta^{-1} = H_{-k}$. Moreover, the BdG transformation evinces a particle-hole symmetry of the model, characterized by $\Xi = \tau_x \mathcal{K}$ (where τ_x is the Pauli matrix acting on the particle-hole space) that satisfies $\Xi H_k \Xi^{-1} = -H_{-k}$. With these two operators, we can build a chiral operator $\Pi = \Theta\,\Xi = \tau_x$ that satisfies $\Pi\, H_k\, \Pi^{-1} = -H_k$. For the operators described above, we have $\Theta^2 = \Xi^2 = \Pi^2 = 1$, classifying this 1D system into the BDI symmetry class [16, 42], whose topological invariant in one dimension

is characterized by a $\mathbb{Z}$-index, as we can see in the Table 2.1.

This global behavior of the eigenstates corresponds to the number of times that a closed path described by the winding vector winds the origin in the complex plane $\mathbb{C}$. For a set of eigenstates in the momentum space, whose Hamiltonian can be written in an off-diagonal form, the winding number is given by

$$\begin{aligned} \mathcal{Z} &= \frac{i}{\pi}\oint dk\langle u_{k,\pm}|\partial_k u_{k,\pm}\rangle && (2.14)\\ &= \frac{1}{2\pi}\int_{k=-\pi/a}^{\pi/a}\partial_k\phi(k) && (2.15)\\ &= \frac{-i}{\pi}\int_{k=0}^{\pi/a}\frac{\partial z_k}{z_k}, && (2.16) \end{aligned}$$

where z_k is the winding vector, which is given by $z_k = \rho(k)/|\rho(k)|$ that has been previously calculated.

In the general case, the winding number can take just integer numbers, corresponding to how many times a closed path covered by z_k in $\mathbb{C}$ includes the origin. In our case, the path to the winding vector covers just one loop in the complex plane, then to know how many times the closed path include the origin we just have to know the value of the middle and the end of the path, that correspond to $\rho(0)$ and $\rho(\pi/a)$, respectively.

An interesting observation we can make about the values of this phase to compute the Zak phase easily is: $\rho(k)$ is a real number when is evaluated in the extremes ($k = \pm\pi/a$) and in the middle ($k = 0$) of the BZ. In fact, the function $\rho(k) = -(\mu + 2t\cos(ka)) + i2\Delta\sin(ka)$ is real just at these values of k, then we have

$$\mathcal{Z} = i\oint dk\langle u_{k,\pm}|\partial_k u_{k,\pm}\rangle = \frac{\pi}{2}\left(sgn\{\rho(\pi/a)\} - sgn\{\rho(0)\}\right), \qquad (2.17)$$

where $\mathcal{Z} = \pi$ when $|\mu| < 2t$ and 0 otherwise. This outcome is represented in Figure (2.4). The first region (I – white) corresponds to the topological phase, where the eigenstates makes one loop in the complex plane, including the origin, and the second region (II – gray), represent the non topological, where the Zak phase is zero and the states do not rotate. They do not acquire a Zak (or Berry) phase.

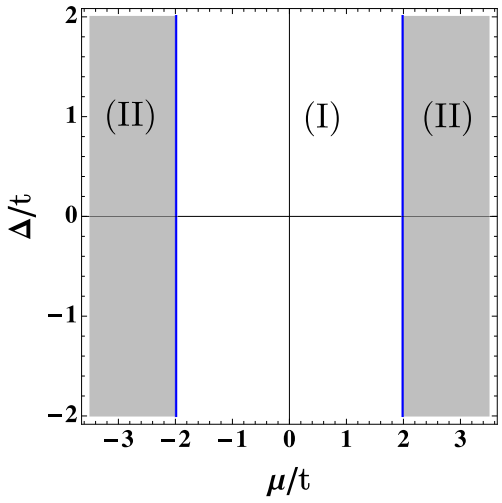

Fig. 2.4: *Topological phase diagram of the homogeneous Kitaev chain. The phase diagram μ/t versus Δ/t is characterized by (I) a white region for $|\mu/t| < 2$ corresponding to the topological phase and (II) two disconnected gray regions corresponding to non-topological phases.*

The signature of the topological phase is the presence of Majorana zero modes at the ends of the wire. This feature can be observed numerically after an exact diagonalization for a finite system with open boundary conditions, whose energy levels are plotted in Figure 2.5 for a chain with $N = 10$ sites and for $\Delta/t = 1$. In the left-hand side, the dashed (continuous) lines represent the energy levels of a chain with periodic (open) boundary conditions as a function of μ/t. We observe that the system with periodic boundary conditions closes the gap for $\mu/t = \pm 2$, while the system with open boundary conditions presents two modes with energy zero for $|\mu/t| < 2$. These zero-modes are characterized by the majorana occupation at the edges of the chain. We plotted its occupation $|\psi|^2$ as a function of μ/t and N at the right-hand side of Figure 2.5. The two white lines represent a region where the topological phase takes place. It is the point where the occupation of the majoranas bound-state grows towards the edges of the chain. To extract such occupation we filtered out the contribution of the zero modes from the wave-function, as seen in the left hand side of Fig. 2.5.

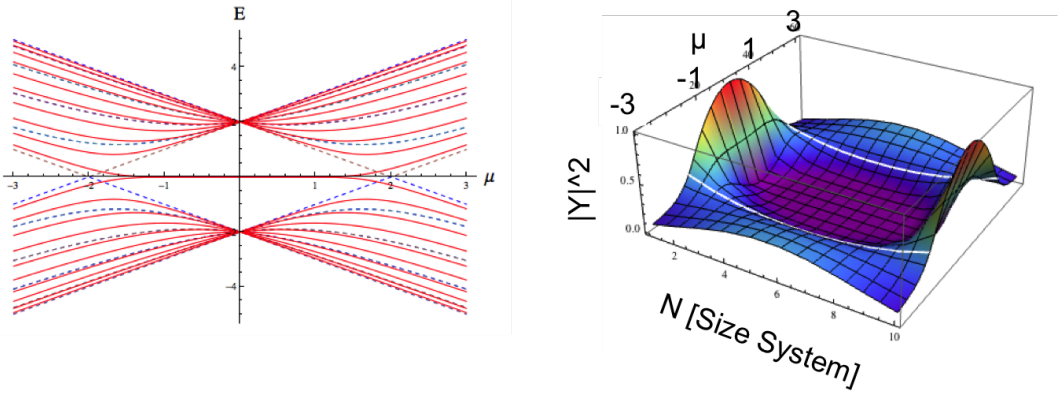

Fig. 2.5: *(left) Energy levels as a function of μ/t from an exact diagonalization for $N = 10$ sites. Dashed lines represent a system with periodic boundary conditions, while solid lines are for a system with open boundary conditions. (right) The Majorana occupation $|\psi|^2$ in the wire for 10 sites.*

The topological invariant calculated above is a way to obtain the Zak phase. On the other hand, Kitaev [1] used the Pfaffian to measure the parity of the eigenstates, while DeGottardi *et al.* [26, 27] used the roots of the characteristic polynomial from a Transfer Matrix Approach to describe the topological phases. All these procedures find topological invariants that are two integer numbers that describe the non-topological and topological phases, therefore a topological invariant of $\mathbb{Z}$-type, in conformity with Table (2.1), for a BDI class in one-dimension ($d = 1$).

2.3 The inhomogeneous Kitaev chain

In this section we will study the effect of inhomogeneities in the Kitaev chain, motivated by the possibility to extend the topological description previously developed to include more realistic cases, like the effect of spatial fluctuations that may appear during the fabrication process of an experimental sample, or due to some randomness of the Rashba coupling, for instance. This kind of defects induces spatial distributions on the parameters of the model. In this work, we pay attention on the modulations of the chemical potential and the hopping, which can be manipulated by external fields in an atomic chain or in optical lattices.

2.3.1 Topological invariant in the enlarged unit-cell method

We have previously discussed the solution of the homogeneous Kitaev chain, where the Topological Invariant is defined by the sign of the functions $\rho(0)$ and $\rho(\pi/a)$. In order to study the effect of spatial distributions, we will develop a procedure to study the topological properties of the system using an enlarged unit cell method. This approach was previously used by Yi Gao *et al.* [4] to study some site distributions for the hopping term. We will extend this approach to study other hopping (off-site) distributions and chemical potential (on-site) landscapes.

Let us start to write the Hamiltonian of the system with site-dependent couplings and with periodic boundary conditions, which is given through an enlarged unit-cell approach. For a system with N sites, we can write such model Hamiltonian as $\mathcal{H} = \sum_{\ell=1}^{N/q} \mathcal{H}_\ell$, where q is the number of sites within each unit-cell, and

$$\begin{aligned} \mathcal{H}_\ell &= \sum_{s=1}^{q} \mu_s \hat{c}^\dagger_{s,\ell}\hat{c}_{s,\ell} + \\ &\sum_{s=1}^{q-1}\left(-t_s\hat{c}^\dagger_{s,\ell}\hat{c}_{s+1,\ell} + \Delta\hat{c}_{s,\ell}\hat{c}_{s+1,\ell}\right) + \\ &\left(-t_q\hat{c}^\dagger_{q,\ell}\hat{c}_{1,\ell+1} + \Delta\hat{c}_{q,\ell}\hat{c}_{1,\ell+1}\right) + \text{H.c.} \end{aligned} \tag{2.18}$$

Upon using the Fourier transformation in each unit cell, $\hat{c}^\dagger_{s,\ell} = \sqrt{q/N}\sum_k \hat{c}^\dagger_{s,k}e^{ikq\ell}$, with $k \in (-\pi/q, \pi/q]$, the reduced BZ, and through the well-known Bogoliubov-de Gennes (BdG) transformation [43], $\widehat{\Psi}^\dagger_k = (\hat{c}^\dagger_{1,k}\dots\hat{c}^\dagger_{q,k}\ \hat{c}_{1,-k}\dots\hat{c}_{q,-k})$, we can write down the Hamiltonian in momentum space in terms of such spinor fields as

$$\mathcal{H} = \frac{1}{2}\sum_k \widehat{\Psi}^\dagger_k H_k \widehat{\Psi}_k = \frac{1}{2}\sum_k \widehat{\Psi}^\dagger_k \begin{pmatrix} M_k & V_k \\ V_k^\dagger & -M^T_{-k} \end{pmatrix} \widehat{\Psi}_k, \tag{2.19}$$

The matrices M_k and V_k have the following nonzero elements:

- $M_k^{s,s+1} = M_k^{s+1,s} = -t_s$ for $s = 1, ..., q-1$
- $V_k^{s,s+1} = -V_k^{s+1,s} = -\Delta$ for $s = 1, ..., q-1$

- $M_k^{s,s} = \mu_s$ for $s = 1, ..., q$
- $M_k^{q,1} = (M_k^{1,q})^* = -t_q e^{-ikq}$
- $V_k^{q,1} = (-V_k^{1,q})^* = -\Delta e^{-ikq}$.

If t_s, μ_s and Δ are real, then H_k satisfies the time-reversal, the particle-hole and the chiral symmetries previously discussed, and it can be unitarily transformed to an off-diagonal matrix as follows

$$UH_kU^\dagger = \begin{pmatrix} 0 & A_k \\ A_{-k}^T & 0 \end{pmatrix}, \quad A_k = M_k + V_k \tag{2.20}$$

$$U = \exp(-i\pi\sigma_y/4) = \frac{1}{2}\begin{pmatrix} I & -I \\ I & I \end{pmatrix} \tag{2.21}$$

where σ_y is the Pauli matrix acting on the particle-hole space. The winding number (or the Zak phase) of this enlarged unit-cell method is given by

$$\mathcal{W} = -\frac{i}{\pi}\int_0^{\pi/q} \frac{dz_k}{z_k}, \tag{2.22}$$

where

$$z_k = e^{i\phi(k)} = \frac{Det(A_k)}{|Det(A_k)|} \tag{2.23}$$

In our approach, the winding number ($\mathcal{W} \in \mathbb{Z}$) can be evaluated through the sign of the function $\mathrm{Det}(A_k)$ at the particle-hole symmetric points, $\kappa = 0$ and π/q

$$\mathcal{W} = \frac{1}{2}\left[\, sgn\{\mathrm{Det}(A_{\pi/q})\} - sgn\{\mathrm{Det}(A_0)\}\,\right]. \tag{2.24}$$

This expression is easy to understand, as a model of nearest-neighbors interactions the winding vector z_k develops a single one-loop in $\mathbb{C}$ as a function of k, which is symmetric with respect to the real axis. We can deduce from its definition that $(A_k)^* = A_{-k}$, so the function $\mathrm{Det}(A_\kappa)$ is real at the extreme points, $\kappa = 0$ and π/q. When the loop encloses the origin of $\mathbb{C}$, the real function $\mathrm{Det}(A_\kappa)$ has opposite signs at these points. In that case, we have from Eq. (2.24): $\mathcal{W} = \pm 1$, *i.e.*, a topological (T) phase. Meanwhile, if the loop does not include the origin of $\mathbb{C}$, we have a

non-topological (NT) phase, with $\mathcal{W} = 0$. This observation can be visualized in the figure (2.6).

The closure of the bulk gap, which occurs only for $\kappa = 0$ and π/q, is given by $\mathrm{Det}(A_\kappa) = 0$. The latter can be inferred from Eq. (2.20), which implies $\mathrm{Det}(U H_k U^\dagger) = \mathrm{Det}(H_k) = \mathrm{Det}(A_k)\,\mathrm{Det}(A^T_{-k})$, therefore, $\mathrm{Det}(A_k)$ can only vanish if H_k has a vanishing determinant or equivalently a zero eigenvalue. The gap-closing specifies the locations where the topological quantum phase transitions take place.

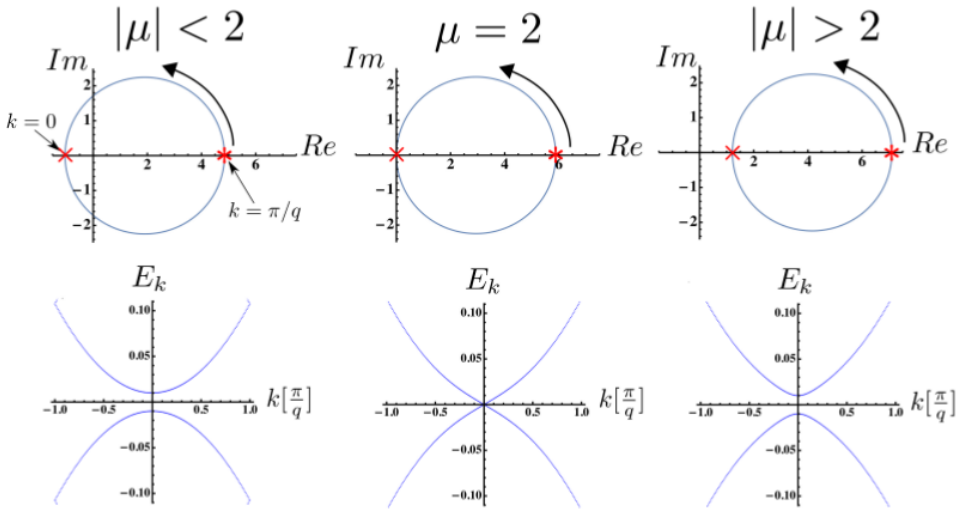

Fig. 2.6: *Winding vector path and energy band structure of the homogeneous Kitaev chain with an enlarged unit-cell of* $q = 10$ *and* $\Delta/t = 0.1$. *The left and the right-hand side pictures are in the topological and non-topological regions, respectively. We see that for* $\mu/t = 2$ *the topological phase transition takes place, where* $Det(A_k) = 0$, *and the band structure is gapless for* $k = 0$.

2.3.2 Spatial distributions

The main advantage of this approach is the possibility to study a spatial modulation in the parameter space. This aim will be presented in this section. Let $\mathcal{H}_\ell$ be our tight-binding model of spinless fermions with a site-dependent chemical potential (μ_s), a site-dependent hopping amplitude (t_s), and a constant triplet p-wave

superconducting pairing (Δ). For the site modulations we use either

$$\mu_s = \mu\,(1+\lambda w_s), \tag{2.25}$$

$$t_s = t\,(1+\lambda w_s), \tag{2.26}$$

for the chemical potential or for the hopping amplitude, respectively, while Δ is kept real and constant[3]. The additional parameter λ, that will be taken as $0 \leq \lambda < 1$, provides the strength of the inhomogeneity and w_s are the spatial distributions, which are taken as

$$w_s = \begin{cases} \delta_{s,1} & , \text{ a single-defect} \quad \text{(S)} \\ \cos(2\pi s/q) & , \text{ commensurate} \quad \text{(C)} \\ \cos(2\pi s\beta) & , \text{ incommensurate} \quad \text{(I)} \end{cases} \tag{2.27}$$

where $\beta = (\sqrt{5}+1)/2$ is the golden ratio. The first of these distributions (S) needs no justification, while the others two (C,I) are in the class of Aubry-André or Harper potentials, useful for study the interrelation of disorder and superconductivity [31, 44–47]

We have chosen some particular values of the parameters to show the variations induced by modulations on the phase diagram. Examples for the spatial distributions (S,C,I), applied separately to the chemical potential and to the hopping amplitude, can be viewed in Fig. 2.7. Due to the particle-hole symmetry, the phase diagrams of Fig. 2.7 are symmetric with respect to Δ/t and μ/t, thus we plot them for $\mu > 0$ only.

Apart from the variations of the Ising transition lines at the well-known values $\mu = \pm 2t$ of the homogeneous case, especially those in Fig. 2.7(b) and (e), we observe in all cases the emergence of non-topological compact domains ("bubbles") around $\Delta/t = 0$. The number and shape of these isolated bubbles depend on the cell size q, on the inhomogeneity strength λ, as well as on the spatial distribution. They

[3] The pairing Δ, which comes from an effective mean-field approach, was kept real and constant to compare with previous works. Another aspect would be to consider a pairing of the form $\Delta = |\Delta|e^{i\theta}$, with a phase constant, which can be eliminated by a gauge transformation. See Ref. [1].

look rather different when spatial modulations are applied either to the chemical potential or to the hopping amplitude, as can be seen from the top and the bottom panels in Fig. 2.7, respectively.

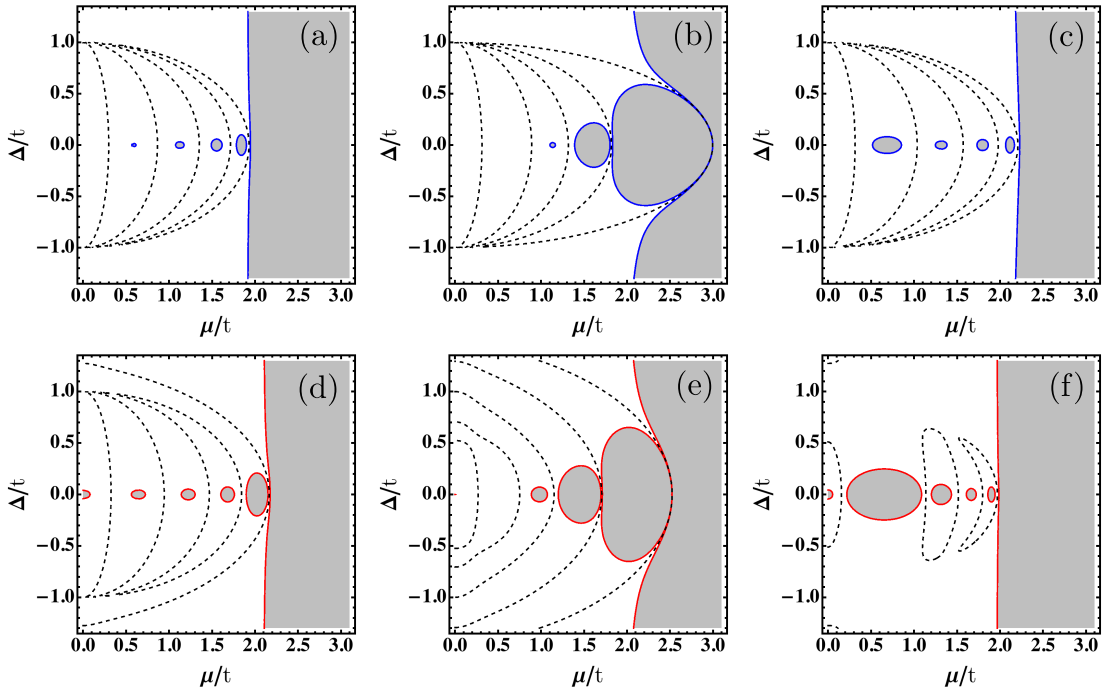

Fig. 2.7: *Topological phase diagrams for modulated chemical potentials (top panels) and modulated hopping terms (bottom panels) in the (a,d) single-defect model, (b,e) commensurate and (c,f) incommensurate potentials. Topological (T) regions are drawn in white and Non-Topological (NT) zones in gray. Blue solid lines (top panels) and red solid lines (bottom panels) demarcate the loci of the T-NT phase transitions, for which* $Det(A_\kappa) = 0$. *Dashed lines depicting ellipses are zeros of the oscillating function* $U(\mu, \Delta, q, \lambda)$, *as given below. All diagrams are symmetric by changing* $\mu \leftrightarrow -\mu$ *and* $\Delta \leftrightarrow -\Delta$. *We have used in all cases* $q = 10$ *and* $\lambda = 0.5$ *in the enlarged unit-cell approach. Emerging features are the non-topological regions ("bubbles") around the anisotropy line* ($\Delta/t = 0$), *and the bending of the Ising transition lines at* $\mu \approx 2t$, *most notably for (b) and (e) cases. Case (f) will be discussed separately.*

2.3.3 Polynomial description

In the previous section we showed how non-topological bubbles emerge in the topological regions of the phase diagram when an inhomogeneity is turned on. In this section we will consider some analytical aspects of the topological invariant to understand the physical origin of these bubbles. First, we rewrite the (real) function $\mathrm{Det}(A_\kappa)$, for $\kappa = 0$ and π/q, as

$$\mathrm{Det}(A_\kappa) = U(\mu, \Delta, q, \lambda) - \Lambda_\kappa(\Delta, q, \lambda), \tag{2.28}$$

where U is a κ-independent polynomial function that carries all the dependence on μ, and Λ_κ is the difference, in our (q, λ) scheme. According to Eq. (2.24), and the discussion following it, we observe that the system is topological ($\mathcal{W} \neq 0$) when U is within the region delimited by both Λ_κ (*viz.*: $\Lambda_0 < U < \Lambda_{\pi/q}$) and non-topological ($\mathcal{W} = 0$) otherwise. For the singular cases where $\mathrm{Det}(A_\kappa) = 0$, namely $U = \Lambda_\kappa$, Eq. (2.24) is undefined, though these points demarcate the *loci* of the T-NT transitions in the phase diagram, namely, the closure of the bulk gap. For the purpose of analysis, we shifted our functions U and Λ_κ according to the sum rule expression (2.31) below and refer, from now on, to the shifted functions. The shift is defined so as to obtain $\Lambda_0 + \Lambda_{\pi/q} = 0$.

To understand the role played by the functions U and Λ_κ, we have plotted in Fig. 2.8 the homogeneous case (left panels) and the inhomogeneous single-defect model applied to the chemical potential (right panels), respectively. The phase diagrams, (a) and (b), are given together with the related behavior of the functions U and Λ_κ, in (c) and (d).

In the homogeneous case, we see from Fig. 2.8(c) that the function U oscillates between the two Λ_κ functions, for $|\mu| \leq 2t$, defining thus a topological phase in that region. Whereas in the single-defect case of Fig. 2.8(d), the function U leaves these two limits because its oscillations are now enhanced by the presence of modulations. These extrapolations of the function U produce the bubbles seen in Fig. 2.8(b). These bubbles have alternating sign, as seen from the figure. The borders of these bubbles, as described above, are the points of gap-closings, location of the topological

quantum phase transitions.

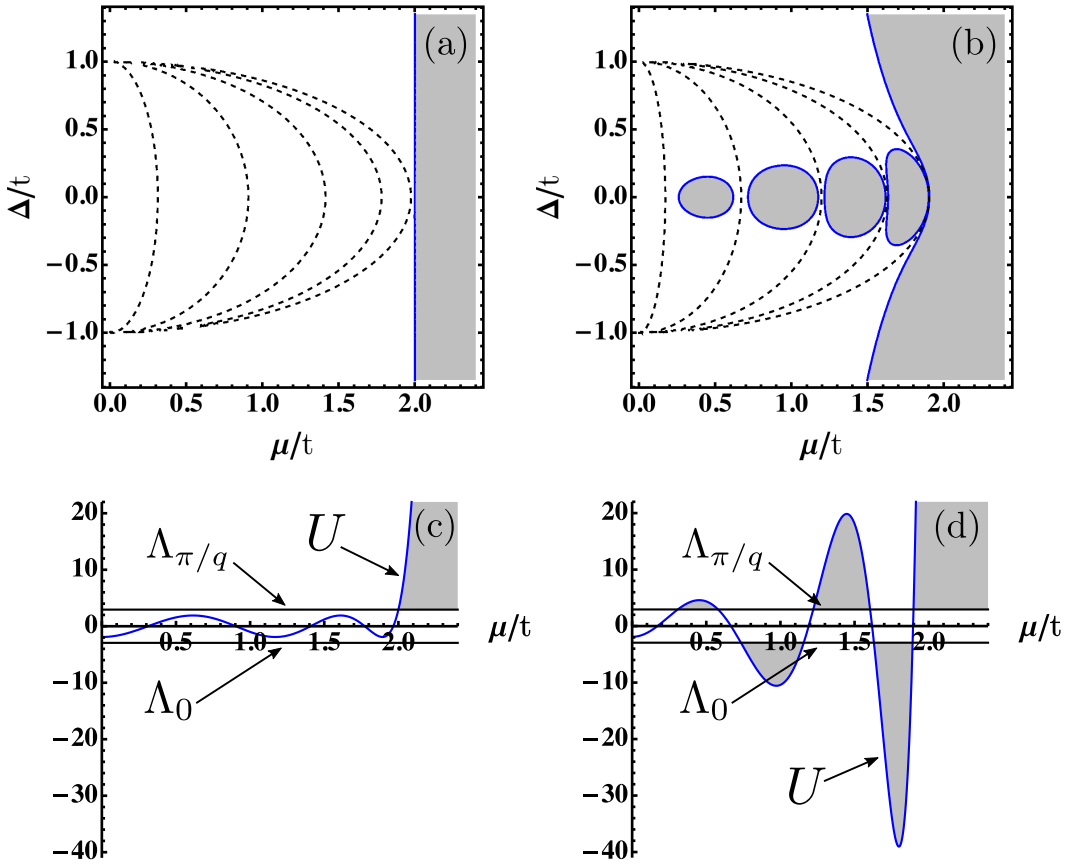

Fig. 2.8: *Comparison of the homogeneous (left panels, $\lambda = 0$) and the inhomogeneous single-defect (right panels, $\lambda = 10$) cases applied to the chemical potential, for $q = 10$. Dashed lines in the phase diagrams (a) and (b) are zeros of the oscillating function U, the outermost one is very close to the ellipse $\bar{\mu} = 2t$, beyond which U is overdamped. The function U (blue curves, for $\Delta/t = 0.1$) in (c) and (d) oscillates with q zeros until it crosses the Ising transition line, at or close to $\mu/t = 2$. In the homogeneous case of Fig. 2(c) U is delimited by the two Λ_κ functions, while in Fig. 2(d) the oscillations of U extrapolate these two limits until it crosses $\Lambda_{\pi/q}$ definitively. This is the origin of the bubbles observed in all inhomogeneous cases. These bubbles have alternating signs, corresponding to the wavefunction fermion parity. For drawing purposes, we shifted the vertical axis to get $U = 0$ as the mean of both Λ_κ functions, see text.*

We observed numerically that at the places where $U = \Lambda_{\pi/q}$ the gap closes at $k = 0$, while at the places where $U = \Lambda_0$ the gap closes at π/q. Beyond the topological phase, in the μ/t axis, the oscillating function U changes character and becomes unbounded in all cases. These are the trends caused by the modulations and they can be explained analytically as given below.

The homogeneous case

After detailed algebraic and numerical manipulations we found, in the homogeneous case ($\lambda = 0$), that the function U can be written as

$$U(\mu, \Delta, q, 0) = \left(\sqrt{1-(\Delta/t)^2}\right)^q \overline{U}_H(\bar{\mu}, q), \tag{2.29}$$

where $\bar{\mu} = \mu/\sqrt{1-(\Delta/t)^2}$ is a scaled chemical potential, identical to the one found in DeGottardi *et al.* [26, 27], while $\overline{U}_H(\bar{\mu}, q)$ is described by a polynomial in $\bar{\mu}$ of degree q, restricted to integers $q \geq 2$

$$\overline{U}_H(\bar{\mu}, q) = \sum_{n=1}^{q} a_n^q \, \bar{\mu}^n, \tag{2.30}$$

whose coefficients $a_n^q \in \mathbb{Z}$ can be obtained through the following recurrence formula: $a_q^q = 1$ for all q, $a_1^q = \mp q$ (alternating) for q odd and $a_1^q = 0$ for q even, while for $1 < n < q$ we have $a_n^q = a_{n-1}^{q-1} - a_n^{q-2}$ for $q - n$ even and $a_n^q = 0$ for $q - n$ odd. Some of these a_n^q coefficients are given in Table 2.2. We notice that the non-zero coefficients of this polynomial expansion have alternating signs for each q. The oscillatory behavior of the function U is due to this fact. It is easily seen that U, as a function of μ is symmetric for q even and antisymmetric for q odd, while it is always symmetric with respect to Δ.

As for the delimiting functions Λ_κ in Eq. (2.28), we found a useful relation in the form of a sum rule

$$\Lambda_{\pi/q} + \Lambda_0 = \left(\sqrt{1-(\Delta/t)^2}\right)^q s^{1/2}\,(1+s)^2, \tag{2.31}$$

Table 2.2: *Some coefficients a_n^q, with $1 \leq n \leq q$, of the polynomial $\overline{U}_H$ in the homogeneous case. Observe the constructing rule $a_n^q = a_{n-1}^{q-1} - a_n^{q-2}$.*

q	n									
	1	2	3	4	5	6	7	8	9	10
2	0	1	0	0	0	0	0	0	0	0
3	-3	0	1	0	0	0	0	0	0	0
4	0	-4	0	1	0	0	0	0	0	0
5	5	0	-5	0	1	0	0	0	0	0
6	0	9	0	-6	0	1	0	0	0	0
7	-7	0	14	0	-7	0	1	0	0	0
8	0	-16	0	20	0	-8	0	1	0	0
9	9	0	-30	0	27	0	-9	0	1	0
10	0	25	0	-50	0	35	0	-10	0	1

where $s = (-1)^q$ and the factor $(1+s)^2$ dictates that this sum is zero for q odd, while for q even the sum rule can be shifted to zero using this expression. All three functions U, $\Lambda_{\pi/q}$ and Λ_0 will be shifted in the same way, keeping Eq. (2.28) unaltered. This is an important point in our approach to get the fermion parity switches locations for homogeneous finite wires.

Using (2.31), we thus need to deal with only one of these polynomials. In this work, we study $\Lambda_0 = \Lambda_0(\Delta, q)$, which is given by an even polynomial in Δ ($b_n^q = 0$ for n odd)

$$\Lambda_0(\Delta, q) = \sum_{n=0}^{q} b_n^q \, \Delta^n. \tag{2.32}$$

Some of these b_n^q coefficients are given in Table 2.3. They do not have a simple constructing rule, although we observe the cyclic pattern '4202' for b_0^q, we also have $b_q^q = 0$ for all q, while $b_{q-1}^q = 2q$ for q odd, also $b_{q-2}^q = q^2$ for q even, etc. Such description is not complete however.

An interesting point is that the alternating integer polynomial $\overline{U}_H(\bar{\mu}, q)$ in (2.30) has more than one root (in fact, q real roots), that yield an oscillatory behavior for

Table 2.3: *Some coefficients b_n^q of the delimiting function $\Lambda_0(\Delta, q)$ in the homogeneous case.*

q	n				
	0	2	4	6	8
2	4	0	0	0	0
3	2	6	0	0	0
4	0	16	0	0	0
5	2	20	10	0	0
6	4	24	36	0	0
7	2	42	70	14	0
8	0	64	128	64	0
9	2	72	252	168	18
10	4	80	440	400	100

U within the dome $\bar{\mu} = 2t$, that is, inside the ellipse $(\mu/2t)^2 + (\Delta/t)^2 = 1$ (see Fig. 2.8(a)). Outside from this elliptical dome U has no more oscillations, as $\overline{U}_H$ turns from an alternating to a positive polynomial in μ in that case. Such analytical behavior is a critical combination of the prefactor $(\sqrt{1-(\Delta/t)^2}\,)^q$ and the scaled $\bar{\mu} = \mu/\sqrt{1-(\Delta/t)^2}$ that appear in Eq. (2.29). This result is quite consistent with those seen in Hegde *et al.* [29,30], about the positions of fermion parity switches for homogeneous finite wires.

Modulated chemical potential

When site modulations are applied to the chemical potential the sum rule (2.31) still applies, the polynomial expansion of $\Lambda_0(\Delta, q)$ is thus the same as in (2.32), *viz.* Table 2.3, while the function U can be written now as

$$U(\mu, \Delta, q, \lambda) = \left(\sqrt{1-(\Delta/t)^2}\right)^q \left(\overline{U}_H + \overline{U}_\lambda\right). \tag{2.33}$$

For the single-defect (S) case, apart from the polynomial $\overline{U}_H$ we have an additional inhomogeneous contribution which is linear on λ, that is $\overline{U}_\lambda = \lambda\,\overline{U}_S(\bar{\mu}, q)$, where $\overline{U}_S$

is a polynomial like in (2.30), with the same recurrence formula for the coefficients a_n^q, except that $a_1^q = \mp 1$ (alternating) for q odd and $a_1^q = 0$ for q even. Some of these a_n^q coefficients are given in Table 2.4.

Table 2.4: *Some coefficients a_n^q of the polynomial $\overline{U}_S(\bar{\mu}, q)$ for the (S) single-defect case in the modulated μ_s.*

q	n									
	1	2	3	4	5	6	7	8	9	10
2	0	1	0	0	0	0	0	0	0	0
3	-1	0	1	0	0	0	0	0	0	0
4	0	-2	0	1	0	0	0	0	0	0
5	1	0	-3	0	1	0	0	0	0	0
6	0	3	0	-4	0	1	0	0	0	0
7	-1	0	6	0	-5	0	1	0	0	0
8	0	-4	0	10	0	-6	0	1	0	0
9	1	0	-10	0	15	0	-7	0	1	0
10	0	5	0	-20	0	21	0	-8	0	1

On the other hand, for the commensurate (C) and the incommensurate (I) potentials applied to μ_s, the extra contributions in (2.33) do not depend on Δ but are nonlinear on λ. That is, we have integer polynomials $\overline{U}_\lambda$ written as $\overline{U}_C(\bar{\mu}, q, \lambda)$ and $\overline{U}_I(\bar{\mu}, q, \lambda)$, respectively. We have not yet found a simple recurrence formula for them, but we can give some examples. For the (C) commensurate case, for $q = 3$, we have

$$\overline{U}_C(\bar{\mu}, q = 3, \lambda) = \frac{1}{4}\lambda^2(\lambda - 3)\,\bar{\mu}^3, \tag{2.34}$$

whilst for the (I) incommensurate case, also for $q = 3$, we have

$$\begin{aligned}
&\overline{U}_I(\bar{\mu}, q=3, \lambda) = \\
&-\left[\cos(2\pi\beta)+\cos(4\pi\beta)+\cos(6\pi\beta)\right]\lambda(\bar{\mu}-\bar{\mu}^3) \\
&+\left[\cos(2\pi\beta)\cos(4\pi\beta)+\cos(2\pi\beta)\cos(6\pi\beta)\right. \\
&\left.+\cos(4\pi\beta)\cos(6\pi\beta)\right]\lambda^2\bar{\mu}^3 \\
&+\left[\cos(2\pi\beta)\cos(4\pi\beta)\cos(6\pi\beta)\right]\ \lambda^3\bar{\mu}^3. \qquad (2.35)
\end{aligned}$$

Modulated hopping amplitude

Significant differences already begin when spatial modulations are applied to the hopping amplitude t_s. For the single-defect (S) case, for example, we found a function U described as

$$\begin{aligned}
U(\mu, \Delta, q, \lambda) &= \left(\sqrt{1-(\Delta/t)^2}\,\right)^q \\
&\times \left(\overline{U}_H + \frac{\lambda(\lambda+2)}{[1-(\Delta/t)^2]}\,\tilde{U}_S\right), \qquad (2.36)
\end{aligned}$$

Likewise, the sum rule for the Λ_κ functions is now

$$\begin{aligned}
\Lambda_{\pi/q} + \Lambda_0 &= \left(\sqrt{1-(\Delta/t)^2}\,\right)^q s^{1/2}\,(1+s)^2 \\
&\times \left(1+\frac{\lambda(\lambda+2)}{[1-(\Delta/t)^2](1+s)}\right). \qquad (2.37)
\end{aligned}$$

In (2.36) we have $\tilde{U}_S = \tilde{U}_S(\bar{\mu}, q)$, which is a polynomial in $\bar{\mu}$ of degree $q \geq 3$, given by the same recurrence formula as in (2.30), except that the largest-power non-zero coefficients are now given by $a^q_{q-2} = -1$ (*viz.*: $a^q_q = a^q_{q-1} = 0$ for all q). Some of these coefficients are given in Table 2.5. Interestingly enough, we see that by eliminating the first column in Table 2.4 and inverting signs we find an equivalence with Table 2.5. We have not yet understood the origin of this similarity.

We notice in Eqs. (2.36) and (2.37) the extra terms in $\lambda(\lambda+2)$, which depend also on Δ. This contribution expands the dome of the oscillations of the function U beyond the limits $\Delta/t = \pm 1$, as is indeed observed in Fig. 2.7(d).

Table 2.5: *Some coefficients a_n^q of the polynomial $\tilde{U}_S(\bar{\mu}, q)$ for the (S) single-defect case in the modulated t_s.*

q	n								
	1	2	3	4	5	6	7	8	9
3	-1	0	0	0	0	0	0	0	0
4	0	-1	0	0	0	0	0	0	0
5	2	0	-1	0	0	0	0	0	0
6	0	3	0	-1	0	0	0	0	0
7	-3	0	4	0	-1	0	0	0	0
8	0	-6	0	5	0	-1	0	0	0
9	4	0	-10	0	6	0	-1	0	0
10	0	10	0	-15	0	7	0	-1	0
11	-5	0	20	0	-21	0	8	0	-1

The sum rule (2.37) of the Λ_κ functions, gives us a selected polynomial $\Lambda_0(\Delta, q, \lambda) = \sum_{n=0}^{q} b_n^q \, \Delta^n$ which is an even polynomial in Δ whose coefficients are nonlinear in λ. Some of these coefficients can be seen from Table 2.6. We notice that when $\lambda = 0$ they match those in Table 2.3, as it should be.

Lastly, for the commensurate (C) and the incommensurate (I) potentials applied to the hopping, a general expression for the function U is

$$U(\mu, \Delta, q, \lambda) = \left(\sqrt{1 - (\Delta/t)^2}\right)^q \overline{U}_H + \tilde{U}_\lambda. \tag{2.38}$$

Namely, the corresponding inhomogeneous $\tilde{U}_\lambda$ terms, $\tilde{U}_C = \tilde{U}_C(\mu, \Delta, q, \lambda)$ or $\tilde{U}_I = \tilde{U}_I(\mu, \Delta, q, \lambda)$, respectively, are now polynomials of degree q in μ and Δ, which cannot be simply factorized as in (2.33) or in (2.36). The latter two cases in (2.38) are examples where the above elliptical description does not apply anymore, as can be inferred from the dashed lines in Figs. 2.7(e) and 2.7(f). The farthest case from an elliptical description is the latter one in Fig.2.7(f), for which the incommensurate (I) distribution provides a rather complex U function. In these cases, we do not have integer polynomials, and a new approach should be devised.

Table 2.6: *Some coefficients b_n^q of the polynomial $\Lambda_0(\Delta, q, \lambda)$ for the (S) single-defect case in the modulated t_s. For $\lambda = 0$ it reproduces Table 2.2*

q	n			
	0	2	4	6
2	$(2+\lambda)^2$	0	0	0
3	$2(1+\lambda)$	$2(3+\lambda)$	0	0
4	$-\lambda^2$	$(4+\lambda)^2$	0	0
5	$2(1+\lambda)$	$4(5+3\lambda)$	$2(5+\lambda)$	0
6	$(2+\lambda)^2$	$2(12+8\lambda-\lambda^2)$	$(6+\lambda)^2$	0
7	$2(1+\lambda)$	$6(7+5\lambda)$	$10(7+3\lambda)$	$2(7+\lambda)$
8	$-\lambda^2$	$(64+48\lambda+3\lambda^2)$	$(128+64\lambda-3\lambda^2)$	$(8+\lambda)^2$

Neither recurrence formulas for $\tilde{U}_C$, $\tilde{U}_I$ nor sum rules for $\tilde{\Lambda}_\kappa$ in the modulated t_s case were yet found, but we can give some examples. The function $\tilde{U}_C$ in the (C) commensurate case applied to the hopping, when $q = 5$, for instance, is given by

$$\tilde{U}_C(\mu, \Delta, q = 5, \lambda) = \\ -5\Delta^2\lambda^2\mu + 5\tfrac{\sqrt{5}+7}{32}\lambda^4\mu - \tfrac{5}{2}\lambda^2\mu^3 - 5\tfrac{\sqrt{5}+1}{2}\lambda^2\mu, \tag{2.39}$$

while the new delimiting function $\tilde{\Lambda}_0^C$, for $q = 5$, is

$$\tilde{\Lambda}_0^C(\Delta, q = 5, \lambda) = \\ 2 + \tfrac{1}{8}\lambda^2\left(140 + 75\lambda^2 + \lambda^3 - 60\Delta^2\right). \tag{2.40}$$

Similarly, the function $\tilde{U}_I$ in the (I) incommensurate case applied to the hopping, for $q = 3$, is given by

$$\tilde{U}_I(\mu, \Delta, q = 3, \lambda) = \\ -\mu\left[2\lambda\left(\cos(2\pi\beta) + \cos(4\pi\beta) + \cos(6\pi\beta)\right)\right. \\ \left.+\lambda^2\left(\cos^2(2\pi\beta) + \cos^2(4\pi\beta) + \cos^2(6\pi\beta)\right)\right], \tag{2.41}$$

while for the new delimiting function $\tilde{\Lambda}_0^I$, for $q = 3$, we have

$$\begin{aligned}\tilde{\Lambda}_0^I(\Delta, q=3, \lambda) &= 2(1+3\Delta^2) \\ &+2\lambda(1+\Delta^2)\left[\cos(2\pi\beta)+\cos(4\pi\beta)+\cos(6\pi\beta)\right] \\ &+2\lambda^2\left[\cos(2\pi\beta)\cos(4\pi\beta)+\cos(2\pi\beta)\cos(6\pi\beta)\right. \\ &\left.+\cos(4\pi\beta)\cos(6\pi\beta)\right] \\ &+2\lambda^3\left[\cos(2\pi\beta)\cos(4\pi\beta)\cos(6\pi\beta)\right]. \end{aligned} \tag{2.42}$$

2.3.4 Concluding remarks

In order to have some insight on the new phases found in this work, we have studied the eigenstates of H_k to see the characteristics of the band structure at both sides of a bubble. We will use a strategy which is successfully employed nowadays in Topological Band Theory [48]. We took as an example the single-defect (S) case applied to the chemical potential, which is given in Fig. 2.8(b), but this analysis is equally valid for other distributions. We can see the comparison of the low-lying bands in Fig. 2.9 at two points that are close in the phase diagram, outside 3(a) and inside 3(b) a bubble, whose gap closes at π/q, as explained in Section 2.3.3. The way our BdG Hamiltonian (2.19) was built in, we can distinguish the particle-part from the hole-part of these eigenstates. We used a particle-projection operator applied to the eigenstates to plot them blue for particle-like (projection above 50%) and red for hole-like (projection below 50%).

What is interesting in these results is that there is a band inversion (change of color) in the band states from $k = 0$ to $\pm\pi/q$ and close to the gap at $E = 0$, when comparing the topological bands in 3(a) with the non-topological bands in 3(b), which is an indication of a change in the fermion parity. The parity inversion between 3(a) and 3(b) indicates a change of occupancy of one non-local fermion state, which is another way of detecting the presence of Majorana edge modes in the topological phase, when the system has open boundaries. This argument is guaranteed by the bulk-edge correspondence. It is also a confirmation example of

the usefulness of our method for detecting the fermion parity switches in the general inhomogeneous cases, as proposed in the Introduction.

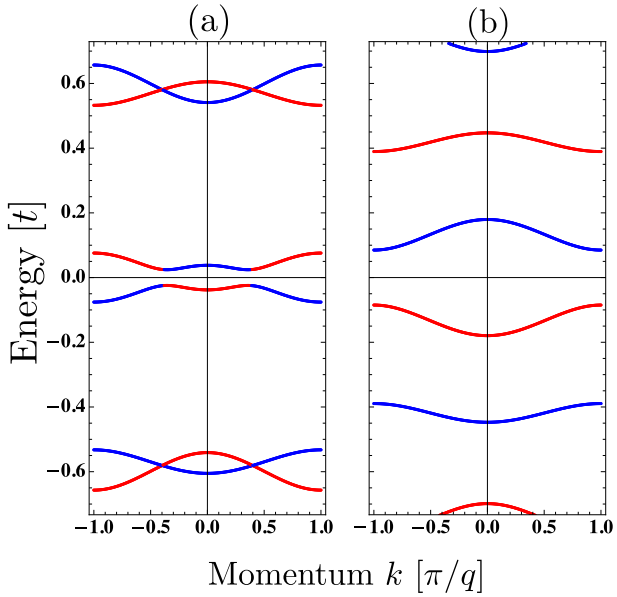

Fig. 2.9: *Calculated bands at opposite sides of a bubble, whose gap closes at π/q, for the single-defect model applied to μ, using $q = 10$, $\lambda = 10$ and $\Delta = 0.05t$, (a) Topological region, outside the bubble, (b) Non-Topological region, inside the bubble. Notice that, in contrast to (b), there is a band inversion in (a) of the band states close to the gap at $E = 0$ as one moves along the reduced Brillouin Zone, from $k = 0$ to $\pm\pi/q$, which indicates a change of the fermion parity.*

In summary, we have studied the effects of spatial inhomogeneities in the 1D p-wave Kitaev model, for which we constructed a polynomial description for the topological invariant using an enlarged-unit cell approach. We applied the method to three different classes of spatial distributions, (S,C,I), although it can be easily expanded to more general cases, like those including longer-range hoppings and pairings [49–51].

A comparative study was made for modulated chemical potentials and modulated hopping amplitudes, using the same site distributions, finding very clear differentiations, as the examples from Fig. 2.7 have demonstrated. The modulations

applied to the chemical potential, for example, preserve the elliptical region of the oscillations in $(\mu/2t)^2 + (\Delta/t)^2 = 1$, as mentioned above, while those applied to the hopping amplitude do not. This marked difference will establish a strong dichotomy for diagonal versus off-diagonal disordered systems. These differentiations would not have been seen if we had applied the modulation in both parameters simultaneously. Additionally, our results are fully consistent with previous works [4, 25–32].

Furthermore, the oscillatory behavior of the polynomial function U and its delimiting functions Λ_κ take account of most of the topological features of the model, not only on the origin of emerging non-topological bubbles around the anisotropy line ($\Delta = 0$) in the topological region of the phase diagram, but also about the exact positions of the ground-state fermion parity switches for homogeneous finite wires which, according to Hegde *et al.* [29, 30], are given by the elliptical curves

$$\bar{\mu} = 2t \cos\left(\frac{\pi p}{q+1}\right) \tag{2.43}$$

where $p = 1, 2, \ldots, [q/2]$, with $[q/2]$ the integer part of $q/2$. Our coincident numerical results are astonishingly precise with this expression.

The fact that our periodic boundary bulk results are consistent with those for open boundary systems, with edge Majorana fermions, obtained otherwise through the large size limit of the transfer matrix approach [29, 30], is a consequence of the bulk-edge correspondence. Therefore, with this validity test we propose to use these results also for the inhomogeneous cases. The new zeros of the shifted function U, like those seen in the examples of Figs. 2.7 and 2.8, should be the positions of the new fermion parity switches in those cases. This proposal was confirmed using a single test, shown in Fig. 2.9, where a fermion parity inversion was obtained.

Moreover, as a by-product, since the Kitaev chain is exactly mapped onto the XY model through a Jordan-Wigner transformation [5, 52], we hope that other authors would be willing to observe paramagnetic bubbles in the ferromagnetic region of the inhomogeneous dual XY model, as well. What would remain to verify is whether the oscillations of the spin correlation function for the XY model will be at the same oscillatory region of the shifted function U, as it is in the homogeneous case.

2.4 One application of our method

In this section, we will show an application of our approach in the characterization of a time-dependent Hamiltonian modulated periodically in time. We will analyze a periodically driven model of interacting spinless fermions in a 1D optical lattice. Since the fermions have no spin, there is no on-site Hubbard interaction, but just a NN two-body term, which, with the help of Feshbach resonances, is tailored to be attractive. In the absence of driving, this model reduces to the Kitaev chain upon applying a mean-field approximation in the particle-particle channel. However, when an additional periodic ac Feshbach magnetic field is applied to the system, the NN-interaction term acquires an ac component. Using the Floquet formalism, we derive an effective model at stroboscopic times, which is time-independent, but much more complex: three-body interaction terms emerge, as well as a dimerization in the NN pairing term. In addition, a next-nearest neighbor (NNN) pairing term arises also. Inspired by these terms, we investigate two simplified toy models, which are both interesting generalizations of the Kitaev chain. The first is a Kitaev chain with dimerized NN pairing, while the second is a longer-range Kitaev chain, with NNN pairing. The enlarged unit-cell method is further applicable to both cases.

2.4.1 Floquet states

Let us start considering a 1D tight-binding model for spinless fermions with nearest-neighbors (NN) attractive interaction and a time-dependent perturbation. The corresponding Hamiltonian is given by

$$H = H_J + H_\mu + H_V + H_d, \tag{2.44}$$

where

$$\begin{aligned} H_J &= -J\sum_i (c_i^\dagger c_{i+1} + h.c.) \quad , \qquad H_\mu = -\mu \sum_i n_i \\ H_V &= V_0 \sum_i n_i n_{i+1} \quad , \qquad H_d = V_1 \cos(\omega t) \sum_i n_i n_{i+1}. \end{aligned} \tag{2.45}$$

The first term describes hopping between NN with amplitude J, whereas the second term accounts for the chemical potential μ, since we are working on the grand

canonical ensemble. The term H_V describes a NN charge interaction, which is attractive ($V_0 < 0$). The last term is an external ac driving term, with amplitude V_1 and frequency ω. Since this driving term H_d is periodic, we may apply the Floquet theory outlined in Ref. [54] and derive an effective time-independent Hamiltonian to describe the system at stroboscopic times. First, we build the Floquet basis as

$$|\{n_j\}, m\rangle = |\{n_j\}\rangle e^{im\omega t} \exp\left[-i\frac{V_1}{\hbar\omega}\sin(\omega t)\sum_j n_j n_{j+1}\right], \tag{2.46}$$

where $|\{n_j\}\rangle$ stands for the Fock states, and m is an integer. Then, we compute the matrix elements of the Floquet Hamiltonian $\mathcal{H} = H - i\hbar\partial_t$, to find a time-independent effective model. By applying the operator $-i\hbar\partial_t$ on the Floquet basis (2.46), we find

$$\begin{aligned} -i\hbar\partial_t|\{n_j\}, m\rangle &= |\{n_j\}\rangle(-i\hbar)\partial_t\left(e^{im\omega t}\exp\left[-i\frac{V_1}{\hbar\omega}\sin(\omega t)\sum_j n_j n_{j+1}\right]\right) \\ &= |\{n_j\}, m\rangle\left(m\hbar\omega - V_1\cos(\omega t)\sum_j n_j n_{j+1}\right) \\ &= |\{n_j\}, m\rangle\left(m\hbar\omega - H_d\right), \end{aligned} \tag{2.47}$$

The last term of eq. (2.47) cancels the driving term in eq. (2.44), thus leading to

$$\langle\langle\{n'_j\}, m'|H_d - i\hbar\partial_t|\{n_j\}, m\rangle\rangle = \delta_{n'n}\delta_{m'm}m\hbar\omega. \tag{2.48}$$

The dc interaction term H_V reads

$$\begin{aligned} \langle\langle\{n'_j\}, m'|H_V|\{n_j\}, m\rangle\rangle &= \frac{1}{T}\int_0^T dt e^{i\omega t(m-m')}\langle\{n'_j\}|H_V|\{n_j\}\rangle \times \\ &\quad \exp\left[-i\frac{V_1}{\hbar\omega}\sin(\omega t)\sum_j(n_j n_{j+1} - n'_j n'_{j+1})\right]. \end{aligned} \tag{2.49}$$

The basis $|\{n_j\}\rangle$ are eigenstates of H_V, and hence

$$\langle\langle\{n'_j\}, m'|H_V|\{n_j\}, m\rangle\rangle = \langle\{n'_j\}|H_V|\{n_j\}\rangle\delta_{m',m}. \tag{2.50}$$

The chemical potential term is given by

$$\begin{aligned} \langle\langle\{n'_j\}, m'|H_\mu|\{n_j\}, m\rangle\rangle &= \frac{1}{T}\int_0^T dt e^{i\omega T(m-m')}\langle\{n'_j\}|H_\mu|\{n_j\}\rangle \times \\ &\quad \exp\left[-i\frac{V_1}{\hbar\omega}\sin(\omega t)\sum_j(n_j n_{j+1} - n'_j n'_{j+1})\right], \end{aligned} \tag{2.51}$$

where the main element $\langle\{n'_j\}|c_i^\dagger c_i|\{n_j\}\rangle$ is non zero when $n'_i = n_i$, leading to

$$\langle\langle\{n'_j\}, m'|H_\mu|\{n_j\}, m\rangle\rangle = \langle\{n'_j\}|H_\mu|\{n_j\}\rangle\delta_{m',m}. \tag{2.52}$$

Finally, the hopping term reads

$$\begin{aligned}\langle\langle\{n'_j\}, m'|H_J|\{n_j\}, m\rangle\rangle &= \frac{1}{T}\int_0^T dt e^{i\omega t(m-m')}\langle\{n'_j\}|H_J|\{n_j\}\rangle \times \\ &\exp\left[-i\frac{V_1}{\hbar\omega}\sin(\omega t)\sum_j(n_j n_{j+1} - n'_j n'_{j+1})\right],\end{aligned} \tag{2.53}$$

where the main element $\langle\{n'_j\}|c_i^\dagger c_{i+1}|\{n_j\}\rangle$ is non zero when $n'_i = n_i + 1$ and $n'_{i+1} = n_{i+1} - 1$. Since the occupation number n can only be zero or one, we find that $n_i = 1$, $n'_i = 0$, $n_{i+1} = 0$, $n'_{i+1} = 1$ and $n'_j = n_j \;\forall\; j \neq \{i, i+1\}$. This information allows us to compute the sum

$$\begin{aligned}\hat{s} = \sum_j(n_j n_{j+1} - n'_j n'_{j+1}) &= n_{i-1}n_i - n'_{i-1}n'_i + n_i n_{i+1} - n'_i n'_{i+1} + n_{i+1}n_{i+2} - n'_{i+1}n'_{i+2} \\ &= n_{i+2} - n_{i-1}.\end{aligned} \tag{2.54}$$

Using the integral representation of the Bessel function, and following a similar procedure as described in Ref. [54], we can then write the effective Hamiltonian as

$$H_{\text{eff}} = -\mu\sum_i n_i + V_0\sum_i n_i n_{i+1} - J\sum_i(c_i^\dagger c_{i+1} + h.c.)\mathcal{J}_0[K(n_{i+2} - n_{i-1})], \tag{2.55}$$

where $K = V_1/\hbar\omega$. Factorizing the sum of the Taylor expansion of the Bessel function as

$$\mathcal{J}_0[K\hat{s}] = \sum_{m=0}^{\infty} c_{2m}K^{2m}\hat{s}^{2m} = 1 - (1 - \mathcal{J}_0[K])\hat{s}^2, \tag{2.56}$$

where $\hat{s}^2 = n_{i+2} + n_{i-1} - 2n_{i+2}n_{i-1}$, we finally find the effective Hamiltonian

$$H_{\text{eff}} = H_J + H_\mu + H_V + J(1 - \mathcal{J}_0[K])\sum_i(c_i^\dagger c_{i+1} + c_{i+1}^\dagger c_i)(n_{i+2} + n_{i-1} - 2n_{i+2}n_{i-1}). \tag{2.57}$$

This effective Hamiltonian describes a kind of correlated-hopping model, with two-body and three-body interacting terms. The next step is then to apply a mean-field approximation and study the topological properties of this system.

2.4.2 Mean-field approximation

In this section, we are going to apply a mean-field approximation to the effective Hamiltonian. In the absence of a driving term ($V_1 = 0$), the Hamiltonian (2.57) simplifies as

$$H = -J\sum_i (c_i^\dagger c_{i+1} + h.c.) - \mu\sum_i n_i + V_0\sum_i n_i n_{i+1}. \tag{2.58}$$

By applying a MF approximation to the interaction part in the particle-particle channel, i.e. $n_i n_{i+1} = c_i^\dagger c_i c_{i+1}^\dagger c_{i+1} = c_i^\dagger c_{i+1}^\dagger c_{i+1} c_i \to \langle c_i^\dagger c_{i+1}^\dagger\rangle c_{i+1}c_i + \langle c_{i+1}c_i\rangle c_i^\dagger c_{i+1}^\dagger - \langle c_{i+1}c_i\rangle\langle c_i^\dagger c_{i+1}^\dagger\rangle = \Delta_1^* c_{i+1}c_i + \Delta_1 c_i^\dagger c_{i+1}^\dagger - |\Delta_1|^2$, where $\Delta_1 = \Delta_1^* \equiv \langle c_{i+1}c_i\rangle = \langle c_i^\dagger c_{i+1}^\dagger\rangle$, we find that the Hamiltonian may be written as

$$H = -J\sum_i (c_i^\dagger c_{i+1} + h.c.) - \mu\sum_i n_i + V_0\Delta_1\sum_i (c_i^\dagger c_{i+1}^\dagger + h.c.) - V_0\Delta_1^2 N, \tag{2.59}$$

where N is the length of the chain and $V_0\Delta_1 \in \mathbb{R}$ acts as the usual 1D p-wave superconducting pairing. This Hamiltonian corresponds to the homogeneous Kitaev chain, which exhibits Majorana edge states for $|\mu/J| < 2$, for open boundary conditions.

Now, we consider the case $V_1 \neq 0$ and apply a mean-field approximation on the many-body operators found in Eq. (2.57). Upon defining $\hat{T} \equiv c_i^\dagger c_{i+1} + h.c.$, we can identify three different terms in Eq. (2.57), $\hat{T}n_{i+2}$, $\hat{T}n_{i-1}$ and $\hat{T}n_{i+2}n_{i-1}$. In this section, we will concentrate on the two-body interaction terms, which are given by

$$\hat{T}n_{i+2} = \Delta_1(c_{i+2}c_i + h.c.) + \Delta_2(c_{i+2}c_{i+1} + h.c.) - (\Delta_1^*\Delta_2 + \Delta_2^*\Delta_1), \tag{2.60}$$

$$\hat{T}n_{i-1} = \Delta_1(c_{i+1}c_{i-1} + h.c.) + \Delta_2(c_i c_{i-1} + h.c.) - (\Delta_1^*\Delta_2 + \Delta_2^*\Delta_1), \tag{2.61}$$

where we used $\Delta_1 = \langle c_{i+1}c_i\rangle = \langle c_{i+2}c_{i+1}\rangle = \langle c_i c_{i-1}\rangle$ (the NN paring term) and defined a next-nearest neighbor (NNN) pairing $\Delta_2 = \langle c_{i+2}c_i\rangle = \langle c_{i+1}c_{i-1}\rangle$. As a first approximation, we neglect the term $\hat{T}n_{i+2}n_{i-1}$, corresponding to a three-body interaction. Upon substituting Eqs. (2.60) and (2.61) in (2.57), we find the mean-field Hamiltonian

$$H_{MF} = H_\mu + H_J + H_{NN} + H_{NNN}^d + H_{NN}^d \tag{2.62}$$

where

$$H_{NN} = V_0\Delta_1 \sum_j (c_{j+1}c_j + h.c.) \tag{2.63}$$

$$H^d_{NNN} = J(1-\mathcal{J}_0[K])\Delta_1 \sum_j (c_{j+1}c_{j-1} + c_{j+2}c_j + h.c.) \tag{2.64}$$

$$H^d_{NN} = J(1-\mathcal{J}_0[K])\Delta_2 \sum_j (c_{j+2}c_{j+1} + c_j c_{j-1} + h.c.) \tag{2.65}$$

which corresponds to a Kitaev chain with a NNN pairing term and an inhomogeneous NN pairing. Indeed, the pairing between $c_{j+1}c_j$ has intensity $V_0\Delta_1$, whereas for the next pairs of sites, $c_{j+2}c_{j+1}$, the intensity is $V_0\Delta_1 + J(1-\mathcal{J}_0[K])\Delta_2$.

2.4.3 Toy models

In the previous section, we applied a mean-field approximation to the effective Hamiltonian (2.62), and obtained a non-interacting spinless fermion model with a dimerized NN and NNN pairing terms. In this section, we study the topological properties of this system using an enlarged unit cell approach (with two sites) and the polynomial description previously applied to the inhomogeneous Kitaev chain. In Fig. (2.10), we depict the coupling in a particle-hole scheme, where we defined $\phi = J(1-\mathcal{J}_0[K])$ to simplify the notation.

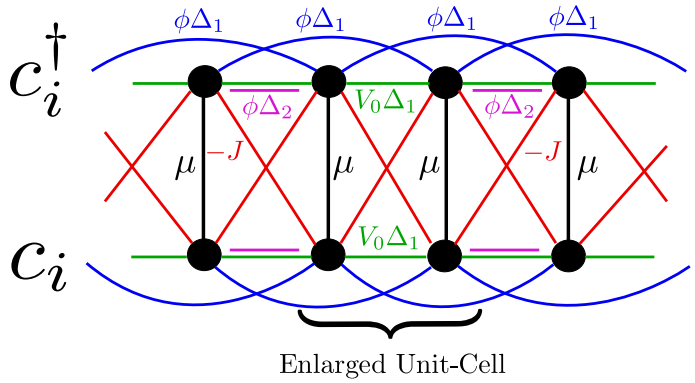

Fig. 2.10: *Coupling scheme for the effective mean-field Hamiltonian (2.62). The presence of a dimer and NNN pairing terms request the use of an enlarged unit-cell approach.*

Kitaev chain with dimerized NN pairing. – For simplicity and pedagogical reasons, let us start by studying the effect of the dimerized NN pairing term and artificially take $H^d_{NNN} = 0$ in the Eq. (2.62), we then get the Hamiltonian

$$\begin{aligned} H_{dim} &= -\mu \sum_j n_j - J \sum_j (c_j^\dagger c_{j+1} + h.c.) + V_0 \Delta_1 \sum_j (c_{j+1} c_j + h.c.) \\ &\quad + \phi \Delta_2 \sum_j (c_{j+2} c_{j+1} + c_j c_{j-1} + h.c.) \end{aligned} \tag{2.66}$$

The last term in Eq. (2.66) adds a coupling only for alternating bonds and turns the system into a dimerized pairing wire. To solve this problem, we are going to use the enlarged unit-cell (EUC) approach [53]. The method consists of taking a unit-cell in the particle-hole space with more than one site (enlarged), and then describing the model by an internal structure in the EUC plus terms that connect the cells (hopping-like matrix). In this case, the Hamiltonian for each EUC is

$$H_l = \sum_{j=1}^{N} \left[-\mu n_{j,l} - J(c_{j,l}^\dagger c_{j+1,l} + h.c) + V_0 \Delta_1 (c_{j,l} c_{j+1,l} + h.c) \right], \tag{2.67}$$

where N is the number of sites in the unit-cell ($N = 2$ for our purpose), and l is the label of each unit-cell. Using the Bogoliubov de Gennes (BdG) transformation, we can write the Hamiltonian (2.67) as

$$H_l = \frac{1}{2} \psi_{j,l}^\dagger \hat{H}_{l,l} \psi_{j,l} \tag{2.68}$$

where $\psi_{j,l}^\dagger = (c_{1,l}^\dagger, ..., c_{N,l}^\dagger, c_{1,l}, ..., c_{N,l})$ is an extended basis given by the BdG transformation. The *hopping* term among the unit-cells is a combination of spatially modulated hopping and pairing terms, given by

$$H^t = \psi_{j,l}^\dagger \hat{H}^t_{l,l+1} \psi_{j,l+1} + \psi_{j,l+1}^\dagger \hat{H}^t_{l+1,l} \psi_{j,l}, \tag{2.69}$$

where $H^t = -J(c_{j+1,l}^\dagger c_{j,l+1} + h.c.) + \phi \Delta_2 (c_{j+1,l} c_{j,l+1} + h.c.)$ is the linking element between two unit-cells (l and $l+1$).

Applying a Fourier transformation to each EUC allows us to write the Hamiltonian in momentum space as

$$H = \sum_k \psi_k^\dagger \hat{H}_k \psi_k, \tag{2.70}$$

where $\psi_k^\dagger = (c_{i,k}^\dagger, c_{i+1,k}^\dagger, c_{i,-k}, c_{i+1,-k})$, and $k \in (-\pi/N, \pi/N]$ is the momentum in the reduced Brillouin Zone. The Hamiltonian H_k then acquires the structure

$$H_k = H_l + H_{l,l+1}^T \exp(iNk) + H_{l+1,l}^T \exp(-iNk). \tag{2.71}$$

such that Eq. (2.70) may be rewritten as

$$H = \frac{1}{2}\sum_k \psi_k^\dagger H_k \psi_k = \frac{1}{2}\sum_k \psi_k^\dagger \begin{pmatrix} V_k & M_k \\ M_k^\dagger & -V_{-k}^T \end{pmatrix} \psi_k, \tag{2.72}$$

where V_k and M_k are $N \times N$ matrices. The Hamiltonian H_k can be brought into an off-diagonal form by a unitary transformation given by

$$\Omega H_k \Omega^\dagger = \begin{pmatrix} 0 & A_k \\ A_k^T & 0 \end{pmatrix}, \tag{2.73}$$

where $A_k = M_k + V_k$, and $\Omega = \exp(-i\tau_y \pi/4)$ is the unitary transformation and τ_y is the suitable Pauli matrix on the particle-hole space. The matrix A_k will give us the information about the topological features of the model. In fact, the winding vector has similar properties to the function $Det(A_k)$ for the same values of k, which describe loops in the complex plane linked with the winding number. From now on, we are going to study this function using a polynomial description [53].

Let us start with the A_k matrix for the dimerized pairing model, given by

$$A_k = \begin{pmatrix} \mu & -e^{-ik}(2J\cos(k) + 2iV_0\Delta_1 \sin(k) - e^{-ik}\phi\Delta_2) \\ -e^{ik}(2J\cos(k) + 2iV_0\Delta_1 \sin(k) + e^{ik}\phi\Delta_2) & \mu \end{pmatrix}. \tag{2.74}$$

The topological phase transition occurs when $Det(A_k) = 0$. For the dimer-pairing model, the phase-transition then takes place when $\mu = \pm\sqrt{(2J)^2 - (\phi\Delta_2)^2}$. This result shows that the Ising lines in the topological phase diagram change their position, getting close to the origin, as long as $\phi\Delta_2$ is smaller than $2J$. After this, the system remains gapped, but is no longer topological. In Fig. (2.11), we show how the topological phase diagram changes when the dimer-pairing term is present in the system.

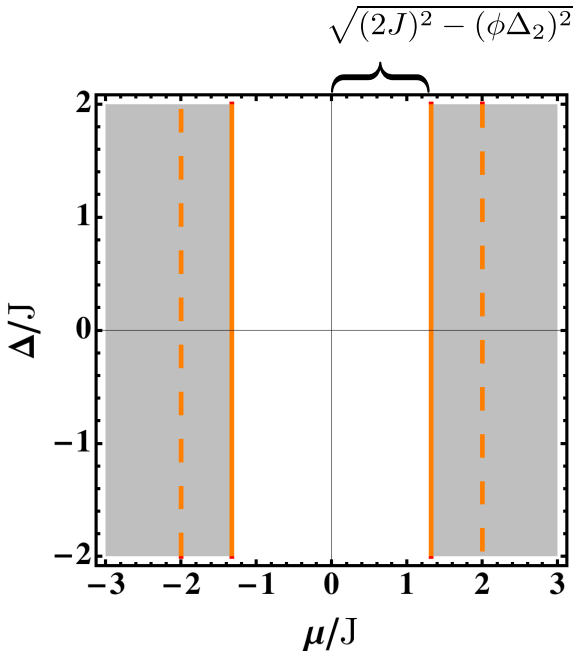

Fig. 2.11: *Topological phase diagram for a system with a dimer-pairing term. The white (gray) zone correspond to the topological (non-topological) phase. The dashed lines represent the topological phase transition for the homogeneous case, and the bold (orange) line is where it occur when the dimer term is non-zero* $\phi\Delta_2 \neq 0$.

Kitaev chain with NNN pairing term – Now, we are going to study the effect of the NNN pairing term. Taking $H_d^{NN} = 0$ in Eq. (2.62), the A_k matrix is now given by

$$A_k = \begin{pmatrix} \mu + 2i\phi\Delta_1 \sin(2k) & -e^{-ik}(2J\cos(k) + 2iV_0\Delta_1 \sin(k)) \\ -e^{ik}(2J\cos(k) + 2iV_0\Delta_1 \sin(k)) & \mu + 2i\phi\Delta_1 \sin(2k) \end{pmatrix}. \quad (2.75)$$

In this case, the topological phase diagram remains the same as the one for the homogeneous Kitaev chain (the system is topological for $|\mu/J| < 2$), but the anisotropy line rotates as a function of the NNN coupling $\phi\Delta_1$. The anisotropy line is where

the path of the winding vector changes its chirality. This transition occurs when $Im[Det(A_k)] = 0$. In the homogeneous case, the anisotropy line is given by $V_0\Delta_1 = 0$ (see Fig. (2.12)-left panel) which separates the phase diagram in two regimes, characterized by the chirality of the winding vector. For $V_0\Delta_1 > 0$, the winding vector rotates counterclockwise (Fig. 2.12 (I)), while is rotates clockwise for $V_0\Delta_1 < 0$ (Fig. 2.12 (II)). Notice that the sense of rotation in Figs. 2.12 (II) and 2.12 (IV) is the same as in 2.12 (I). The difference is that in Fig. 2.12 (I) it encloses the origin because this phase is topological. These features hold also for the phase diagram in Fig. (2.11), simply with the topological region.

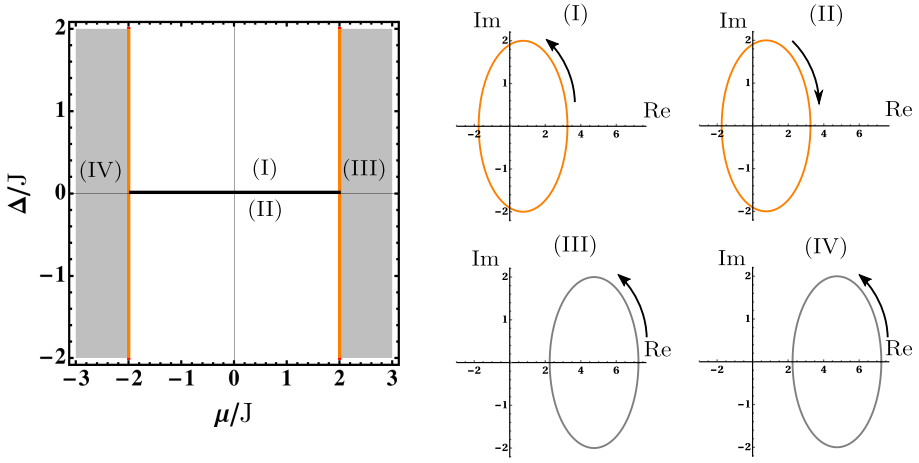

Fig. 2.12: *(left panel) Topological phase diagram of the homogeneous Kitaev chain and (right panel) the path of the winding vector and its chirality for different regions on the parameter space. In the right panels we plot the trajectory of the winding vector for the parameters* $(\mu/J, V_0\Delta_1/J)$ *given by (I):* $(1.5, 1.5)$*, (II):* $(1.5, -1.5)$*, (III):* $(2.5, 1.5)$ *and (IV):* $(-2.5, 1.5)$*.*

When the NNN pairing is added, then $Im[Det(A_k)] = V_0\Delta_1 - \phi\Delta_1\mu$, hence the anisotropy transition is described by either $\Delta_1 = 0$ or $V_0 = \phi\mu$. Since the effective p-wave superconducting pairing of this system is given by $\Delta \equiv V_0\Delta_1$, we can think that the anisotropy line rotates by the angle $\theta = \arctan(\phi\Delta_1)$ with respect to the homogeneous case, as shown in the left panel of Fig. (2.13). Across this line, the chirality of the winding vector changes, as in the homogeneous case, with the

difference that this line is no longer at $\Delta = 0$ This behavior can be observed in the right panel of Fig. (2.13).

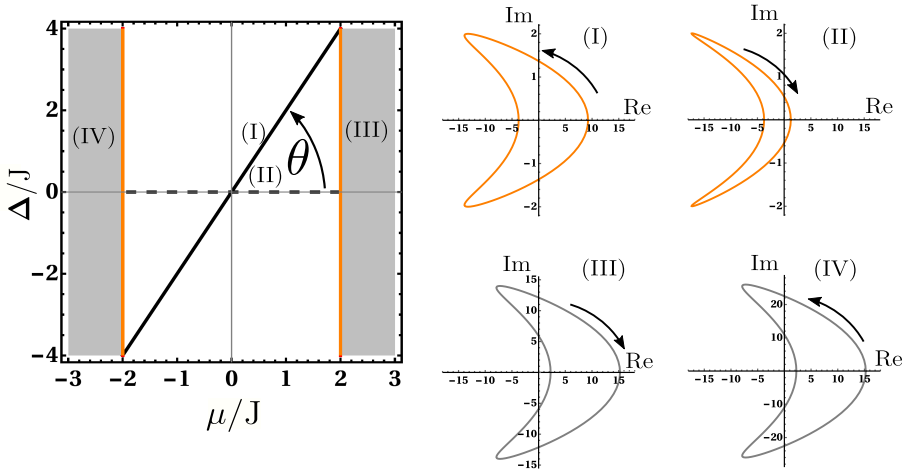

Fig. 2.13: *(left) Topological phase diagram of the inhomogeneous case and (right) the path of the winding vector and their chirality for different regions on the parameter space. In the right panel, we plot the winding vector for* $\phi\Delta_1/J = 2$ *and the parameters* $(\mu/J, V_0\Delta_1/J)$ *given by (I):* $(1.5, 3.5)$*, (II):* $(1.5, 2.5)$*, (III):* $(2.5, 2.5)$ *and (IV):* $(-2.5, 2.5)$*.*

Another interesting finding is the shape of the path described by the winding vector. While in the homogeneous case the path is an ellipse, when the NNN pairing is added, the shape of the path becomes a boomerang (see right panels of Fig. 2.13).

Kitaev chain with dimerized-NN and NNN pairing – When the dimerized-NN and the NNN pairings are both included, the Hamiltonian in its off-diagonal form is described by the following A_k matrix

$$A_k = \begin{pmatrix} \mu + 2i\phi\Delta_1 \sin(2k) & -e^{-ik}(2J\cos(k) + 2iV_0\Delta_1 \sin(k) - e^{-ik}\phi\Delta_2) \\ -e^{ik}(2J\cos(k) + 2iV_0\Delta_1 \sin(k) + e^{ik}\phi\Delta_2) & \mu + 2i\phi\Delta_1 \sin(2k) \end{pmatrix}. \quad (2.76)$$

The topological phase diagram is then a mixture of previous results. In fact, since each kind of pairing distribution is present in different parts of the matrix A_k (diagonal for NNN paring and off-diagonal for the dimer-NN pairing), the topological phase diagram exhibits the features of both systems combined. In this case, the

Ising line changes as the dimer-NN case: the topological transition takes place when $|\mu| = \sqrt{(2J)^2 - (\phi\Delta_2)^2}$, and the condition that describes the anisotropy line is given by $V_0\Delta_1 - \phi\Delta_1\mu + \phi\Delta_2/2 = 0$.

In Fig. (2.14), we display the topological phase diagram of this system. In this case, the anisotropy line is a linear equation, given by $\Delta/J = \phi\Delta_1\mu/J - \phi\Delta_2/2$.

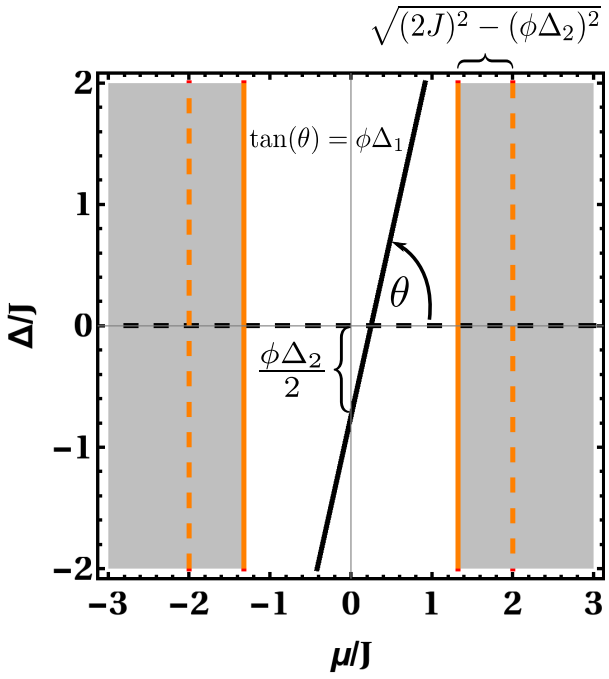

Fig. 2.14: *Topological phase diagram for the system with dimerized NN and NNN pairings. While the topological phase transition is descirbed by* $\mu = \pm\sqrt{(2J)^2 - (\phi\Delta_2)^2}$*, the anisotropy line is given by the equation* $V_0\Delta_1 - \phi\Delta_1\mu + \phi\Delta_2/2 = 0$*. In this plot we used the parameters* $\phi = 3$*,* $\Delta_2 = 0.5$ *and* $\Delta_1 = 1/3$*.*

2.4.4 Concluding remarks

In this Section, we studied the effect of a periodically driving perturbation in a 1D spinless fermion interacting model. After applying the Floquet formalism and a mean-field approximation, we found an effective model equivalent to a p-wave superconductor wire with an inhomogeneous pairing distribution. The distribution added to the system a dimer pairing and a NNN pairing term, which was solved

using an enlarged unit-cell approach, allowing us to describe a topological phase diagram as a function of the driving frequency.

While the MF is not a good approximation in one-dimensional systems as we neglected the three-body term, our approach allows us to identify effects linked to the parameters that drive the time-dependent perturbation, and to understand how to modify the boundaries and properties of the topological regions. It would be interesting to investigate the full time-dependent problem using numerical approaches like DMRG, including 6th order term, long-range hopping, dimerized hopping and interaction.

All these studies helped us to acquire a deeper understanding of the paradigmatic Kitaev model and its stability, thus setting the theoretical basis for Majorana qubits. (back to quantum computing)

This application of our method of the enlarged unit-cell, described in Section 2.4, was worked out in collaboration with Professor Cristiane Morais Smith (Utrecht University, The Netherlands) and it is being processed as a preprint for publication purposes.

All the Sections previous to this one in this Chapter were the main contributions to this thesis for the inhomogeneous Kitaev chain, and the results were published in Journal of Physics: Condensed Matter **29**, 475503 (Nov. 2017).

Chapter 3

The Haldane-Shastry model with a chiral interaction

3.1 Integrability of many-body systems

Integrable systems play an important role in the comprehension of interacting many-particle models in one dimension. Integrability is better, and perhaps only, understood through the Bethe ansatz method [55], where an infinite set of conserved quantities are reduced analytically to a set of Bethe ansatz equations, whose solutions would eventually give all the quasi-momenta of the exact many-body wavefunction [56]. It is an intricate set of solutions whose practical limitations took more than 50 years to read off the non-trivial physical concepts involved. Among these concepts there is a prominent one, which is the fractional quantization of spin in antiferromagnetic spin-1/2 chains. Fadeev and Takhatajan [57] discovered in 1981 that the elementary excitations, now called *spinons*, of the spin-1/2 Heisenberg chain solved by Hans Bethe fifty years earlier carry spin-1/2, contrary to spin flips which carry spin-1. This is now known as fractionalization of spin and it is conceptually similar to the fractional quantization of charge in quantized Hall liquids [13]. One of the reasons underlying practical uses of the Bethe ansatz is that the solutions are given as distributions of pseudomomenta, in which spinon excitations appear as defects. Spinons hence play the role of defects or solitons in the solutions of the Bethe ansatz equations, either for spins in the Heisenberg model as for electrons in

the one-dimensional Hubbard model.

The spinon Hilbert space cannot be decomposed into a product space of single particle states, as the Fock space for the familiar cases of fermions or bosons. Indeed, such peculiarity is the kernel of the difficulties to develop a perturbative method in the spinon field directly.

The work in this thesis confronts such possibility by coupling a chiral perturbation to the Haldane-Shastry model. The chiral perturbation will be related to the Yangian algebra and involves the z-component of the rapidity vector.

The spin and the rapidity operators define the Yangian algebra for the Haldane-Shastry spin chain, as we shall see below. To construct the spinon Hilbert space of the Haldane-Shastry model, one has to deal with tensor products of the fundamental representations of the associated Yangian algebra. It is shown here that the representation theory of the Yangian is intimately related to the fractional statistics of the spinons.

In this Chapter we present our study of the Haldane-Shastry model with a chiral interaction given by the rapidity operator. In section 3.2, we summarize the Haldane-Shastry model and detail the most important properties of the ground-state and its spectrum. In section 3.3 we introduce the Haldane-Shastry model with a chiral interaction and show our numerical results and the analytic description that explain the features of the exact diagonalization in finite clusters. In doing this we discovered how to use the Modified Young Tableaus formalism [63] to describe the representation theory of the Yangian algebra that operates in the elementary excitations of the Haldane-Shastry model. Finally, we discuss some aspects about our findings related to the thermodynamic limit and the comparison with other medium-range spin chain models.

3.2 A summary of the Haldane-Shastry model

In this section, we summarize the most important features of the spin-1/2 chain model with $1/r^2$-exchange interactions, which was independently solved by F. D.

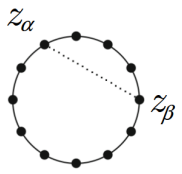

$$z_\alpha = \exp\left(i\frac{2\pi}{N}\alpha\right)$$

Fig. 3.1: *Scheme representing N sites of spin-1/2 on the unit circle. The chord distance $|z_\alpha - z_\beta|$ between the sites α and β is drawn with a dotted line. Positions are given by $z_\alpha = \exp\left(i\frac{2\pi}{N}\alpha\right)$.*

M. Haldane [7] and B. S. Shastry [8] in 1988, and is part of the exclusive list of many-body models which are exactly solved [58].

3.2.1 The Hamiltonian and its symmetries

Let us consider a chain of N Heisenberg spins (with N even), located in a unit-circle embedded in the complex plane, as seen in Fig. 3.1. The positions of the spins-1/2 on the unit circle are uniformly distributed

$$z_\alpha = \exp\left(i\frac{2\pi}{N}\alpha\right) \quad \text{with} \quad \alpha = 1, ..., N. \tag{3.1}$$

The Hamiltonian of the Haldane-Shastry model (HSM) is described by exchange interactions between the spins depending on the inverse of the distance square $(1/r^2)$ among the spins, given by the expression

$$H^{HS} = \left(\frac{\pi}{N}\right)^2 \sum_{\alpha<\beta}^{N} \frac{\mathbf{S}_\alpha \cdot \mathbf{S}_\beta}{|z_\alpha - z_\beta|^2} \tag{3.2}$$

where $|z_\alpha - z_\beta|$ is the chord distance (r) between the sites α and β, as shown in Fig. 3.1.

The spin-chain models are usually characterized by the time-reversal symmetry, stemming for the invariance under space translations due to their periodic boundary condition or rotations of the unit circle; the parity symmetry, which can be studied after a Jordan-Wigner transformation; and the global SU(2) spin rotations

symmetry, which is generated for the HSM by the spin operator

$$\mathbf{S}_{tot} = \sum_{\alpha=1}^{N} \mathbf{S}_\alpha, \qquad \left[H^{HS}, \mathbf{S}_{tot}\right] = 0. \tag{3.3}$$

The HSM possesses an additional symmetry generated by the rapidity vector operator which measures the spin current and is given by

$$\mathbf{\Lambda} = \frac{i}{2} \sum_{\alpha,\beta=1\alpha\neq\beta}^{N} \frac{z_\alpha + z_\beta}{z_\alpha - z_\beta} \mathbf{S}_\alpha \times \mathbf{S}_\beta, \qquad \left[H^{HS}, \mathbf{\Lambda}\right] = 0. \tag{3.4}$$

The total spin trivially satisfies the standard commutation relations for angular momentum

$$\left[S^i_{tot}, S^j_{tot}\right] = i\epsilon^{ijk} S^k_{tot}, \tag{3.5}$$

and the rapidity operator transforms as a vector operator under spin rotations,

$$\left[S^i_{tot}, \Lambda^j\right] = i\epsilon^{ijk} \Lambda^k. \tag{3.6}$$

Note that even though both $\mathbf{S}_{tot}$ and $\mathbf{\Lambda}$ commute with the Hamiltonian, they do not commute mutually, generating an infinite dimensional associative algebra with certain defining relations and consistency conditions, named the Yangian $\mathrm{Y}(sl_2)$ [58]. This symmetry is indirectly related with the integrability of this model, whose solution was found by the asymptotic Bethe ansatz [59, 60] that will be commented below.

3.2.2 The Haldane-Shastry eigenstates: Modified Young Tableaux

The ground state of this model is given by the Gutzwiller projector over the free Fermi sea described by the N-particle Slater determinant. This projection eliminates configurations with more than one particle on any site, and reads as follows

$$|\psi_0^{HS}\rangle = P_G |\psi_{SD}^N\rangle \tag{3.7}$$

where

$$|\psi_{SD}^N\rangle = \prod_{q\,\in\,\mathcal{I}} c^\dagger_{q\uparrow} c^\dagger_{q\downarrow} |0\rangle, \quad \text{and} \quad P_G = \prod_{i=1}^{N} (1 - c^\dagger_{i\uparrow} c_{i\uparrow} c^\dagger_{i\downarrow} c_{i\downarrow}). \tag{3.8}$$

P_G is the *Gutzwiller projector* and $\mathcal{I}$ is a set of $N/2$ adjacent momenta, which has to be occupied by two particles of different spins [61]. The state $|\psi_{SD}^N\rangle$ is a singlet by construction and P_G commutes with SU(2) rotations, then the ground-state $|\psi_0^{HS}\rangle$ is a SU(2) singlet as well. In fact, we have that

$$[P_G, \mathbf{S}_\alpha] = [P_G, \mathbf{S}_{\text{tot}}] = 0, \tag{3.9}$$

and $\mathbf{S}_{\text{tot}}|\psi_{SD}^N\rangle = 0$, hence

$$\mathbf{S}_{\text{tot}}|\psi_0^{HS}\rangle = 0. \tag{3.10}$$

The ground state has momentum

$$p_0 = -\frac{\pi}{2}N \tag{3.11}$$

where we have adopted a convention according to which the *vacuum* state, which is $|\downarrow\downarrow \ ...\downarrow\rangle$, has momentum $p = 0$ (and the empty state $|0\rangle$ has $p = \pi(N-1)$). The energy of this ground-state is

$$E_0 = -\frac{\pi^2}{4N}. \tag{3.12}$$

Let us comment and summarize some results about the whole spectrum of HSM. The elementary excitations of this model can be constructed by the annihilation of a particle from the Slater determinant state before Gutzwiller projection. This annihilation creates a spinon with opposite spin orientation and spin 1/2. The two-spinon polarized state can be mapped to the exact eigenstates of the HSM, and the total energy of this eigenstate takes the form of free particles if and only if each spinon momenta is shifted [62]. The shift is due to the fractional statistics of the spinons. In another way, the whole spectrum can be solved by the asymptotic Bethe ansatz (ABA) [59, 60], giving us the pseudomomenta of each spinon (p_i) and their single spinon spectra. For a chain with even number of spins, the dispersion relation of a single spinon is

$$\epsilon(p) = \frac{\pi^2}{8N^2} + \frac{1}{2}p(\pi - p). \tag{3.13}$$

The momentum and energy of each eigenstate of HSM is given by

$$p = p_0 + \sum_{i=1}^{L} p_i, \quad E = E_0 + \sum_{i=1}^{L} \epsilon(p_i) \tag{3.14}$$

where $L \leq N$ is the number of spinons.

The methodology to find the pseudomomenta by the ABA is rather complicate. Greiter and Schuricht [63] has found a new, clear and heuristic approach to describe the spinon spectra. The method consists in modifying the Young tableaux initially used to describe the SU(2) spectrum of the Heisenberg model. The modification give us a set of numbers, which can be identified as spinon momentum numbers (SMN) that coincide with the motifs used in the ABA, and enabling us to compute the Hilbert space representation of the free spinons and their single momenta spectrum.

The formalism found by Greiter and Schuricht works as follows. For our system, the Hilbert space can be decomposed into a representation of the total spin ($\mathbf{S}_{\text{tot}}$). Since this operator commutes with the Hamiltonian described in the Eq. (3.2), we can classify this decomposition by the energy eigenstates. This representation can be expressed in terms of Young tableaux, which give us a set of tableaus that depict an irreducible representation of SU(2). The procedure to obtain the tableaus works as follow: each spin is represented by a box numbered, then the Hilbert space is build by the tensor product of these boxes. For instance, a system with two spins is composed by boxes as follows

$$\boxed{1} \otimes \boxed{2} \,. \tag{3.15}$$

The SU(2) representation is constructed by putting the boxes together such as the numbers assigned to them increase in each row from left to right and in each column from top to bottom. Each tableau obtained in this way represents an irreducible representation of SU(2). For our example, the Young tableaux for two spins as given by the direct sum is

$$\boxed{1} \otimes \boxed{2} = \underbrace{\begin{array}{|c|}\hline 1 \\ \hline 2 \\ \hline \end{array}}_{S=0} \oplus \underbrace{\begin{array}{|c|c|}\hline 1 & 2 \\ \hline \end{array}}_{S=1} \tag{3.16}$$

where the tableaux represent a basis composed by a singlet state ($S = 0$) and a triplet state ($S = 1$). The boxes distribution indicates symmetrization over all boxes in the same row, and antisymmetrization over all boxes in the same column,

which implies that we cannot have more than 2 boxes on each column, because exists just one possibility to antisymmetrize states composed by spin-1/2. In our example we have that the first tableau represents a singlet because the two boxes are in the same column, then the state have to be antisymmetrized. Using the spin quantum numbers (the total spin S and the z-spin component S^z) and the spin distribution to describe any state, we summarized the previous observation as follows

$$\underbrace{\begin{array}{|c|}\hline 1 \\ \hline 2 \\ \hline \end{array}}_{S=0} \equiv |S=0, S^z=0\rangle \equiv |\uparrow\downarrow\rangle - |\downarrow\uparrow\rangle \tag{3.17}$$

For $N = 4$, the Young tableaux are given by direct sums as follows

$$\begin{array}{|c|}\hline 1 \\ \hline \end{array} \otimes \begin{array}{|c|}\hline 2 \\ \hline \end{array} \otimes \begin{array}{|c|}\hline 3 \\ \hline \end{array} \otimes \begin{array}{|c|}\hline 4 \\ \hline \end{array} = \left\{ \begin{array}{l} \begin{array}{|c|c|}\hline 1 & 3 \\ \hline 2 & 4 \\ \hline \end{array} \oplus \begin{array}{|c|c|c|}\hline 1 & 2 & 4 \\ \hline 3 \\ \cline{1-1} \end{array} \oplus \\ \begin{array}{|c|c|}\hline 1 & 2 \\ \hline 3 & 4 \\ \hline \end{array} \oplus \begin{array}{|c|c|c|}\hline 1 & 2 & 3 \\ \hline 4 \\ \cline{1-1} \end{array} \oplus \\ \begin{array}{|c|c|c|}\hline 1 & 3 & 4 \\ \hline 2 \\ \cline{1-1} \end{array} \oplus \begin{array}{|c|c|c|c|}\hline 1 & 2 & 3 & 4 \\ \hline \end{array} \end{array} \right. \tag{3.18}$$

where we can see that each tableau has up to two rows.

Now, we will introduce the modified Young tableaux, which create a one-to-one correspondence between the Young tableaux and the non-interacting spinon states. For each Young tableau we shift boxes to the right such as each box is below or in the column to the right of the box with the preceding number. Each missing box in the resulting extended tableau represents a spinon, to which we assign a spinon momentum number (SMN) a_i given by the number in the same column. This number is the main feature of the one-to-one correspondence by the single spinon momenta given by

$$p_i = \frac{\pi}{N}\left(a_i - \frac{1}{2}\right). \tag{3.19}$$

The modification of the Young tableaux described above, give us the complete set of pseudomomenta that provides us with the solution of the HSM for a complete

description of each supermultiplet. In Table (3.1), we can see the Young tableaux and their modifications for $N = 4$, including the SMN and the total energy related to the ground-state $\Delta E = E_i - E_0$.

Table 3.1: *Spectrum for $N = 4$ including the SU(2) Young tableaux, the total spin $\mathbf{S}_{\text{tot}}$ and its degeneracy (deg), the modified Young tableaux (MYT), the spinon momentum number (SMN) and its relative energy ΔE.*

Young Tab.	$\mathbf{S}_{\text{tot}}$ (deg)	MYT	SMN $\{a_i\}$	$\Delta E/E_0$
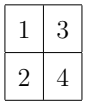	0 (1)	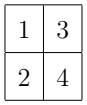	–	0
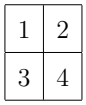	0 (1)	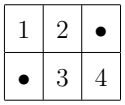	$\{1,4\}$	2
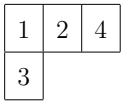	1 (3)	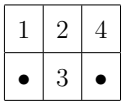	$\{1,4\}$	2
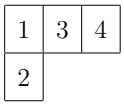	1 (3)	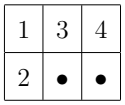	$\{3,4\}$	3
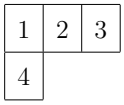	1 (3)	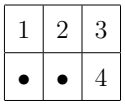	$\{1,2\}$	3
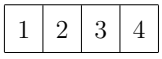	2 (5)	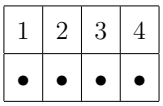	$\{1,2,3,4\}$	6

Using this approach, we can summarize the information required to describe the whole spectrum of the HSM for any chain size. To finish this section, we show in the Tables (3.2), (3.3) and (3.4) the spectrum for $N = 4$, 6 and 8 sites, respectively, given by the SU(2) configuration, the SMN distribution $\{a_i\}$ and the energy ΔE of each supermultiplet.

Table 3.2: *Eigenstates characterization of the HSM for $N = 4$ sites.* n *labels the supermultiplets described by its SU(2) representation, the spinon momentum number distribution $\{a_i\}$ and their energy difference from the ground-state. We have 4 different supermultiplets.*

n	SU(2)	$\{a_i\}$	$\Delta E/E_0$
0	0	–	0
1	$0 \oplus 1$	$\{1, 4\}$	2
2	1	$\{1, 2\}$	3
2	1	$\{3, 4\}$	3
3	2	$\{1, 2, 3, 4\}$	6

Table 3.3: *Eigenstates characterization of the HSM for $N = 6$ sites.* n *labels the supermultiplets, which are described by its SU(2) representation, the spinon momentum number distribution $\{a_i\}$ and their energy difference from the ground-state. We have 9 different supermultiplets.*

n	SU(2)	$\{a_i\}$	$\Delta E/E_0$
0	0	–	0
1	$0 \oplus 1$	$\{1, 6\}$	2
2	1	$\{1, 2\}$	10/3
2	1	$\{5, 6\}$	10/3
3	$0 \oplus 1$	$\{1, 4\}$	4
3	$0 \oplus 1$	$\{3, 6\}$	4
4	1	$\{3, 4\}$	6
5	$0 \oplus 1 \oplus 2$	$\{1, 2, 5.6\}$	20/3
6	$1 \oplus 2$	$\{1, 4, 5, 6\}$	22/3
6	$1 \oplus 2$	$\{1, 2, 3, 6\}$	22/3
7	2	$\{3, 4, 5, 6\}$	28/3
7	2	$\{1, 2, 3, 4\}$	28/3
8	3	$\{1, 2, 3, 4, 5, 6\}$	38/3

Table 3.4: *Eigenstates characterization of the HSM for $N = 8$ sites.* n *labels the supermultiplets, which are described by its SU(2) representation, the spinon momentum number distribution $\{a_i\}$ and their energy difference from the ground-state. There are 19 supermultiplets in this case.*

n	SU(2)	$\{a_i\}$	$\Delta E/E_0$	n	SU(2)	$\{a_i\}$	$\Delta E/E_0$
0	0	–	0	10	$1 \oplus 2$	$\{3,6,7,8\}$	21/2
1	$0 \oplus 1$	$\{1,8\}$	2	10	$1 \oplus 2$	$\{1,2,3,6\}$	21/2
2	1	$\{1,2\}$	7/2	11	$0 \oplus 1 \oplus 2$	$\{3,4,7,8\}$	11
2	1	$\{7,8\}$	7/2	11	$0 \oplus 1 \oplus 2$	$\{1,2,5,6\}$	11
3	$0 \oplus 1$	$\{3,8\}$	9/2	11	2	$\{5,6,7,8\}$	11
3	$0 \oplus 1$	$\{1,6\}$	9/2	11	2	$\{1,2,3,4\}$	11
4	$0 \oplus 1$	$\{5,8\}$	5	12	$1 \oplus 2$	$\{3,4,5,8\}$	25/2
4	$0 \oplus 1$	$\{1,4\}$	5	12	$1 \oplus 2$	$\{1,4,5,6\}$	25/2
5	$0 \oplus 1$	$\{3,6\}$	7	13	$0 \oplus 1 \oplus 2 \oplus 3$	$\{1,2,3,6,7,8\}$	14
5	$0 \oplus 1 \oplus 2$	$\{1,2,7,8\}$	7	14	$1 \oplus 2 \oplus 3$	$\{1,2,5,6,7,8\}$	29/2
6	1	$\{3,4\}$	15/2	15	2	$\{3,4,5,6\}$	15
6	1	$\{5,6\}$	15/2	16	$1 \oplus 2 \oplus 3$	$\{1,2,3,4,7,8\}$	16
7	$1 \oplus 2$	$\{1,6,7,8\}$	8	16	$2 \oplus 3$	$\{1,4,5,6,7,8\}$	16
7	$1 \oplus 2$	$\{1,2,3,8\}$	8	16	$2 \oplus 3$	$\{1,2,3,4,5,8\}$	16
8	$0 \oplus 1 \oplus 1 \oplus 2$	$\{1,4,7,8\}$	17/2	17	3	$\{3,4,5,6,7,8\}$	37/2
8	$0 \oplus 1 \oplus 1 \oplus 2$	$\{1,2,5,8\}$	17/2	17	3	$\{1,2,3,4,5,6\}$	37/2
9	$0 \oplus 1 \oplus 1 \oplus 2$	$\{1,4,5,8\}$	10	18	4	$\{1,2,3,4,5,6,7,8\}$	22

This model is integrable and exactly solvable even for chains with finite length, allowing us to derive an explicit wave-function for the ground-state and their elementary spinon excitations [7]. An interesting discussion about the physics of these excitations was developed in the last decades. Bernevig *et al.* [64] studied the spinon-spinon scattering matrix for the two spinon wave-function and found effects of the interaction between the spinons. Later on, Greiter and Schuricht [62] made a critical revision, and found that the interaction effects are in fact due to the fractional statistics (Yangian statistics) of free particles, which results in non-trivial quantization rules for a single spinon momenta, which are linked with the approach previously discussed.

3.3 The chiral interaction

In this section, we will introduce a new model given by HSM plus the z-component of the rapidity operator $\mathbf{\Lambda}$ given by the eq. (3.4), which acts as a long-range chiral interaction. The chiral Hamiltonian reads as follows

$$H^{HS-Ch} = H^{HS} + D\left(\frac{\pi}{N}\right)^2 \Lambda^3, \tag{3.20}$$

where D is a real number that modulates the interaction strength, and Λ^3 is the z-component of the rapidity operator, i.e.,

$$\Lambda^3 \equiv \mathbf{\Lambda} \cdot \hat{z}. \tag{3.21}$$

In the previous section, we showed how the whole spectrum of the HSM can be described using a SU(2) representation of free-spinons provided by the MYT. Although this picture diagonalizes the HSM, it cannot solve the chiral Hamiltonian H^{HS-Ch}. In fact, the commutation relation given by eq. (3.6) show us that the rapidity interaction does not commute with the spin operator and then it is impossible to find a common basis between SU(2) and Λ^z. In fact, the rapidity interaction is a generator of the Yangian algebra (Y(sl_2)), which describes both the HSM and the rapidity.

Schuricht [9] visualized the problem about the kind of states that the MYT gives us, and he extended the description, previously developed, by means of the Yangian Y(sl_2) representation over the spinon distributions, which can be described by the spectral parameter of the representation that are related with the previous SMN findings. The key ingredient is the identification of the Yangian Highest Weight State (YHWS) of each representation and the construction of the other states from that, which will be discussed below.

First, we will develop a numerical approach based on exact diagonalization, including a discussion about the eigenstates and the energy distribution after the rapidity interaction was turned on. Next, we summarize the representation theory of the Yangian algebra Y(sl_2), applying it to the spectrum of $N = 4$. Finally we summarize our results and discuss the outcomes in the large-size limit ($N \to \infty$).

3.3.1 Numerical approach

In this section, we present the numerical results by exact diagonalization of the HSM with the rapidity interaction presented above. We studied chains with $N = 4,\ 6$ and 8 spin-1/2, homogeneously distributed in a unit-circle in the complex plane. The whole spectrum of each chain will be labeled by the supermultiplet (n) and the Λ^z expectation value, as well as by the total spin S and its z-component through the kets $|n, S, S^z, \Lambda^z\rangle$. Furthermore, we will study the parameters where the ground-state transition takes place and discuss the projection of the eigenstates onto a suitable SU(2) basis, which describes the spectrum of the HSM but it is not useful when the rapidity interaction is added.

Finite chain for N = 4 sites:

The HSM spectrum with $N = 4$ spin-1/2 is composed by 4 supermultiplets. The ground-state ($n = 0$) is a singlet, while the excited states are degenerated, composed by 4, 6 and 5 states, respectively. The projection in a SU(2) basis show us that the 1st excited state ($n = 1$) is composed by a singlet plus a triplet ($S = 0 \oplus 1$), the 2nd excited state by two triplets ($S = 1 \oplus 1$) and the 3rd excited state by a quintet ($S = 2$) in agreement with theoretical results previously discussed using the MYT. See Table 3.2. While the representation above allow us to describe the HSM spectrum it is not useful when the rapidity interaction is added, where the degenerate states of each supermultiplet split, turning the spin not a good quantum number. The split is handled by the Λ^z expectation value and its effect can be seen in Fig. (3.2). We found that the ground-state and the 3rd supermultiplet have a rapidity expectation value equal to zero. For the 2nd supermultiplet we found that each triplet is outlined independently. One of them is described by the states $|2, 1, 1, 1\rangle$, $|2, 1, 0, 0\rangle$, $|2, 1, -1, -1\rangle$, and the other by the states $|2, 1, 1, -1\rangle$, $|2, 1, 0, 0\rangle$, $|2, 1, -1, 1\rangle$, where we should pay attention in how the rapidity expectation has opposite signs between two states with the same S^z. Similarly, we found that two states with $S^z = 0$ split in the 1st supermultiplet, while two other states do not split. The last two states are $|1, 1, \pm 1\rangle$, while the splitted states are a linear combination of two states with $S^z = 0$, with

different total spin and $|\langle\Lambda^z\rangle| = \sqrt{2}$. The linear combination is given by

$$|1,0\oplus 1,0,-\sqrt{2}\rangle = \frac{1}{\sqrt{2}}\left(|1,0,0\rangle - i|1,1,0\rangle\right) \tag{3.22}$$

$$|1,0\oplus 1,0,\sqrt{2}\rangle = \frac{1}{\sqrt{2}}\left(|1,0,0\rangle + i|1,1,0\rangle\right) \tag{3.23}$$

where in the right hand we have written the states with the SU(2) basis representation. $|n,S,S^z\rangle$.

The whole spectrum, including the split can be seen in the Fig. (3.2).

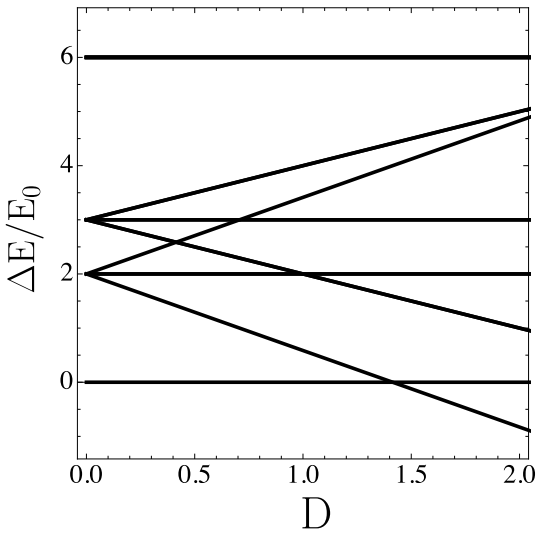

Fig. 3.2: *Level splittings of the HSM supermultiplets, as a function of D for $N = 4$.*

The split observed in the energy spectrum allows us to identify a ground-state transition. In fact, we observe that since the ground-state of the HSM is not perturbed with the rapidity interaction, the state $|1,0\oplus 1,0,-\sqrt{2}\rangle$ turns into the ground state for a specific value of the interaction strength D. Let the ground-states of this model be given by

$$|GS,1\rangle = |0,0,0\rangle \tag{3.24}$$

$$|GS,2\rangle = \frac{1}{\sqrt{2}}\left(|1,0,0\rangle - i|1,1,0\rangle\right) \tag{3.25}$$

The energy of the ground-state can be represented as following

$$E_{GS}(D) = \begin{cases} E_0 & D < D_1 \\ E_1 - \left(\frac{\pi}{N}\right)^2 D\lambda_1^z & D \geq D_1 \end{cases} \tag{3.26}$$

where $E_0 = -\frac{7}{2}\frac{\pi^2}{N^2}$ is the energy of the HS ground-state ($n = 0$), until $D_1 \approx 1.41421$, and $E_1 = -\frac{3}{2}\frac{\pi^2}{N^2}$ is the energy of the first excited ($n = 1$) state, and $-\left(\frac{\pi}{N}\right)^2\sqrt{2}$ is the expectation value of the rapidity interaction in the state $|GS, 2\rangle$.

D_1 can be found numerically if we know the HSM spectrum and the splitting. For the system with $N = 4$ we know that $E_0 = -\frac{7}{2}\frac{\pi^2}{N^2}$ and $E_1 = -\frac{3}{2}\frac{\pi^2}{N^2}$, then D_1 can be expressed as follows

$$D_1 = \frac{E_1 - E_0}{\sqrt{2}(\pi/N)^2} = \frac{2(\pi/N)^2}{\sqrt{2}(\pi/N)^2} = \sqrt{2} \approx 1.41421 \tag{3.27}$$

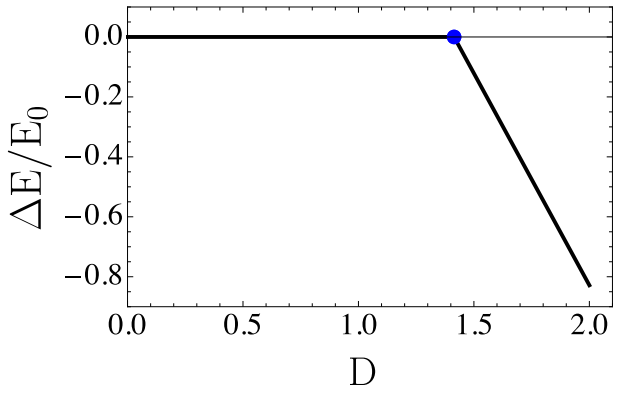

Fig. 3.3: *Ground-state energy as a function of D for $N = 4$. There is a crossing of levels at $D = D_1 = 1.41421$, from $|GS, 1\rangle$ to $|GS, 2\rangle$.*

Finite chain for N = 6 sites:

The HSM spectrum with $N = 6$ spins is composed by 9 supermultiplets (labeled by $n = 0, \ldots, 8$). The ground-state is a singlet, while the rest of the spectrum is composed by degenerate states that split when the rapidity interaction is added. The degeneracies of these states are 4, 6, 8, 3, 9, 16, 10, and 7, respectively. The SU(2) representations of these states are the same that those given by the MYT approach. For instance, the first supermultiplet is composed by a singlet and a triplet ($0 \oplus 1$), states previously discussed for $N = 4$ and in the description of the MYT. The whole spectrum including the splitting due to the interaction can be seen in the Fig. (3.4).

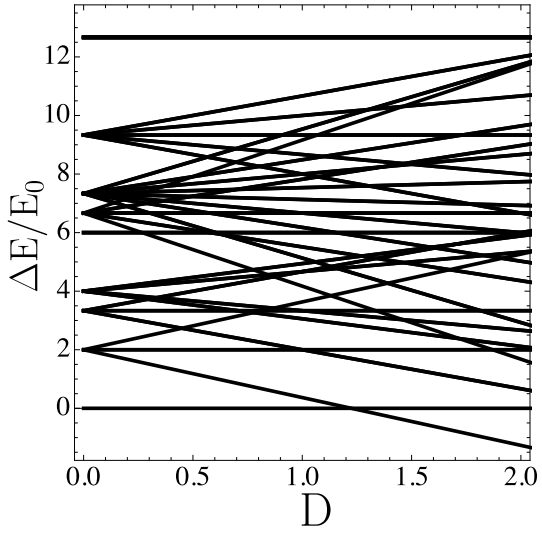

Fig. 3.4: *Level splittings of the HS supermultiplets, as a function of D for $N = 6$.*

In this system, we observe two ground-state transitions. Numerically, we found that the first transition occurs at $D_1 = 0.6413$, while the second is at $D_2 = 2.8364$. The S and S_z expectation values of the ground-states have similar behaviors as the system with $N = 4$: the total spin S grows in steps, and S_z is always zero. This observation can be seen in figure 3.5.

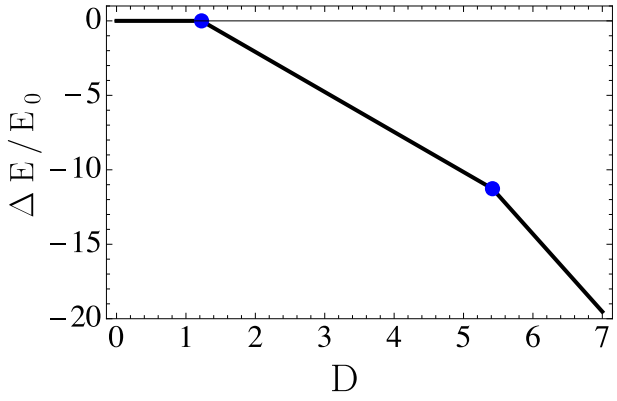

Fig. 3.5: *Ground-state as a function of D for $N = 6$. There are level crossings at $D_1 = 1.11072$ and $D_2 = 2.8364$, from $|GS, 1\rangle$ to $|GS, 2\rangle$ and $|GS, 3\rangle$.*

The different ground-states can be represented as following:

$$|GS,1\rangle = |0,0,0\rangle \tag{3.28}$$

$$|GS,2\rangle = \frac{1}{\sqrt{2}}\left(|1,0,0\rangle - i|1,1,0\rangle\right) \tag{3.29}$$

$$|GS,3\rangle = \frac{1}{\sqrt{2}}\left(|5,0\oplus 2,0\rangle - i|5,1,0\rangle\right) \tag{3.30}$$

We found that the 3rd ground-state is a linear combination of states $|5,1,0\rangle$ and $|5,0\oplus 2,0\rangle$, while the latter state is a linear combination of $|5,0,0\rangle$ and $|5,2,0\rangle$. It shows us that the basis that we built is not a good representation for the chiral model, because it mixes states with different total spin.

Numerically, we found that the linear combination of mixed state $|5,0\oplus 2,0\rangle$ is given by

$$|5,0\oplus 2,0\rangle = -\sqrt{\frac{5}{7}}|5,0,0\rangle - \sqrt{\frac{2}{7}}|5,2,0\rangle. \tag{3.31}$$

In the previous subsection, we showed how to compute the value D where the ground-state transition occurs. Using this procedure, we calculated an analytic expression to the energy of the ground-state transition to find the values of D where this occurs. The energy can be written as

$$E_{GS}(D) = \begin{cases} E_0 & D \leq D_1 \\ E_1 - \left(\frac{\pi}{N}\right)^2 D\lambda_1^z & D_1 \leq D \leq D_2 \\ E_5 - \left(\frac{\pi}{N}\right)^2 D\lambda_5^z & D_2 \leq D \end{cases} \tag{3.32}$$

where E_0 is the energy of the HSM ground-state, E_1 and E_5 are the HSM eigenenergies of the supermultiplets $n=1$ and $n=5$, respectively. Expressions $-\left(\frac{\pi}{N}\right)^2\lambda_1^z$ and $-\left(\frac{\pi}{N}\right)^2\lambda_5^z$ are the expectation values of the rapidity interaction to the first and fifth excited states, where $\lambda_1^z = \sqrt{6}$ and $\lambda_5^z = \sqrt{14}$. As we said before, we can calculate the exact value of D for each transition. A general expression can be deduced to find the value of D between two different ground-states A and B, as following

$$D_{A\to B} = \frac{E_A - E_B}{(\pi/N)^2(\lambda_A^z - \lambda_B^z)}. \tag{3.33}$$

For our system, we know that $E_i = (\pi/N)^2\epsilon_i$ for supermultiplet i, and in the transition $E_B > E_A$, that is $\lambda_B^z > \lambda_A^z$. The last inequality allows us to create an algorithm

to find the HSM supermultiplet that has a combination of HSM eigenstates which is going to be a ground-state of the full system.

Equation (3.33) can be rewritten as follows

$$D_{A\to B} = \frac{\epsilon_B - \epsilon_A}{\lambda_B^z - \lambda_A^z} \tag{3.34}$$

For the system with $N = 6$, we have: $\epsilon_0 = -41/4$, $\epsilon_1 = -29/4$, $\epsilon_5 = -1/4$, $\lambda_0 = 0$, $\lambda_1 = \sqrt{6}$, $\lambda_5 = \sqrt{14}$, then

$$D_1 = \frac{-29/4 + 41/4}{\sqrt{6} - \sqrt{0}} = \sqrt{\frac{3}{2}} \approx 1.22474 \tag{3.35}$$

$$D_2 = \frac{-1/4 + 29/4}{\sqrt{14} - \sqrt{6}} = \frac{7}{\sqrt{14} - \sqrt{6}} \approx 5.41725 \tag{3.36}$$

Finite chain for N = 8 sites:

For $N = 8$ sites we have 19 supermultiplets. Their degeneracies are 1, 4, 6, 8, 8, 13, 6, 16, 24, 12, 16, 28, 16, 16, 30, 5, 24, 14, 9, respectively. Their energies and the SU(2) description match with the one given by MYT. The whole spectrum can be observed in Figure 3.6.

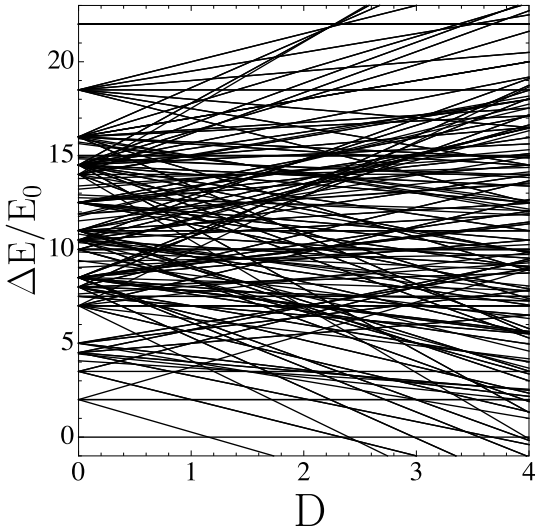

Fig. 3.6: *Level splittings of the HS supermultiplets, as a function of D for $N = 8$.*

In this system we observe that the ground-state has three transition points, characterized by the following $D_1 = 0.4534$, $D_2 = 1.6591$ and $D_3 = 4.523$, while $S_z = 0$ for all ground-states.

To build the ground-state SU(2) composition, we used the information collected in the previous subsections. The three first states have the same structure that the systems with $N = 4$ and $N = 6$, but different values of λ^z (0, 12 and 34, respectively). The ground-states are given by

$$
\begin{aligned}
|GS,1\rangle &= |0,0,0\rangle && (3.37)\\
|GS,2\rangle &= \frac{1}{\sqrt{2}}\left(|1,0,0\rangle - i|1,2,0\rangle\right) = \frac{1}{\sqrt{2}}\left(i|1,0,0\rangle + |1,2,0\rangle\right) && (3.38)\\
|GS,3\rangle &= \frac{1}{\sqrt{2}}\left(|5,0?6,0\rangle - i|5,2,0\rangle\right) = \frac{1}{\sqrt{2}}\left(i|5,0?6,0\rangle + |5,2,0\rangle\right) && (3.39)\\
|GS,4\rangle &= \frac{1}{\sqrt{2}}\left(|13,2?12,0\rangle - i|13,0?6,0\rangle\right)\\
&= \frac{1}{\sqrt{2}}\left(i|13,2?12,0\rangle + |13,0?6,0\rangle\right) && (3.40)
\end{aligned}
$$

The states $|13,2?12,0\rangle$ and $|13,0?6,0\rangle$ have the following linear combination of HSM eigenstates:

$$
\begin{aligned}
|13,2?12,0\rangle &\approx -0.250807|13,2,0\rangle - 0.968037|13,12,0\rangle && (3.41)\\
|13,0?6,0\rangle &\approx -0.75248|13,0,0\rangle - 0.658615|13,6,0\rangle && (3.42)
\end{aligned}
$$

The expectation value of $(\Lambda^z)^2$ for $|GS,4\rangle$ is now not an integer number, but interesting results are observed in the supermultiplet 13 that host these states. In the HSM supermultiplet $n = 13$, we have a set of eigenstates that has the same S_z expectation value. Here, we have two linear combinations that create two eigenstates with different values of $\langle\Lambda^z\rangle$ where the sum of these squared is an integer number, which in this case is equal to 54. For the ground-state of phase four, we have $\lambda_4^z \approx -7.04624$ that has a partner eigenstate with $\lambda \approx -2.08578$.

Using the equation (3.34) we can identify a numerical expression for the parameter D in the different ground-state transitions. If $\epsilon_0 = -23$, $\epsilon_1 = -19$, $\epsilon_2 = -9$ and $\epsilon_3 = 5$, we obtain that

$$D_1 = \frac{-23+19}{\sqrt{0}-\sqrt{12}} = \frac{2}{\sqrt{3}} \approx 0.4534 \tag{3.43}$$

$$D_2 = \frac{-19+9}{\sqrt{12}-\sqrt{34}} = \frac{10}{\sqrt{34}-2\sqrt{3}} \approx 1.6591 \tag{3.44}$$

$$D_3 = \frac{-9-5}{\sqrt{34}-7.04624} \approx 11.5199 \tag{3.45}$$

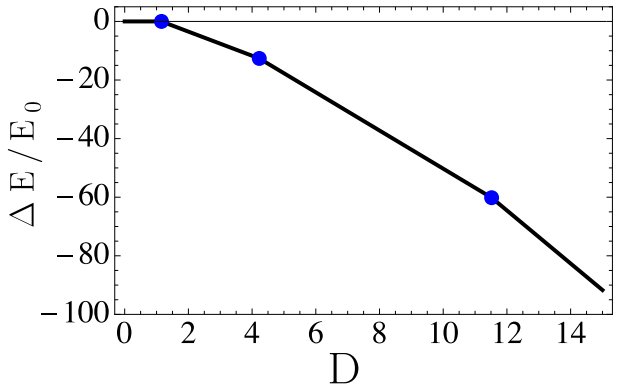

Fig. 3.7: *Ground-state energy as a function of D for $N = 8$. The ground-state transitions occur for $D_1 = 0.4534$, $D_2 = 1.6591$ and $D_3 = 11.5199$*

3.3.2 Early conclusion

In this subsection, we have shown a numerical description of finite chains of spin-1/2 whose interaction is described by the chiral Hamiltonian (3.20). We observed that the degeneracy in each supermutliplet is splitted, mixing the total spin component of the state previously described by a SU(2) representation obtained by the MYT. Althought S^z is a good quantum number, the formalism developed by Greiter and Schuricht [63], and discussed in the sections above, is not suitable to study our chiral model, as we observed on the ground-state description. The main outcome of this section was the description of the ground-state transitions. The splitting due to the rapidity interaction enable the system to have ground-state transitions. The different ground-states are characterized by a null S^z expectation value and they come from specific supermultiplets of HSM, as long as the chain size increases.

The split on each supermultiplet and the fact that a SU(2) description is not useful to characterize the splitted state, give us arguments to introduce a description using the Yangian $\mathrm{Y}(sl_2)$ algebra, which also describe the HSM spectrum in a different way that the SU(2) basis given by the MYT. In the next section we will follow a representation theory approach of the Yangian algebra, developed in [9] by Schuricht.

3.3.3 Analytical approach

In this section, we present the representation theory of the Yangian algebra $\mathrm{Y}(sl_2)$ to describe the spectrum of the HS model with a rapidity interaction following the approach of Schuricht [9]. The numerical calculation showed us that the states split when the interaction is turn on. The split is driven by the expectation value of Λ^z, which can be computed theoretically using the representation theory of $\mathrm{Y}(sl_2)$. This approach maps the Hilbert space of HSM into independent descriptions of the elementary excitations using the Yangian, where each representation is described by their respective spectral parameters. (For more details see [65]).

Let us start summarizing the Yangian algebra for spin-1/2 ($\mathrm{Y}(sl_2)$). It is composed by an orthonormal basis given by $S^a = \sigma^a/2$, where σ^a are the Pauli matrices with $a = 1, 2, 3$. The $\mathrm{Y}(sl_2)$ is a infinite-dimensional associative algebra over $\mathbb{C}$ generated by the elements S^a and Λ^a, with the following relations

$$[S^a, S^b] = i\epsilon^{abc} S^c \tag{3.46}$$

$$[S^a, \Lambda^b] = i\epsilon^{abc} \Lambda^c \tag{3.47}$$

where ϵ^{abc} is the Levi-Civita symbol. On the other hand, $\mathrm{Y}(sl_2)$ has a Hopf algebra structure with comultiplications $\Delta : \mathrm{Y}(sl_2) \to \mathrm{Y}(sl_2) \otimes \mathrm{Y}(sl_2)$ given by

$$\Delta(S^a) = S^a \otimes 1 + 1 \otimes S^a, \tag{3.48}$$

$$\Delta(\Lambda^a) = \Lambda^a \otimes 1 + 1 \otimes \Lambda^a - i\epsilon^{abc} S^b \otimes S^c. \tag{3.49}$$

The representation theory of the Yangian can be understood naively as a set of states sorted by the *weight* given by the Laurent expansion of a monic polynomial

known as Drinfel'd polynomial [9, 66]. The weight of the first state in this set depends on the spectral parameters that describe the representation. This state is known as the Yangian Highest Weight State (YHWS) and is the main element on the representation.

Let us apply this algebra in the most simple case for spin-1/2: a single spinon basis, which corresponds to two-dimensional Yangian representation, with a spectral parameter ξ, denoted by $V(\mathbf{\frac{1}{2}}, \xi)$. Let $\{|\uparrow\rangle, |\downarrow\rangle\}$ be the basis of our two-dimensional space. The YHWS of this representation is the state $|\uparrow\rangle$, which is described as follows

$$S^z|\uparrow\rangle = \frac{1}{2}|\uparrow\rangle, \quad S^+|\uparrow\rangle = 0, \quad S^-|\uparrow\rangle = |\downarrow\rangle$$
$$\Lambda^z|\uparrow\rangle = \frac{\xi}{2}|\uparrow\rangle, \quad \Lambda^+|\uparrow\rangle = 0, \quad \Lambda^-|\uparrow\rangle = 2\xi|\downarrow\rangle.$$

By completeness, the state $|\downarrow\rangle$ is described by

$$S^z|\downarrow\rangle = -\frac{1}{2}|\downarrow\rangle, \quad S^+|\downarrow\rangle = |\uparrow\rangle, \quad S^-|\downarrow\rangle = 0$$
$$\Lambda^z|\downarrow\rangle = -\frac{\xi}{2}|\downarrow\rangle, \quad \Lambda^+|\downarrow\rangle = \xi|\uparrow\rangle, \quad \Lambda^-|\downarrow\rangle = 0.$$

Schuricht [9] found the connection between this spectral parameter and the spinon momentum number (SMN) given by the Modified Young Tableaux (MYT). The Modified Young Tableaux for one spinon is described by a SMN a. This number is linked with the expectation value of Λ^z by the expression

$$\Lambda^z|\uparrow\rangle = \frac{1}{2}\left(a - \frac{N+1}{2}\right)|\uparrow\rangle \tag{3.50}$$

where N is the size of the spin chain. The expression above enable us to map the complete spectrum for each MYT using the representation theory of $\mathrm{Y}(sl_2)$.

For the two spinons case, the Yangian representation can be build by the tensor product of two single-spinon representation with different spectral parameter, $V_1 \otimes V_2 = V(\mathbf{\frac{1}{2}}, \xi_1) \otimes V(\mathbf{\frac{1}{2}}, \xi_2)$. Although the YHWS of this representation is given by the $v_1 \otimes v_2$, where v_i is the respective YHWS of V_i, the tensor product between V_1 and V_2 is not isomorphic, therefore the other states are not easy to build. In fact, since the

comultiplication relation given by the Eqs. (3.48) and (3.49) are not commutative, the expectation value of $\mathrm{Y}(sl_2)$ operators does not have a simple structure.

Now, we will show how the two spinons representation is build by the tensor product of two single spinon and the comultiplication relation. Let us start with the YHWS of this space, which is given by $|\uparrow\uparrow\rangle = |\uparrow\rangle \otimes |\uparrow\rangle$ and characterized by

$$S^+|\uparrow\uparrow\rangle = \Lambda^+|\uparrow\uparrow\rangle = 0. \tag{3.51}$$

Using the comultiplication relation described in Eq. (3.49), we can find that

$$\Lambda^z|\uparrow\uparrow\rangle = \lambda^z|\uparrow\uparrow\rangle \tag{3.52}$$

$$S^z|\uparrow\uparrow\rangle = |\uparrow\uparrow\rangle. \tag{3.53}$$

where $\lambda_z = \xi_1/2 + \xi_2/2$. $\xi_i = a_i - (N+1)/2$ for a_i read from the MYT with $a_2 > a_1$.

This state is also eigenstate of both HSM and the chiral model to each set of SMN extracted from the MYT. Moreover, the other state that is also eigenstate of the chiral model, and the HSM too, can be found by means of the Yangian algebra. For instance, Schuricht [9] describe the spectrum when $a_2 - a_1 = 1$, finding that a singlet state is part of the basis. Next, we will extend this results for any $\delta = a_2 - a_1 \geq 1$, where we will see that the singlet state is just a limiting case.

Let us start to study the state $S^-|\uparrow\uparrow\rangle$, which turns down one spinon forming a singlet as follows

$$S^-|\uparrow\uparrow\rangle = |\downarrow\uparrow\rangle + |\uparrow\downarrow\rangle \tag{3.54}$$

where we used the comultiplication relation given by Eq. (3.49). While the z-spin component of this state is zero, hence is an eigenstate of S^z, the expectation value of Λ^z is a linear combination of two elements of the algebra. In fact, using the commutation relation $[\Lambda^z, S^-] = -\Lambda^-$, we found that

$$\Lambda^z S^-|\uparrow\uparrow\rangle = -\Lambda^-|\uparrow\uparrow\rangle + \lambda^z S^-|\uparrow\uparrow\rangle, \tag{3.55}$$

where

$$\Lambda^-|\uparrow\uparrow\rangle = (2\lambda_1^z + 1/2)|\downarrow\uparrow\rangle + (2\lambda_2^z - 1/2)|\uparrow\downarrow\rangle. \tag{3.56}$$

We can see that $\Lambda^-|\uparrow\uparrow\rangle \propto S^-|\uparrow\uparrow\rangle$ just when $a_2 - a_1 = 1$ that corresponds to $\lambda_2^z - \lambda_1^z = 1/2$. In fact, we have that

$$\Lambda^-|\uparrow\uparrow\rangle = \lambda^z S^-|\uparrow\uparrow\rangle, \tag{3.57}$$

which allow us to identify the state $S^-|\uparrow\uparrow\rangle$ as an eigenstate of Λ^z with null expectation value.

Let us verify this result using the MYT for a 2nd supermultiplet of the HSM for $N = 4$. The SMNs are $a_2 = 4$ and $a_1 = 3$, which can be seen in Table 3.1. The tableau, which initially describes a triplet state, is a representation of three Yangian states, given by

- $|\uparrow\uparrow\rangle$, where $\langle\Lambda^z\rangle = 1$ and $\langle S^z\rangle = 1$ (YHWS),
- $S^-|\uparrow\uparrow\rangle$, where $\langle\Lambda^z\rangle = 0$ and $\langle S^z\rangle = 0$,
- $S^-S^-|\uparrow\uparrow\rangle$, where $\langle\Lambda^z\rangle = -1$ and $\langle S^z\rangle = -1$.

These results agree with the numerical approach, including the last state, which we will name Yangian Lowest Weight State (YLWS), that is build by applying S^- over the YHWS twice.

Now, we are going to study the states created by the YHWS with two spinons whose SMN satisfy $a_2 - a_1 > 1$. The Eq. (3.56) show us that these states have to be a combination of states given by the application of the operators S^- and Λ^- over YHWS.

Motivated by the splitting observed in our numerically approach, we will propose an educated guess given by the following state

$$|\lambda^-\rangle = aS^-|\uparrow\uparrow\rangle + b\Lambda^-|\uparrow\uparrow\rangle \tag{3.58}$$

where a and b are complex numbers. The eqs. (3.54) and (3.56) allow us to write the previous equation as

$$\begin{aligned} |\lambda^-\rangle &= (a + b(2\lambda_1^z + 1/2))\,|\downarrow\uparrow\rangle + (a + b(2\lambda_2^z - 1/2))\,|\uparrow\downarrow\rangle & (3.59)\\ &= \alpha\,|\downarrow\uparrow\rangle + \beta\,|\uparrow\downarrow\rangle & (3.60)\end{aligned}$$

This state has to be an eigenstate of the rapidity operator, and then an eigenstate of the chiral model, which is described by its eigenvalue

$$\Lambda^z|\lambda^-\rangle = \lambda^-|\lambda^-\rangle. \tag{3.61}$$

To expand the left hand of the equation above we need to use the relations

$$\Lambda^z|\downarrow\uparrow\rangle = \delta|\downarrow\uparrow\rangle + \frac{1}{2}|\uparrow\downarrow\rangle \tag{3.62}$$

$$\Lambda^z|\uparrow\downarrow\rangle = -\delta|\uparrow\downarrow\rangle - \frac{1}{2}|\downarrow\uparrow\rangle \tag{3.63}$$

$$\tag{3.64}$$

where $\delta = \lambda_2^z - \lambda_1^z$, and the comultiplication relation was used. Then we find that

$$\Lambda^z|\lambda^-\rangle = \left(\delta\alpha - \frac{\beta}{2}\right)|\downarrow\uparrow\rangle + \left(\frac{\alpha}{2} - \beta\delta\right)|\uparrow\downarrow\rangle = \lambda^-|\lambda^-\rangle \tag{3.65}$$

comparing with the state given in Eq. (3.60), we find the condition

$$\frac{\alpha}{\beta} = \frac{1}{2(\delta - \lambda^-)} = 2(\delta + \lambda^-) \tag{3.66}$$

which gives us the result

$$\lambda^- = \pm\sqrt{\delta^2 - \frac{1}{4}}\,. \tag{3.67}$$

This expression shows interesting features of the state $|\lambda^-\rangle$. First, if $\delta = 1/2$ then $\lambda^- = 0$, identifying the state $S^-|\uparrow\uparrow\rangle$ as an eigenstate, outcome that was discussed by Schuricht and summarized by us previously.

In general, $\lambda^- \neq 0$, taking two possible signs and describing two eigenstates. These states are a combination of states arising from two tableaux with the same set of SMN, such as the first excited state in the HSM with the rapidity interaction for any N.

Let us show how to build these states for the $N = 4$ case. The first excited state is described by two MYT, as we can seen in Table 3.1. The second tableau describes a triplet state (where YHWS is located), while the first tableau represents a singlet state. Both have the same set of SMN, $a_i = 1, 4$, and then belong to the same supermultiplet. For these SMN, $|\lambda^-| = \sqrt{2}$, describing two eigenstates with the same energy, the same z-spin component ($S^z = 0$) and with the same absolute

value of λ^-, but with opposite sign. This outcome can be observed in the spectrum of HSM with rapidity interaction for $N = 4$ (see fig. 3.2). Here, we can see how two states split from the 1st supermultiplet in *opposite* directions. These states are composed by a linear combination of two states with different total spin but the same z-component, in agreement with our analytic description. To complement this discussion, we found that $\lambda^z = 0$, then the YHWS and YLWS do not split, as we can see in our numerical results.

In summary, we found a general result that describes any representation with two spinons. The YHWS is described by the state $|\uparrow\uparrow\rangle$ and the YLWS by $S^-S^-|\uparrow\uparrow\rangle$. When $a_2 - a_1 > 1$ we found that the supermultiplet is represented by two tableaux, forming two states that are a linear combination of states with different total spin, which split with the same $|\lambda^-|$ but with opposite signs.

Since our model is composed by even numbers of spins, we will find tableaux with even numbers of spinons. We found that the 1st excited state will be always characterized by two tableaux with two spinons, which can be described by the discussion above.

$|\lambda^-\rangle$ for n-spinon state. – Let us proceed our discussion with a generalized $|\lambda^-\rangle$ state from a general n-spinon state, where n is an even number that describes the number of spinons in the representation. We will start defining the YHWS spinon state as

$$|\uparrow^{\otimes n}\rangle = |\underbrace{\uparrow ... \uparrow}_{n-spinon}\rangle. \tag{3.68}$$

The S^- operator over this state can be generalized as follows

$$S^-|\uparrow^{\otimes n}\rangle = \sum_{i=1}^{n} S_i^-|\uparrow^{\otimes n}\rangle \tag{3.69}$$

where the operator S_i^- turns down the i-th up-spinon. This result can be found applying the comultiplication relation recursively, keeping each operator on their single-spinon representation. This procedure allows us to write the comultiplication relation of S^- as

$$\Delta(S^-) = \sum_{i=1}^{n} S_i^- \tag{3.70}$$

where n is the number of spinons in this representation. In a similar way, we find that the operator Λ^- can be generalized as follows

$$\Delta(\Lambda^-) = \sum_{i=1}^{n} \Lambda_i^- - \sum_{i<j}^{n} S_i^z S_j^- + \sum_{i>j}^{n} S_i^- S_j^z. \tag{3.71}$$

Applying to the n-spinon state we find that

$$\Lambda^- | \uparrow^{\otimes n} \rangle = \sum_{i=1}^{n} \left(2\lambda_i^z + \kappa_i^n\right) S_i^- | \uparrow^{\otimes n} \rangle, \tag{3.72}$$

where $2\lambda_i^z = \xi_i$, the i-th spectral parameter, and κ_i^n is given by

$$\kappa_i^n = \frac{1}{2} \sum_{j=1}^{n} \theta_{ij}, \tag{3.73}$$

where $\theta_{ij} = sign(j - i)$.

Replaying the previous procedure, we propose the following state

$$|\lambda^-\rangle = (a\Lambda^- + bS^-) | \uparrow^{\otimes n} \rangle \tag{3.74}$$

where a and b are complex numbers, and $|\lambda^-\rangle$ is an eigenstate of Λ^z, whose eigenvalue equation gives two possible solutions: $\pm\lambda^-$. To find these values and the suitable a and b, we have to solve the following set of equations

$$(\lambda^- - \lambda^z + 2\lambda_i^z)(a + b(2\lambda_i^z + \kappa_i^n)) = -\frac{1}{2} \sum_{j=1}^{n} \theta_{ij}(a + b(2\lambda_j^z + \kappa_j^n)) \tag{3.75}$$

where each equation is labeled by the i-index that runs from $i = 1$ to n.

Although each equation can give the value of λ^-, this result is not complete because the normalization condition has not yet been satisfied. In fact, we found just two possible values for λ^-, with the same module but with opposite signs. This result shows an internal structure about the construction of eigenstates in each representation. While the YHWS (and the YLWS also) is only one, the other states come in pairs, coming from a suitable operator composed by a linear combination of Λ^- and S^-.

This linear combination is tailored by the distributions of the SMN, specially by their differences. For example, we have that the SMN distribution for the four

spinon state is $\{a_i\} = \{1, 2, 3, 4\}$. Here, we can observe that $a_{i+1} - a_i = 1 \ \forall \ i$, which implies that the rapidity expectation value is zero for the whole set of states describing the last tableau for $N = 4$. With this last comment we finish our analysis for $N = 4$. Larger clusters with even numbers follow the same analysis.

3.4 General comments

3.4.1 A large limit result

The exact solution of the HSM in the infinite limit is given by the Yangian symmetry the same as the Heisenberg model at the same limit. Entirely different is the finite size case, where the Heisenberg cannot be exactly solved using the Yangian algebra, while the HSM keeps that symmetry which supports the integrability up to the infinite system. This feature allows us to extrapolate the results previously presented in this chapter up to chains with infinite length. One feature of the solution took our attention related to the behavior of the system at the low energy level. We observed that the 1st supermultiplet is always characterized by two tableaux described by a two spinon state. The SMN of this tableaux are $\{a_i\} = \{1, N\}$, where N is the chain size. One state on this supermutliplet will become the ground-state, and its energy is given by

$$E_1 = E_0 + \frac{\pi^2}{2N} - D\frac{\pi^2}{2N^2}\sqrt{N(N-2)}. \tag{3.76}$$

Now, taking the limit $N \gg 1$, we obtain that the difference with the HSM ground-state is given by

$$\Delta E = E_1 - E_0 = \frac{\pi^2}{2N}(1 - D), \tag{3.77}$$

where we can see that the ground-state phase transition in the thermodynamic limit takes place when $D = 1$, as seen in Fig. (3.8). We also observe that the system is gapless in the thermodynamic limit, the gap closes as $\Delta E \sim 1/N$. This means that the symmetry of the HS model with chiral interaction does not change in that limit, having the same properties of the HS alone.

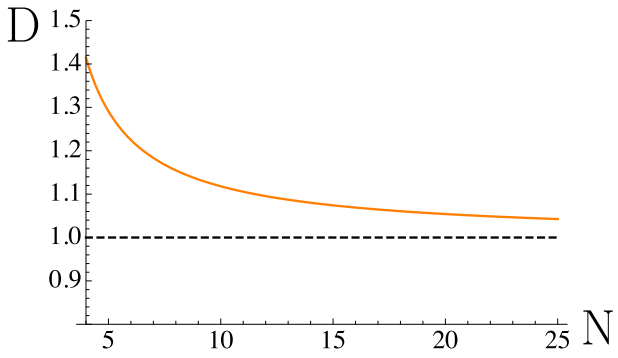

Fig. 3.8: *Critical D values for which the ground-state transition takes place as a function of the chain length. The large size limit value is $D = 1$.*

3.4.2 Spin chains with chiral medium-range interactions

The aim of this last section is to study a family of spin chains with a suitable chiral interaction, which is classified by its medium-range terms of the HSM. The range is related to the farther neighbor where the HSM will be truncated. For a chain with N spins, we have that the Heisenberg model has range 1, while the HSM has range N.

For useful comparison purposes, we fix the exchange interaction term among the different neighbor spins and the corresponding chiral interaction constant from the HSM and for the rapidity operator, respectively, by the truncation of the Hamiltonian and the interaction up to a specific range as follows. The HSM and the rapidity interaction can be rewritten as follows

$$H^{HS} = -\frac{4\pi^2}{N^2} \sum_{\alpha<\beta} \frac{z^\alpha z^\beta}{(z^\alpha - z^\beta)^2} \mathbf{S}_\alpha \cdot \mathbf{S}_\beta \tag{3.78}$$

$$\Lambda^z = -\frac{\pi^2}{N^2} i \sum_{\alpha<\beta} \frac{z^\alpha + z^\beta}{z^\alpha - z^\beta} \left(S^+_\alpha S^-_\beta - S^-_\alpha S^+_\beta \right) \tag{3.79}$$

where N is the number of spins that lie homogeneously distributed in the unit-circle in the complex plane, whose positions are $z^m = \exp(2\pi i m/N)$, from $m = 1$ to N.

We can split the Hamiltonian and gather their components by the distance, allowing us to study the effect of each part of the interaction. The nearest neighbors

(NN) interaction is given by $\beta = \alpha + 1$, obtaining the Heisenberg model with a suitable $J_1 = \frac{(\pi/N)^2}{\sin^2(\pi/N)}$. In this case the Hamiltonain is given by

$$H^{J_1} = \frac{(\pi/N)^2}{\sin^2(\pi/N)} \sum_{\alpha} \mathbf{S}_{\alpha} \cdot \mathbf{S}_{\alpha+1}. \tag{3.80}$$

In a similar way we obtain the coupling for the system with next nearest neighbor (NNN) interaction doing $\beta = \alpha + 2$. In this case the Hamiltonian is given by

$$H^{J_2} = \frac{(\pi/N)^2}{\sin^2(2\pi/N)} \sum_{\alpha} \mathbf{S}_{\alpha} \cdot \mathbf{S}_{\alpha+2} \tag{3.81}$$

The truncation of the rapidity interaction is developed in the same way as the HSM, where the terms for NN and NNN ranges take the following expressions

$$\Lambda^{z,J_1} = \frac{(\pi/N)^2}{\tan(\pi/N)} \sum_{\alpha} \left(S^+_{\alpha} S^-_{\alpha+1} - S^-_{\alpha} S^+_{\alpha+1} \right) \tag{3.82}$$

$$\Lambda^{z,J_2} = \frac{(\pi/N)^2}{\tan(2\pi/N)} \sum_{\alpha} \left(S^+_{\alpha} S^-_{\alpha+2} - S^-_{\alpha} S^+_{\alpha+2} \right). \tag{3.83}$$

A generalized l-range terms can be defined and they read as

$$H^{J_l} = \frac{(\pi/N)^2}{\sin^2(l\pi/N)} \sum_{\alpha} \mathbf{S}_{\alpha} \cdot \mathbf{S}_{\alpha+l} \tag{3.84}$$

$$\Lambda^{z,J_l} = \frac{(\pi/N)^2}{\tan(l\pi/N)} \sum_{\alpha} \left(S^+_{\alpha} S^-_{\alpha+l} - S^-_{\alpha} S^+_{\alpha+l} \right), \tag{3.85}$$

where the HSM is re-defined as $H^{HS} = \sum_{l=1}^{N} H^{J_l}$ and the rapidity as $\Lambda^z = \sum_{l=1}^{N} \Lambda^{z,J_l}$.

In order to characterize this family of models, we notice that the first element corresponds to the Heisenberg model with a Dzyaloshinskii-Moriya interaction, which was exactly solved by Alcaraz et al. [2]. Motivated by this result, we studied our chiral model following the approach developed by Alcaraz et al. [2]. We found that the method useful for the XXZ model does not work to solve our chiral model (for more details, see the Appendix A), which can be solved by the representation theory of the Yangian $\mathrm{Y}(sl_2)$, as we have shown in this thesis. This result opens the question about the approaches that solve this family of spin models from finite sizes, up to the thermodynamic limit.

To complement this discussion we developed an exact diagonalization for a chain with $N = 6$ with range one (Heisenberg with a Dzyaloshinskii-Moriya interaction),

two ($J_1 - J_2$ model with a Dzyaloshinskii-Moriya interaction up to next-nearest-neighbors) and six (the chiral model, subject of this thesis). In Fig. (3.9) we can see the spectrum of these models. The subject is open for discussions since we believe that this family of medium range models involves a rich structure of levels and their theoretical characteristics are still unveiled.

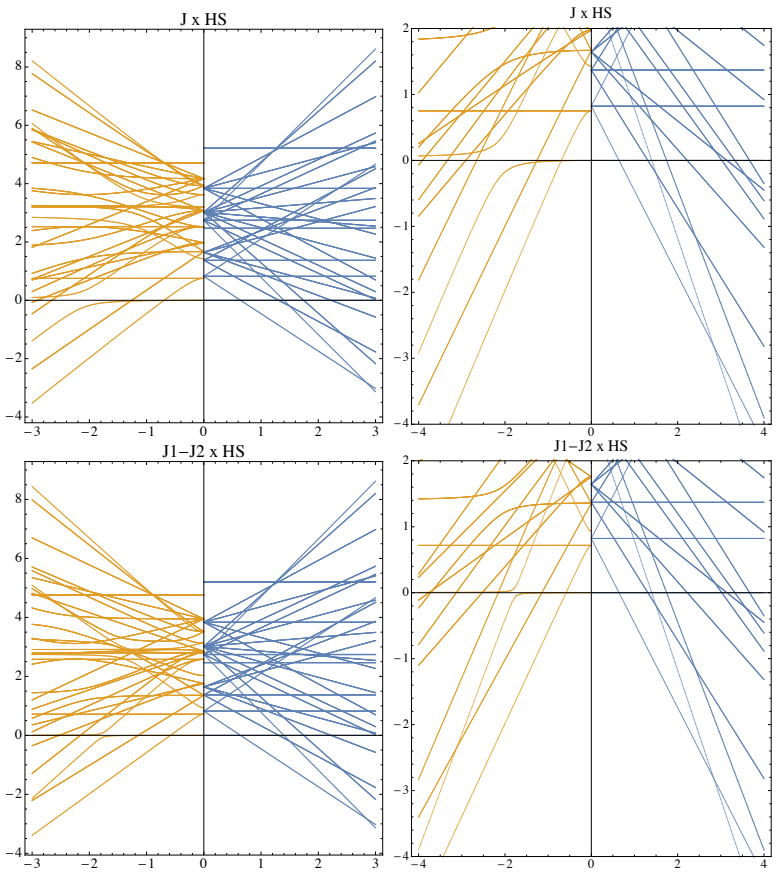

Fig. 3.9: *left panels: Energy spectrum of (top-left) the Heisenberg model, (bottom-left) the $J_1 - J_2$ model and (in the same panel) the HS model with a suitable rapidity interaction for $N = 6$. At the right panels we see a zoom of the low-energy levels from the left panels.*

3.5 Conclusion

In this Chapter, we summarized the exact solution of the HSM introduced by the Modified Young Tableaux (MYT) that describe the elementary excitations of this

model (the spinons) by the spinon momentum number (SMN), which are related with the Yangian algebra through the representation theory. Using this approach, we studied the HSM with a chiral interaction outlined by the rapidity operator, keeping the Yangian symmetry of the system. We developed a numerical description of our chiral model for finite chains with sizes $N = 4,\ 6$ and 8 sites. We observed that the ground-state and the top level (higher spinon state) of the HSM do not split when the rapidity interaction is turned on, however, the remaining eigenstates of the spectrum split in pairs which have the same z-spin component and the same Λ^z expectation value but with opposite signs.

The spectrum of our chiral model satisfied the Yangian algebra, not allowing to use the SU(2) representation given by the usual Young tableaux. This was also observed numerically when the total spin was not useful to describe the splitted eigenstates. Motivated by these results, we used the intricate representation theory of the Yangian to develop an analytic characterization of the spectrum. The splitting observed numerically inspired us an educated guess to build the spectrum from the principal element of the Yangian representation, the YHWS, which is fully described by the MYT. The split of the states generated a set of ground-state transitions, which are characterized by a linear combination of states hosted in the same supermultiplet that has $S^z = 0$, keeping the nature of the ground-state of the model as a Luttinger Liquid.

The finite size characterization of the ground-state allows us to extend our results up to the thermodynamic limit, finding that the ground-state transition for an infinite chain at low energy takes place at $D = 1$ and is composed by an unusual linear combination given by the exotic quantization rules provided by the Yangian algebra, which mix two states with null z-spin component and different total spin (in this case, $0 \oplus 1$).

Finally, we suggest the study of a family of spin chain models with a chiral interaction, which links the Heisenberg model with a Dzyaloshinskii-Moriya interaction and the chiral model at intermediate-ranges, as studied in this work. All intermediate cases are left to the new comers to this fascinating area of quantum

spin liquids.

This part of the thesis, presented in Chapter 3, was partially worked out in collaboration with Professor Germán Sierra (IFT-Madrid, Spain) during my visit to Madrid in November 2017, and is being prepared for publication.

Appendix A

The XXZ model with a Dzyaloshinskii-Moriya interaction

In this Appendix, we deal with the anisotropic Heisenberg chain with nearest-neighbor exchange interactions, while in a second part we deal with an integrable model which has long range (inverse squared) exchange terms, known as the Haldane-Shastry (HS) model. For the Heisenberg model, the Dzyaloshinskii-Moriya (DM) interaction can be argued to come from spin-orbit coupling, while for the HS model we have taken as the chiral term the long-range "rapidity operator." The latter commutes with the HS Hamiltonian, which has a different symmetry group named the Yangian, $\mathrm{Y}(\mathrm{sl}_2)$, which is a quantum deformation of the SU(2) Lie group.

A.1 The XXZ case with a DM term

Let us start from the spin-1/2 XXZ Hamiltonian with a Dzyaloshinskii-Moriya (DM) interaction along z-axis [2, 67]

$$H = J \sum_{n=1}^{L} \left[S_n^x S_{n+1}^x + S_n^y S_{n+1}^y + \delta S_n^z S_{n+1}^z + \Delta \left(S_n^x S_{n+1}^y - S_n^y S_{n+1}^x \right) \right] \tag{A.1}$$

where δ is the anisotropy parameter and Δ is the DM coupling. This model allows to study in an exact manner the magneto-electric effect in quantum spin chains [67]. In reference [2] it was shown that a gauge transformation maps the Hamiltonian

(A.1) into another XXZ Hamiltonian without the DM term. We will reproduce this argument here and try to do the same for the Haldane-Shastry model.

The Hamiltonian (A.1) can be written as

$$H = J\sum_{n=1}^{N}\left[\frac{1}{2}\left(S_n^+S_{n+1}^- + S_n^-S_{n+1}^+\right) + \delta S_n^zS_{n+1}^z + \frac{i\Delta}{2}\left(S_n^+S_{n+1}^- - S_n^-S_{n+1}^+\right)\right] \quad \text{(A.2)}$$

where $S_n^{\pm} = S_n^x \pm iS_n^y$. Notice that for $\delta \neq 0$, H is a complex function and therefore the time-reversal symmetry is broken. The unitary transformation, defined as a site-dependent rotation

$$S_n^{\pm} \to e^{\pm in\phi}S_n^{\pm}\,, \qquad S_n^z \to S_n^z \quad \text{(A.3)}$$

with the choice

$$\Delta = \tan\phi\,, \qquad -\frac{\pi}{2} < \phi < \frac{\pi}{2} \quad \text{(A.4)}$$

brings equation (A.2) back into the form

$$H = J'\sum_{n=1}^{N}\left[\frac{1}{2}\left(S_n^+S_{n+1}^- + S_n^-S_{n+1}^+\right) + \delta' S_n^zS_{n+1}^z\right] \quad \text{(A.5)}$$

where

$$J' = \frac{J}{\cos\phi}\,, \qquad \delta' = \delta\cos\phi = \delta/\sqrt{1+\Delta^2}, \quad \text{(A.6)}$$

therefore, the gauge transformation mentioned in (A.3) transform the original XXZ chain with a nearest-neighbor DM term into an exact integrable model (a new XXZ model with J' and δ'), supplemented by twisted boundary conditions (not discussed here, see [2] for further details), which can be dealt with the method of quantum transfer matrices to determine the exact free energy and to obtain exact thermodynamics functions, like in [67].

If we call the original Hamiltonian, equation (A.2), as

$$H_N^{DM}(\delta,\Delta) = H_N^{XXZ}(\delta) + V_N^{DM}(\Delta) \quad \text{(A.7)}$$

the canonical transformation, equation (A.3), means that

$$H_N^{DM}(\delta,\Delta) = \frac{1}{\cos\phi}H_N^{XXZ}(\delta\cos\phi) \quad \text{(A.8)}$$

except for the boundary conditions, which need to be dealt with separately [2]. Since in the thermodynamics limit ($N \to \infty$) the boundary conditions do not affect the critical behavior, then the Hamiltonian $H_\infty^{DM}(\delta, \Delta)$ will have the same critical properties as $H_\infty^{XXZ}(\delta \cos\phi)$. Hence, the phase diagram of the Hamiltonian $H_\infty^{DM}(\delta, \Delta)$ will be the same as the one for the well-known XXZ model. Figure A.1 shows this phase diagram, where a critical (massless) phase C is separated from the massive phases A (antiferro) and F (ferro) by the lines $\delta' = \pm 1$, namely $\delta = \pm\sqrt{1+\Delta^2}$. A dashed line indicates where the critical exponents in the phase diagram are constant. The particular line $\delta = 0$ (XY model) represent a case where the Dzyaloshinskii-Moriya interaction is inoperant. It does not modify the critical behavior.

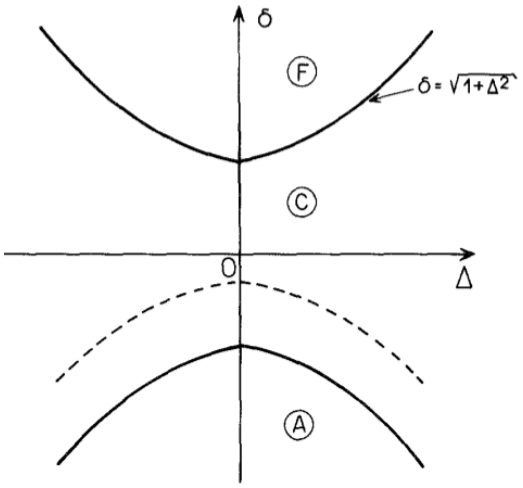

Fig. A.1: *The phase diagram of $H_\infty^{DM}(\delta, \Delta)$. The critical lines $\delta = \pm\sqrt{1+\Delta^2}$ separate the massless phase C from massive phases A and F. On the dashed line as well on the line $\delta = 0$ (XY model) the critical exponents are constant. Figure taken from [2].*

In the rotation (A.3), we shall take $\phi \in [0, \pi/2)$. The value $\phi = \pi/2$ is singular, because then $\Delta = \infty$. This means that the model $\delta' = 0$ cannot be reached with this transformation (except when $\delta = 0$). If the unperturbed XXZ model is critical, i.e. $-1 < \delta \leq 1$, the perturbed model by the DM term is also critical because $-1 < \delta' \leq 1$.

A.2 The HS model with a chiral term

The Haldane-Shastry (HS) Hamiltonian is given by

$$H_{HS} = \frac{J\pi^2}{N^2}\sum_{n<m}^{N}\frac{\tilde{\mathbf{S}}_n\cdot\tilde{\mathbf{S}}_m}{\sin^2\left(\pi(n-m)/N\right)} = -\frac{4J\pi^2}{N^2}\sum_{n<m}^{N}\frac{z_n z_m}{(z_n-z_m)^2}\tilde{\mathbf{S}}_n\cdot\tilde{\mathbf{S}}_m, \tag{A.9}$$

where N is the number of sites. If $N \gg 1$ the HS Hamiltonian can be expanded as

$$H_{HS} = J\sum_{n}^{N}\left(\tilde{\mathbf{S}}_n\cdot\tilde{\mathbf{S}}_{n+1} + \frac{1}{4}\tilde{\mathbf{S}}_n\cdot\tilde{\mathbf{S}}_{n+2} + ...\right) \tag{A.10}$$

The Hamiltonian (A.9) commutes with the rapidity operator

$$\tilde{\mathbf{\Lambda}} = -\frac{\pi}{N}\sum_{n<m}^{N}\cot\left(\frac{\pi(n-m)}{N}\right)\tilde{\mathbf{S}}_n\times\tilde{\mathbf{S}}_m = -\frac{i\pi}{N}\sum_{n<m}^{N}w_{nm}\tilde{\mathbf{S}}_n\times\tilde{\mathbf{S}}_m, \tag{A.11}$$

where

$$w_{nm} = \frac{z_n+z_m}{z_n-z_m}, \qquad \text{and} \qquad z_n = \exp(i2\pi n/N). \tag{A.12}$$

For $N \gg 1$ equation (A.11) can be expanded as

$$\vec{\Lambda} = \sum_{n}^{N}\left(\tilde{\mathbf{S}}_n\times\tilde{\mathbf{S}}_{n+1} + \frac{1}{2}\tilde{\mathbf{S}}_n\times\tilde{\mathbf{S}}_{n+2} + ...\right) \tag{A.13}$$

We shall define the HS model with a chiral perturbation (along z-axis) as

$$\begin{aligned} H_{HS-DM} &= H_{HS} + JD\Lambda^z \\ &= \frac{J\pi^2}{N^2}\sum_{n<m}^{N}\frac{\tilde{\mathbf{S}}_n\cdot\tilde{\mathbf{S}}_m}{\sin^2\left(\pi(n-m)/N\right)} \\ &\quad -\frac{JD\pi}{N}\sum_{n<m}^{N}\cot\left(\frac{\pi(n-m)}{N}\right)(S_n^xS_m^y - S_n^yS_m^x). \end{aligned} \tag{A.14}$$

Notice that the direction of the $\tilde{\mathbf{\Lambda}}$ vector is irrelevant since the HS hamiltonian is SU(2) invariant. In the limit $N \gg 1$, one finds

$$\begin{aligned} H_{HS-DM} &= J\sum_{n}\Big\{\left(\tilde{\mathbf{S}}_n\cdot\tilde{\mathbf{S}}_{n+1} + \frac{1}{4}\tilde{\mathbf{S}}_n\cdot\tilde{\mathbf{S}}_{n+2} + ...\right) \\ &\quad +D(S_n^xS_{n+1}^y - S_n^yS_{n+1}^x) + \frac{D}{2}(S_n^xS_{n+2}^y - S_n^yS_{n+2}^x) + ...\Big\} \end{aligned} \tag{A.15}$$

Therefore, up to the nearest-neighbor coupling it coincides with the equation (A.1) for $\delta = 1$ and $D = \Delta$. In the $S_n^{\pm}$ basis, equation (A.14) becomes

$$\begin{aligned} H_{HS-DM} &= \frac{J\pi^2}{N}\sum_{n<m}^{N}\frac{1}{\sin^2\left(\pi(n-m)/N\right)}\left[\frac{1}{2}(S_n^+S_m^- + S_n^-S_m^+) + \delta S_n^z S_m^z\right] \\ &\quad -\frac{iJD\pi}{2N}\sum_{n<m}^{N}\cot\left(\frac{\pi(n-m)}{N}\right)(S_n^+S_m^- - S_n^-S_m^+) \end{aligned} \tag{A.16}$$

where we have introduced again the anisotropy parameter δ in the z-component. This expression is the corresponding of (A.2) and it will be used in Chapter 3 to extract information from a numerical approach. The question is: can we map this model in the same way as was done for the Heisenberg model with a Dzyaloshinkii-Moriya term? The answer is in the next Section.

A.3 The negative result for the HS+chiral case

We have tried to implement the same gauge transformation as for the XXZ chain, with a negative result. We will show this attempt to see where are the difficulties in finding such global unitary transformation for the Haldane-Shastry with the chiral term. Let us focus on the $S^{\pm}$ terms

$$\begin{aligned} H_{HS-DM}^{XY} &= \frac{J\pi^2}{2N}\sum_{n<m}^{N}\frac{1}{\sin^2\left(\pi(n-m)/N\right)}(S_n^+S_m^- + S_n^-S_m^+) \\ &\quad -\frac{iJD\pi}{2N}\sum_{n<m}^{N}\cot\left(\frac{\pi(n-m)}{N}\right)(S_n^+S_m^- - S_n^-S_m^+) \end{aligned} \tag{A.17}$$

Under the unitary transformation (A.3) one finds

$$S_n^{\pm}S_m^{\mp} \to e^{\pm(n-m)\phi}S_n^{\pm}S_m^{\mp} \tag{A.18}$$

so the transformed operator is

$$\begin{aligned} H_{HS-DM}^{XY} &= \frac{J\pi^2}{2N}\sum_{n<m}^{N}\left\{\frac{1}{\sin^2\left(\pi(n-m)/N\right)} - \frac{iD}{\pi}\cot\left(\frac{\pi(n-m)}{N}\right)\right\}e^{(n-m)\phi}S_n^+S_m^- \\ &+ \frac{J\pi^2}{2N}\sum_{n<m}^{N}\left\{\frac{1}{\sin^2\left(\pi(n-m)/N\right)} + \frac{iD}{\pi}\cot\left(\frac{\pi(n-m)}{N}\right)\right\}e^{-(n-m)\phi}S_n^-S_m^+. \end{aligned}$$

Now, the question is: what is value of D that makes the two coefficients of $S_n^+ S_m^-$ and $S_n^- S_m^+$ in equation above equal? After some algebra, the answer is

$$D = \frac{\pi}{N} \tan\{(n-m)\phi\} \left[\cos\left(\frac{\pi(n-m)}{N}\right) \sin\left(\frac{\pi(n-m)}{N}\right)\right]^{-1} . \tag{A.19}$$

Introducing this result into the equation (A.17), and restoring the z-terms, we finally have

$$\begin{aligned} H_{HS-DM} &= \frac{J\pi^2}{2N^2} \sum_{n<m}^{N} \frac{1}{\sin^2(\pi(n-m)/N)} \left(\frac{1}{\cos\{(n-m)\phi\}} \left[\frac{1}{2}(S_n^+ S_m^- + S_n^- S_m^+)\right] \right. \\ &\left. + \delta \cos\{(n-m)\phi\} S_n^z S_m^z \right) . \end{aligned} \tag{A.20}$$

Therefore, the new HS-DM Hamiltonian is equivalent to a pure HS model, with the site-dependent exchange and anisotropy parameters changed to

$$J'_{nm} = \frac{J_{nm}}{\cos\{(n-m)\phi\}}, \qquad \delta'_{nm} = \delta_{nm} \cos\{(n-m)\phi\} \tag{A.21}$$

where, the original J_{nm} and δ_{nm} Haldane-Shastry parameters were $1/r^2$-type

$$J_{nm} = \frac{1}{\sin^2(\pi(n-m)/N)}, \qquad \delta_{nm} = \frac{\delta}{\sin^2(\pi(n-m)/N)} . \tag{A.22}$$

Although, interestingly similar to the results for the XXZ model, this transformation is, however, not a global gauge transformation, as it was in the nearest-neighbor Heisenberg case, since the DM terms are defined term-by-term in the further-neighboring list, eq. (A.21). We cannot define a unitary (global) operator U that makes $H' = UHU^\dagger$, as in the previous XXZ case.

References

[1] A. Yu. Kitaev. Unpaired majorana fermions in quantum wires. *Physics-Uspekhi*, 44(10S):131, 2001.

[2] F. C. Alcaraz and W. F. Wreszinski. The heisenberg xxz hamiltonian with dzyaloshinsky-moriya interactions. *Journal of Statistical Physics*, 58(1):45–56, 1990.

[3] Lucile Savary and Leon Balents. Quantum spin liquids: a review. *Reports on Progress in Physics*, 80(1):016502, 2017.

[4] Yi Gao, Tao Zhou, Huaixiang Huang, and Ran Huang. Majorana zero modes in the hopping-modulated one-dimensional p-wave superconducting model. *Scientific Report*, 5:17049, Nov 2015.

[5] J. E. Bunder and Ross H. McKenzie. Effect of disorder on quantum phase transitions in anisotropic xy spin chains in a transverse field. *Phys. Rev. B*, 60:344–358, Jul 1999.

[6] G. Mussardo. *Statistical Field Theory: An Introduction to Exactly Solved Models in Statistical Physics*. Oxford Graduate Texts. OUP Oxford, 2009.

[7] F. D. M. Haldane. Exact jastrow-gutzwiller resonating-valence-bond ground state of the spin-(1/2 antiferromagnetic heisenberg chain with $1/r^2$ exchange. *Phys. Rev. Lett.*, 60:635–638, Feb 1988.

[8] B. Sriram Shastry. Exact solution of an s=1/2 heisenberg antiferromagnetic chain with long-ranged interactions. *Phys. Rev. Lett.*, 60:639–642, Feb 1988.

[9] Dirk Schuricht. Many-spinon states and representations of yangians in the su(n) haldane–shastry model. *Journal of Physics A: Mathematical and Theoretical*, 41(1):015208, 2008.

[10] K. v. Klitzing, G. Dorda, and M. Pepper. New method for high-accuracy determination of the fine-structure constant based on quantized hall resistance. *Phys. Rev. Lett.*, 45:494–497, Aug 1980.

[11] R. B. Laughlin. Quantized Hall conductivity in two dimensions. *Phys. Rev. B*, 23:5632–5633, May 1981.

[12] D. J. Thouless, M. Kohmoto, M. P. Nightingale, and M. den Nijs. Quantized hall conductance in a two-dimensional periodic potential. *Phys. Rev. Lett.*, 49:405–408, Aug 1982.

[13] R. B. Laughlin. Anomalous quantum hall effect: An incompressible quantum fluid with fractionally charged excitations. *Phys. Rev. Lett.*, 50:1395–1398, May 1983.

[14] M. V. Berry. Quantal phase factors accompanying adiabatic changes. *Proceedings of the Royal Society of London Series A*, 392:45–57, March 1984.

[15] J. Zak. Berry's phase for energy bands in solids. *Phys. Rev. Lett.*, 62:2747–2750, Jun 1989.

[16] Alexander Altland and Martin R. Zirnbauer. Nonstandard symmetry classes in mesoscopic normal-superconducting hybrid structures. *Phys. Rev. B*, 55:1142–1161, Jan 1997.

[17] C. L. Kane and E. J. Mele. Quantum spin hall effect in graphene. *Phys. Rev. Lett.*, 95:226801, Nov 2005.

[18] F. D. M. Haldane. Model for a quantum hall effect without landau levels: Condensed-matter realization of the "parity anomaly". *Phys. Rev. Lett.*, 61:2015–2018, Oct 1988.

[19] B. Andrei Bernevig and Shou-Cheng Zhang. Quantum spin hall effect. *Phys. Rev. Lett.*, 96:106802, Mar 2006.

[20] Markus König, Steffen Wiedmann, Christoph Brüne, Andreas Roth, Hartmut Buhmann, Laurens W. Molenkamp, Xiao-Liang Qi, and Shou-Cheng Zhang. Quantum spin hall insulator state in hgte quantum wells. *Science*, 318(5851):766–770, 2007.

[21] S. Sachdev. *Quantum Phase Transitions*. Cambridge University Press, 2001.

[22] Steven R. Elliott and Marcel Franz. Colloquium. *Rev. Mod. Phys.*, 87:137–163, Feb 2015.

[23] V. Mourik, K. Zuo, S. M. Frolov, S. R. Plissard, E. P. A. M. Bakkers, and L. P. Kouwenhoven. Signatures of majorana fermions in hybrid superconductor-semiconductor nanowire devices. *Science*, 336(6084):1003–1007, 2012.

[24] W. Chang, V. E. Manucharyan, T. S. Jespersen, J. Nygård, and C. M. Marcus. Tunneling spectroscopy of quasiparticle bound states in a spinful josephson junction. *Phys. Rev. Lett.*, 110:217005, May 2013.

[25] Li-Jun Lang and Shu Chen. Majorana fermions in density-modulated p-wave superconducting wires. *Phys. Rev. B*, 86:205135, Nov 2012.

[26] Wade DeGottardi, Diptiman Sen, and Smitha Vishveshwara. Majorana fermions in superconducting 1d systems having periodic, quasiperiodic, and disordered potentials. *Phys. Rev. Lett.*, 110:146404, Apr 2013.

[27] Wade DeGottardi, Manisha Thakurathi, Smitha Vishveshwara, and Diptiman Sen. Majorana fermions in superconducting wires: Effects of long-range hopping, broken time-reversal symmetry, and potential landscapes. *Phys. Rev. B*, 88:165111, Oct 2013.

[28] Ryohei Wakatsuki, Motohiko Ezawa, Yukio Tanaka, and Naoto Nagaosa. Fermion fractionalization to majorana fermions in a dimerized kitaev superconductor. *Phys. Rev. B*, 90:014505, Jul 2014.

[29] Suraj Hegde, Vasudha Shivamoggi, Smitha Vishveshwara, and Diptiman Sen. Quench dynamics and parity blocking in majorana wires. *New Journal of Physics*, 17(5):053036, 2015.

[30] Suraj S. Hegde and Smitha Vishveshwara. Majorana wave-function oscillations, fermion parity switches, and disorder in kitaev chains. *Phys. Rev. B*, 94:115166, Sep 2016.

[31] Qi-Bo Zeng, Shu Chen, and Rong Lü. Generalized aubry-andré-harper model with p-wave superconducting pairing. *Phys. Rev. B*, 94:125408, Sep 2016.

[32] T. Liu, P. Wang, S. Chen, and G. Xianlong. Phase diagram of a generalized off-diagonal Aubry-Andr\'{e} model with p-wave pairing. *ArXiv e-prints*, May 2017.

[33] Jason Alicea. Majorana fermions in a tunable semiconductor device. *Phys. Rev. B*, 81:125318, Mar 2010.

[34] Davide Vodola, Luca Lepori, Elisa Ercolessi, Alexey V. Gorshkov, and Guido Pupillo. Kitaev chains with long-range pairing. *Phys. Rev. Lett.*, 113:156402, Oct 2014.

[35] P. Cats, A. Quelle, O. Viyuela, M. A. Martin-Delgado, and C. Morais Smith. Staircase to Higher-Order Topological Phase Transitions. *ArXiv e-prints*, October 2017.

[36] Gerardo Ortiz, Jorge Dukelsky, Emilio Cobanera, Carlos Esebbag, and Carlo Beenakker. Many-body characterization of particle-conserving topological superfluids. *Phys. Rev. Lett.*, 113:267002, Dec 2014.

[37] I. Adagideli, M. Wimmer, and A. Teker. Effects of electron scattering on the topological properties of nanowires: Majorana fermions from disorder and superlattices. *Phys. Rev. B*, 89:144506, Apr 2014.

[38] Raquel Queiroz, Eslam Khalaf, and Ady Stern. Dimensional hierarchy of fermionic interacting topological phases. *Phys. Rev. Lett.*, 117:206405, Nov 2016.

[39] Lukasz Fidkowski and Alexei Kitaev. Effects of interactions on the topological classification of free fermion systems. *Phys. Rev. B*, 81:134509, Apr 2010.

[40] Evelyn Tang and Xiao-Gang Wen. Interacting one-dimensional fermionic symmetry-protected topological phases. *Phys. Rev. Lett.*, 109:096403, Aug 2012.

[41] Niklas M. Gergs, Lars Fritz, and Dirk Schuricht. Topological order in the kitaev/majorana chain in the presence of disorder and interactions. *Phys. Rev. B*, 93:075129, Feb 2016.

[42] Andreas P. Schnyder, Shinsei Ryu, Akira Furusaki, and Andreas W. W. Ludwig. Classification of topological insulators and superconductors in three spatial dimensions. *Phys. Rev. B*, 78:195125, Nov 2008.

[43] P. G. de Gennes. *Superconductivity of Metals and Alloys.* Advanced Books Classics Series. Westview Press, 1999.

[44] S. Aubry and G. André. Analyticity breaking and anderson localization in incommensurate lattices. *Ann. Israel Phys. Soc.*, 3:133, 1980.

[45] Xiaoming Cai, Li-Jun Lang, Shu Chen, and Yupeng Wang. Topological superconductor to anderson localization transition in one-dimensional incommensurate lattices. *Phys. Rev. Lett.*, 110:176403, Apr 2013.

[46] X. Cai. Quantum phase transitions and phase diagram for a one-dimensional p-wave superconductor with an incommensurate potential. *J. Phys.: Condens. Matter*, 26(15):155701, 2014.

[47] J. C. C. Cestari, A. Foerster, and M. A. Gusmão. Fate of topological states in incommensurate generalized aubry-andré models. *Phys. Rev. B*, 93:205441, May 2016.

[48] A. Bansil, Hsin Lin, and Tanmoy Das. Colloquium. *Rev. Mod. Phys.*, 88:021004, Jun 2016.

[49] O. Viyuela, D. Vodola, G. Pupillo, and M. A. Martin-Delgado. Topological massive dirac edge modes and long-range superconducting hamiltonians. *Phys. Rev. B*, 94:125121, Sep 2016.

[50] Antonio Alecce and Luca Dell'Anna. Extended kitaev chain with longer-range hopping and pairing. *Phys. Rev. B*, 95:195160, May 2017.

[51] Kristian Patrick, Titus Neupert, and Jiannis K. Pachos. Topological quantum liquids with long-range couplings. *Phys. Rev. Lett.*, 118:267002, Jun 2017.

[52] Elliott Lieb, Theodore Schultz, and Daniel Mattis. Two soluble models of an antiferromagnetic chain. *Ann. Phys. (N.Y.)*, 16(3):407, 1961.

[53] Marcos Pérez and Gerardo Martínez. Polynomial description of inhomogeneous topological superconducting wires. *Journal of Physics: Condensed Matter*, 29(47):475503, 2017.

[54] M. Di Liberto, C. E. Creffield, G. I. Japaridze, and C. Morais Smith. Quantum simulation of correlated-hopping models with fermions in optical lattices. *Phys. Rev. A*, 89:013624, Jan 2014.

[55] H. Bethe. Zur theorie der metalle. *Zeitschrift für Physik*, 71(3):205–226, Mar 1931.

[56] Anatoli G. Izergina Filippo Colomo and Andrei G. Pronko. Lecture notes: Introduction to the bethe ansatz solvable models., 2000.

[57] L.D. Faddeev and L.A. Takhtajan. What is the spin of a spin wave? *Physics Letters A*, 85(6):375 – 377, 1981.

[58] M. Greiter. *Mapping of Parent Hamiltonians: From Abelian and non-Abelian Quantum Hall States to Exact Models of Critical Spin Chains*. Springer Tracts in Modern Physics. Springer Berlin Heidelberg, 2011.

[59] Z. N. C. Ha and F. D. M. Haldane. Squeezed strings and yangian symmetry of the heisenberg chain with long-range interaction. *Phys. Rev. B*, 47:12459–12469, May 1993.

[60] Norio Kawakami. Asymptotic bethe-ansatz solution of multicomponent quantum systems with $\frac{1}{r^2}$ long-range interaction. *Phys. Rev. B*, 46:1005–1014, Jul 1992.

[61] Z. N. C. Ha and F. D. M. Haldane. Models with inverse-square exchange. *Phys. Rev. B*, 46:9359–9368, Oct 1992.

[62] Martin Greiter and Dirk Schuricht. No attraction between spinons in the haldane-shastry model. *Phys. Rev. B*, 71:224424, Jun 2005.

[63] Martin Greiter and Dirk Schuricht. Many-spinon states and the secret significance of young tableaux. *Phys. Rev. Lett.*, 98:237202, Jun 2007.

[64] B. A. Bernevig, D. Giuliano, and R. B. Laughlin. Coordinate representation of the two-spinon wave function and spinon interaction in the haldane-shastry model. *Phys. Rev. B*, 64:024425, Jun 2001.

[65] V. Chari and A.N. Pressley. *A Guide to Quantum Groups*. Cambridge University Press, 1995.

[66] V. G. Drinfeld. A new realization of yangians and quantized affine algebras. *Sov. Math. Dokl.*, 36:212–216, 1988.

[67] Michael Brockmann, Andreas Klümper, and Vadim Ohanyan. Exact description of magnetoelectric effect in the spin-$\frac{1}{2}$ xxz chain with dzyaloshinskii-moriya interaction. *Phys. Rev. B*, 87:054407, Feb 2013.